HIGH-PRESSURE EXPONENT BREAK OF AP/HTPB-COMPOSITE PROPELLANTS

A Dissertation

by

CATHERINE ANNE MARIE DILLIER

Submitted to the Graduate and Profession School of
Texas A&M University
in partial fulfillment of the requirements for the degree of

DOCTOR OF PHILOSOPHY

Chair of Committee,	Eric L. Petersen
Committee Members,	Waruna Kulatilaka
	Timothy Jacobs
	Chad Mashuga
Head of Department,	Andreas A. Polycarpou

August 2021

Major Subject: Mechanical Engineering

ABSTRACT

At higher pressures, the burning rates of AP/HTPB-composite propellants become less controllable as it experiences a transition regime often referred to as an "exponent break" typically between 20.7 and 34.5 MPa. The pressure exponent drastically increases to values greater than 1, making the burning rate extremely sensitive to pressure fluctuations. This study systematically evaluated the effects of AP characteristics, micron-aluminum, and catalytic additives on the exponent break and high-pressure burning rates of AP/HTPB-composite propellants. A total of sixteen formulations containing varying AP characteristics (particle size, concentration, and distribution) and either Mach I iron oxide or titania nanoparticles or in-situ titania as a catalyst were evaluated between pressures of 6.89 MPa and 68.9 MPa. All formulations with the exception of two, 46.0-μm AP with Mach I titania and 138.9-μm AP with 0.50% in-situ titania, showed an exponent break. Decreasing the AP particle size decreased both the characteristic pressure where the exponent break occurred (or P*) and the pressure exponent after the break. AP size distribution also affected P*, whereas changes in AP concentration did not. The inclusion of aluminum lowered P* compared to the non-aluminized formulations. Additionally, increasing the aluminum concentration appeared to lower the post-break pressure exponent. For the formulations containing catalytic additives, the characteristic pressure increased and was dependent on the corresponding baseline burning rates, occurring where the additive burning rate curve intersected with its respective baseline burning rate curve. These burning rate

results along with the Thomas et al. composite propellant burning model were subsequently used to evaluate existing exponent break mechanisms in the literature. The existence of an AP barrier and the general theory in the literature that AP decomposition dominates in the very-high-pressure regime were corroborated. Additionally, it was shown that both crack propagation and formation in AP crystals and series-burning, proposed by Irwin et al. and Cole, respectively, are promising as components of the exponent break mechanism. This study adds new data to the severely limited database for very-high-pressure, AP-based, composite propellant burning rates in the open literature and provides one of the first fundamental studies on the exponent break feature.

DEDICATION

This dissertation is dedicated to my parents, James and Doreen Dillier, for their unceasing love and support and in loving memory of my grandfather and cousin, Vincent Carr and Jeremy Brady.

ACKNOWLEDGMENTS

I would like to thank my committee chair and advisor, Dr. Petersen, for his support, guidance, and confidence in me. I will be forever grateful for the opportunity he provided me with as a senior in undergrad. His patience and direction these past seven years have enabled me to grow as both a researcher and person. The dedication he shows for his students and the environment he creates is unparalleled and allows not only for his students to succeed, but also to thrive.

I also offer my gratitude to my other committee members, Dr. Kulatilaka, Dr. Jacobs, and Dr. Mashuga, as well as Dr. David Reid (Helicon Chemical) for their support and insight throughout the course of this research and graduate career. Thank you also to all of the faculty and staff who have taught me and provided me with countless resources and help during my time at Texas A&M University.

To my friends and colleagues in the Petersen Research Group, thank you. Your advice, support, and laughter has sustained me throughout graduate school. Thank you particularly to Erica for your help, especially with all the late-night testing and supply of caffeinated beverages, and Tom for your wisdom and advice.

Finally, gratitude also goes to my family, particularly my parents, James and Doreen Dillier, and my grandmother, Patricia Carr. Their selfless and unconditional love, advice, patience, and care packages have sustained me throughout my college career and life. I will never be able to repay them and will be forever grateful for them.

CONTRIBUTORS AND FUNDING SOURCES

Contributors

This work was supervised by a dissertation committee consisting of Professor Eric L. Petersen, Professor Waruna Kulatilaka, and Professor Timothy Jacobs of the J. Mike Walker ’66 Department of Mechanical Engineering and Professor Chad Mashuga of the Artie McFerrin Department of Chemical Engineering.

The particle size distributions were measured using a Beckman Coulter LS 13 320 XR Laser Diffraction Particle Size Analyzer provided by Professor Chad Mashuga of the Artie McFerrin Department of Chemical Engineering. The *in-situ* TiO_2 was provided by Dr. David Reid and the Helicon Chemical Company.

All other work conducted for the thesis (or) dissertation was completed by the student independently.

Funding Sources

A portion of this work was supported by a Ralph-James Fellowship from the TEES Turbomachinery Laboratory. Additional funding came from the Petersen Research Group and the TEES Turbomachinery Laboratory.

NOMENCLATURE

a	Burning Rate Constant (also named temperature coefficient)
AP	Ammonium Perchlorate
HTPB	Hydroxyl-terminated Polybutadiene
IPDI	Isophorone Diisocyanate
n	Pressure Exponent
P	Chamber Pressure
r	Burning Rate
$m_{chamber}$	Mass in Rocket Motor Chamber
m_g	Gas Generated from the Propellant Burning
m_d	Mass Discharged Through Nozzle Throat
ρ_P	Propellant Density
A_b	Propellant Burn Area
c*	Characteristic Velocity
A_t	Nozzle Throat Area
CTPB	Carboxyl-terminated Polybutadiene
PBAA	Polybutadiene-acrylic Acid
BDP	Beckstead-Derr-Price
LabRAM	Laboratory Resonance Acoustic Mixer

TABLE OF CONTENTS

Page

LIST OF FIGURES

Page

LIST OF TABLES

Page

CHAPTER I

INTRODUCTION

Composite propellants have been used for over 60 years in a variety of applications such as space flight and missiles due to their reliability and tailor-ability. They typically consist of a hydrocarbon binder such as hydroxyl-terminated polybutadiene (HTPB) and a crystalline oxidizer, ammonium perchlorate (AP). A variety of factors including oxidizer particle size, concentration, distribution, inclusion of catalysts, etc. can be used to tailor composite propellant burning rate behavior and other properties to fit mission-specific requirements. Their burning rate behavior is typically described by Vielle's burning rate law as seen in Eq. (1) where P is the chamber pressure, n the experimentally determined pressure exponent with values typically ranging from 0.3 – 0.6, and an experimentally determined coefficient. Figure 1 provides examples of typical burning rate curves.

$$r = aP^n \tag{1}$$

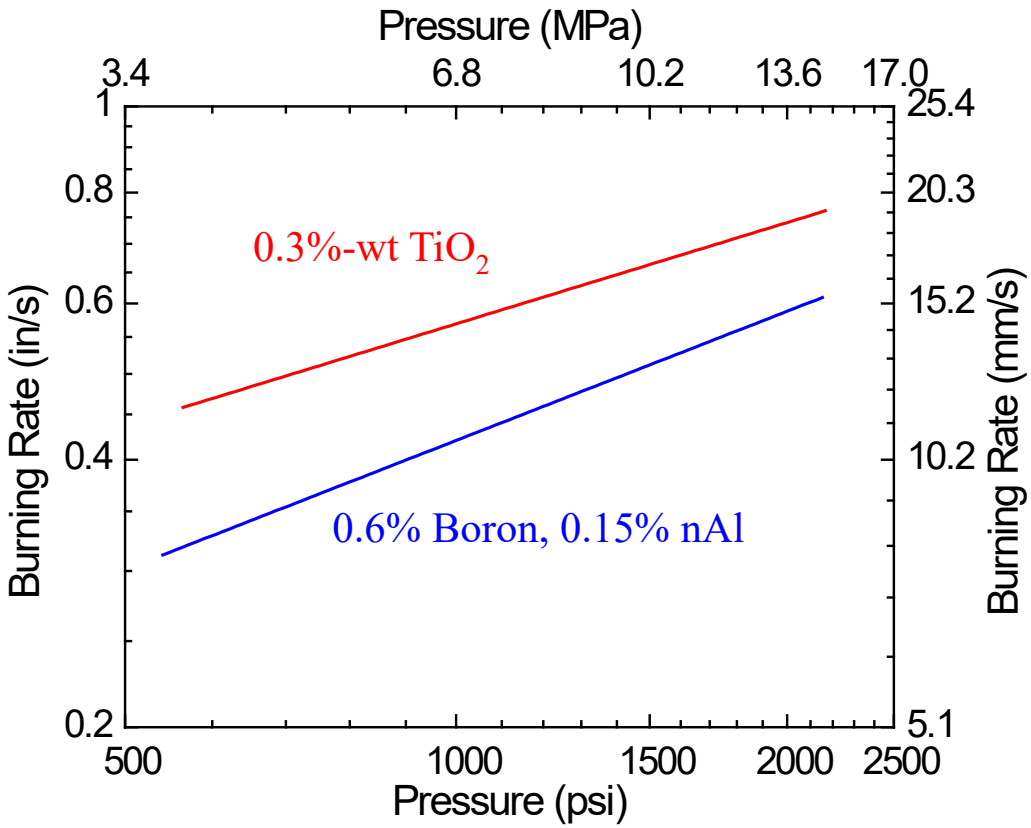

Figure 1. Typical burning rate curves for AP/HTPB-based solid composite propellants. The burning rates presented are for AP/HTPB-based formulations with 85% solids loadings, bimodal AP distributions, and 0.3% in-situ TiO_2 and 0.75% aluminum-coated boron (0.6% boron, 0.15% nAl).

As seen in Fig. 1 and implied in Eq. (1), the burning rate increases linearly with pressure when plotted on a log-log scale. Figure 1 also illustrates the effect of the pressure exponent on the burning rates. As the pressure exponent increases, so do the burning rate values and their sensitivity to chamber pressure, eventually leading to unstable chamber pressure and potentially disastrous over-pressurization when the pressure exponent approaches or exceeds a value of one. As n nears 1, the burning rate becomes extremely sensitive to the chamber pressure and vice versa, potentially leading

to a catastrophic pressure increase in mere milliseconds. Similarly, if n>1, then any deviation from the ideal operating pressure can lead to unstable combustion. This effect of large n is explained by a 1-D mass balance analysis of a typical solid rocket motor chamber and nozzle, as shown Fig. 2 and Eq. (2).

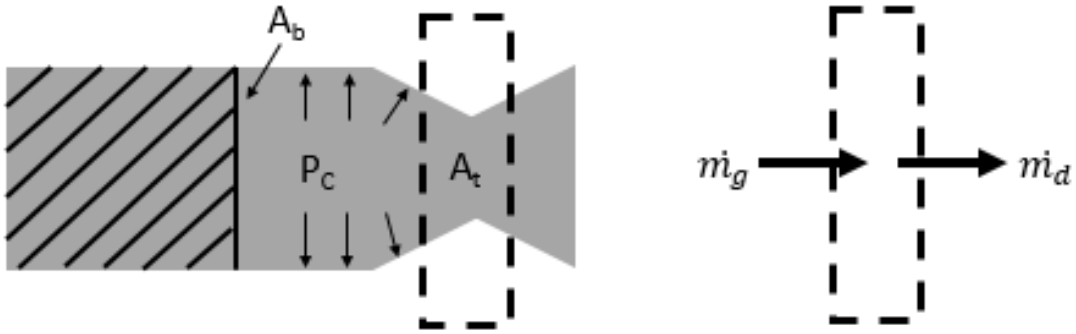

Figure 2. 1-D mass balance analysis of typical solid rocket motor.

$$\frac{dm_{chamber}}{dt} = \dot{m}_g - \dot{m}_d \tag{2}$$

where $m_{chamber}$ is the mass in the rocket motor chamber; m_g, the gas generated from the propellant burning; and m_d, the mass discharged through the nozzle throat. The rate of mass generated and rate of mass discharged through the nozzle can be described as,

$$\dot{m}_g = \rho_p r A_b \tag{3}$$

$$\dot{m}_d = \frac{P_c A_t}{c*} \tag{4}$$

where ρ_P is the propellant density; r, burning rate; A_b, propellant burn area; c*, characteristic velocity; P_c, chamber pressure; and A_t, throat area **[1-2]**. The steady-state chamber pressure is therefore the pressure where these mass flows are equivalent. This

pressure and maintaining steady-state operation are both heavily dependent on the pressure exponent as evidenced in Eq. (1, 3-4) and plotted in Fig. 3.

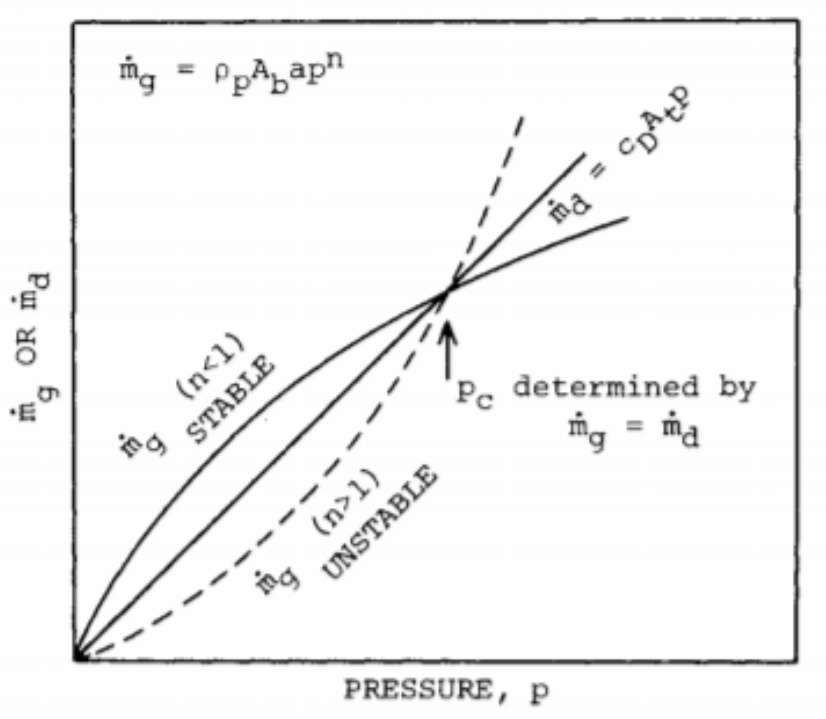

Figure 3. Effect of pressure exponent on the mass generated and discharged and the subsequent effect on pressure stability. Reprinted from Kubota [1].

If the chamber pressure strays from ideal, the pressure exponent dictates the consequences. If the operating pressure decreases slightly, then the rate of mass produced must be greater than the rate discharged and vice versa if the operating pressure increases slightly. As Fig. 3 demonstrates, this is the case for n<1. To an extent, the system is self-regulating in terms of operating pressure [2]. However, if n>1, then the pressure rapidly drops to atmosphere if the operating pressure decreases and exponentially rises if the operating pressure increases slightly. Maintaining a pressure exponent less than 1 is not an issue under typical operating chamber pressures of 1000-

3000 psi. If the chamber pressure exceeds 3000 psi, however, most AP-based solid composite propellants begin to exhibit a secondary burning rate feature called the exponent break.

The exponent break is characterized by a dramatic increase in pressure exponent to values greater than 1, resulting in a heightened burning rate sensitivity to pressure. This exponent break typically occurs at pressures above 2000 psi, and the pressure where it occurs is referred to as the characteristic pressure, P*. Figure 4 provides a typical burning rate curve where the exponent break feature is present. Characterizing and understanding this feature is extremely important in terms of safety and overall rocket motor design. As technology and materials improve, higher chamber operating pressures become more feasible and desirable since propellant specific impulse and thrust increase with pressure. While this exponent break feature has been well-documented and explored in pure AP and other inert-binder/AP-composite propellants such as carboxyl-terminated polybutadiene (CTPB), polysulfide, and PBAA, there is a significant lack of high-pressure data past 5000 psi in the literature and current research regarding AP/HTPB-composite propellants [3-17]. Therefore, the objective of this thesis was to obtain new data at very high pressures, understand the key parameters impacting the AP exponent break, and identify the underlying fundamental physical and chemical mechanisms.

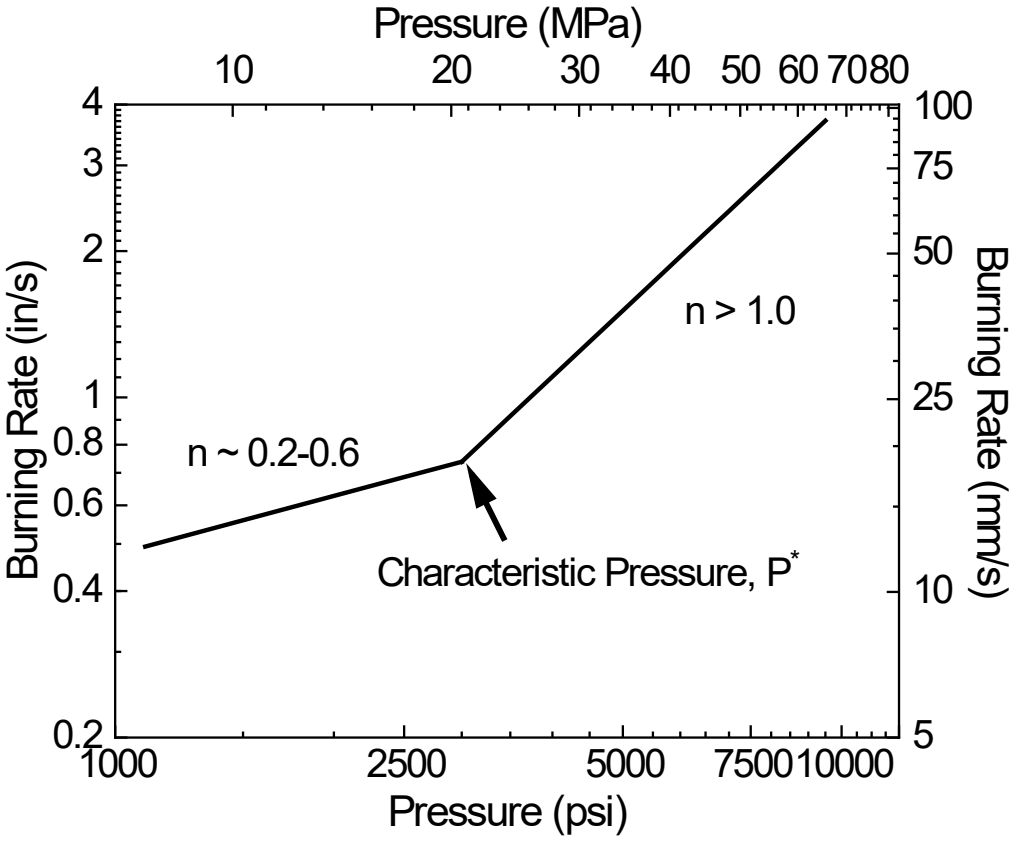

Figure 4. Example burning rate curve with exponent break feature.

This dissertation provides a literature review of AP/HTPB-based composite propellant combustion fundamentals including AP decomposition and combustion and AP/HTPB combustion. It also reviews the effects of aluminum and catalytic additives on AP/HPTB combustion followed by a summary of existing high-pressure studies on AP and AP-based propellants. Chapter III describes the methods and facilities used to perform the high-pressure burning rate experiments for AP/HTPB-composite propellants containing various AP characteristics, aluminum, and/or catalytic additives. It also provides a burning rate uncertainty analysis. The high-pressure burning rate results are presented, and the effects of each formulation detail are assessed in Chapters IV and V,

respectively. Chapter VI provides an evaluation of existing exponent break theories and models as they pertain to the burning rates presented in Chapter IV. Initial exponent break modeling results based on an existing composite propellant model are presented in Chapter VII along with sensitivity analyses performed on the model input parameters. The final chapter summarizes the dissertation and concluding theories from this study.

CHAPTER II

BACKGROUND AND LITERATURE REVIEW

2.1 AP Combustion

This section provides an overview of AP combustion in terms of decomposition and deflagration. The subsequent section provides a summary and description of AP/HTPB-composite propellant combustion where AP decomposition and deflagration continues to play a role when incorporated into solid propellants.

2.1.1 Decomposition

Ammonium perchlorate (AP) has been used as a crystalline oxidizer since the late 1940s when the Jet Propulsion Laboratory and Thiokol first introduced it and started using it in rocket motors in the 1950s [18]. As a result, many papers were published between 1950 and 1970 investigating AP decomposition. Jacobs and Whitehead provided an extensive review of these studies in 1969 [19]. Research in AP decomposition fell off after 1970 as evidenced by Kishore and Prasad's review in 1979, where the majority of studies included were conducted before 1970 [20]. As diagnostics have improved, more AP decomposition studies have appeared lately as described and summarized by Brill and Budenz in 1999 and later on by Boldyrev in his review of AP thermal decomposition [21-22].

Overall, it is generally agreed that AP (NH_4ClO_4) decomposition starts with a proton transfer from the cation NH_4+ to the anion ClO_4- to form the first decomposition products, ammonia (NH_3) and perchloric acid ($HClO_4$). At temperatures below 240°C, the crystalline structure remains orthorhombic and decomposition occurs below the surface. As the temperature increases past 240°C, the crystal lattice transitions to a cubic structure and begins to melt to form a liquid layer. At this point, the decomposition primarily takes place at the surface with the adsorption and desorption of ammonia and perchloric acid. The secondary reactions taking place are complicated and still remain largely unconfirmed [23]. More than 1000 possible chemical reactions could be involved in AP decomposition if the oxidation states of all four elements, N, H, Cl, and O, are considered [21]. However, it is generally agreed that at lower temperatures, NH_3 retards the decomposition rate but accelerates it at higher temperatures, and $HClO_4$ accelerates decomposition regardless of temperature [24-28].

2.1.2 Deflagration

Like AP decomposition, the majority of AP deflagration studies were performed in the 1960s and 70s. The studies ranged from single AP crystals to pressed AP pellets with and without inhibitors [3-4,6,8-9,29-36]. Similarly, various attempts have been made to model AP combustion, including the NWC model created by Price, Boggs, and Derr which is still used today when modeling composite propellant combustion [37]. While specific reactions and reaction rates vary depending on the model, the general consensus is that AP deflagration is primarily dependent on condensed-phase kinetics

rather than physical properties [21]. As described by AP decomposition, the AP crystals experience a crystal phase transition from orthorhombic to cubic around 240°C and begin to melt as the temperature continues to increase. It is in this melt layer that exothermic reactions affecting about 70% of the AP take place, producing the final combustion products, particularly oxygen, O_2. The remaining 30% of the AP endothermically sublimes into ammonia and perchloric acid which react exothermically in a pre-mixed flame close to the surface to form the final combustion products such as O_2, NO, and N_2O [38]. As pressure increases, the primary AP deflagration mechanism begins to change producing drastically different burning rate profiles. This feature is described in detail in Section 2.3.1.

At lower pressures around 290 psi, AP ceases to deflagrate [9]. This low-pressure deflagration limit is thought to exist due to the surface temperature decreasing as the premixed flame moves away from the surface as pressure decreases [38]. The heat feedback to the surface is not enough to maintain surface pyrolysis, which is highly endothermic, since the temperature drops lower than the melting point of AP. The liquid melt layer where the primary exothermic reactions take place is no longer present, and therefore AP deflagration cannot be sustained.

2.2 AP/HTPB Composite Propellant Combustion

This section provides an overview of AP/HTPB-based solid propellant combustion and common performance and burning rate modifiers. The following sections provide a summary of existing high-pressure composite propellant studies and

proposed exponent break mechanisms found in literature, including the suggestion of an "AP barrier".

2.2.1 AP/HTPB Flame Structure

The most widely accepted theoretical illustration of AP/HTPB combustion comes from the Beckstead-Derr-Price (BDP) model first introduced in 1970 [39]. This model introduced a three-flame structure including a primary diffusion flame consisting of AP decomposition and binder decomposition products, the AP monopropellant flame, and a final diffusion flame between the AP monopropellant flame products and the binder products mixed with the primary diffusion flame products. The BDP model also explains the effects of AP particle size and pressure on the burning rate in terms of their impact on the primary diffusion flame. Figure 5 provides the theoretical picture developed as part of the BDP model [39].

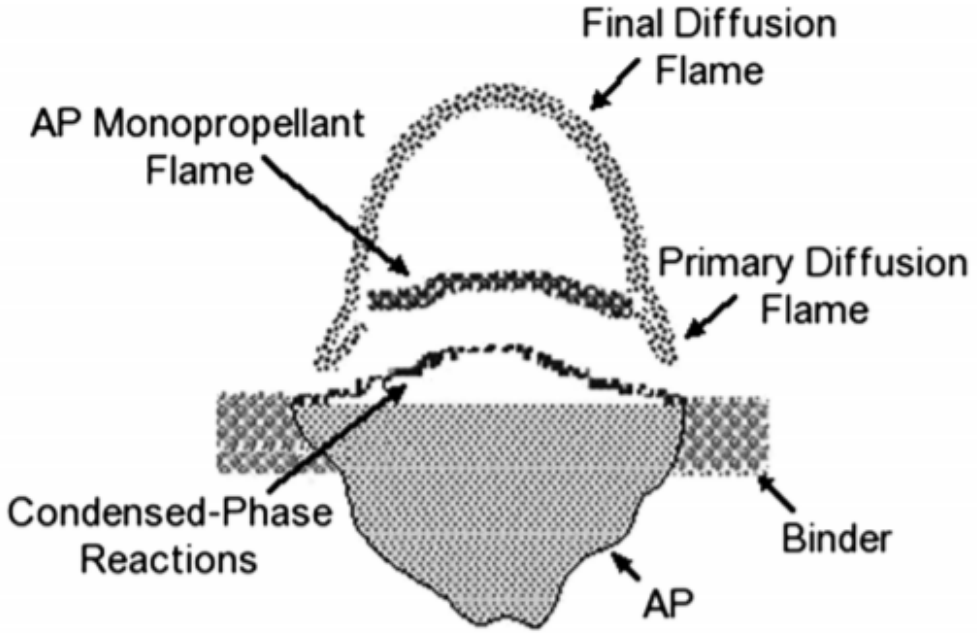

Figure 5. AP/HTPB flame structure proposed in the BDP model. Reprinted from Beckstead et al. [39]

As aforementioned, both AP particle size and pressure impact the primary diffusion flame. As pressure decreases, especially for fine AP particles, the unreacted AP decomposition gases mix with the binder pyrolysis products to form a premixed flame. In this case, the kinetic aspect of the primary diffusion flame dominates rather than the diffusion aspect [40]. Contrastingly, at higher pressures, the characteristic time for gas phase reactions decrease, so the AP decomposition products react with one another, burning as a monopropellant before reacting with the binder products [41]. Overall, at lower pressures, the kinetic rates are slow and the decomposition products are allowed to diffuse extensively above the surface [39]. At higher pressures, the kinetics dominate,

resulting in less species diffusion and the formation of premixed flames very close to the surface [39]. The effects of particle size will be elaborated on in the subsequent section.

The BDP model has served as the starting point for most subsequent AP/HTPB combustion models, with most improving on microstructure (propellant morphology – AP size distributions, packing, etc.), condensed- and gas-phase kinetics, mechanical stresses, etc. features of the original BDP model. Jackson and Beckstead recently provided reviews of the current status of these improvements [42-43].

2.2.2 Effects of AP Characteristics on Solid Propellant Burning Rates

One common method of tailoring AP-based composite propellant burning rates is altering the AP characteristics such as concentration, distribution, and average particle size. Modifying the AP concentration can either increase or decrease the burning rate as it relates directly to the adiabatic flame temperature. As the AP concentration increases, so does the adiabatic flame temperature, which has a maximum value around 89% AP at approximately 3060 K. Additionally, increasing the AP concentration provides additional sites for the AP and binder to interact, generating the primary and diffusion flames which provide heat feedback to the propellant surface. Typical AP concentrations range between 80-90%.

Contrastingly, altering the AP distribution does not necessarily increase or decrease the burning rate. Several studies found that using wide or multimodal AP produced plateau burning rates where the pressure exponent is close to or equal to zero [44-49]. The primary purpose of multimodal distributions, however, is related to

propellant manufacturing. Due to the preferable high AP concentrations (which provide higher performance), mix viscosity can become very high, making it difficult to cast void-free motors. Distributions, such as bimodal and trimodal, drastically reduce the mix viscosity while maintaining a high AP concentration due to better particle packing within the propellant. In these formulations, the effect of distribution on burning rate and combustion is primarily driven by the AP particle sizes incorporated.

It has been noted in many studies that altering the AP particle size significantly affects the burning rate and combustion of AP composite propellants, with smaller AP particle sizes yielding higher burning rates [47,50-58]. The BDP model first explained the particle size effect in terms of the primary diffusion flame. For very small particles, the propellant burns as a pre-mixed flame due to the AP decomposition products mixing with the binder pyrolysis products before reacting. Larger particles, on the other hand, burn primarily as AP monopropellants. Intermediate sizes will have a dominant diffusion flame. Figure 6 illustrates this particle size effect and denotes the relative combustion mechanism regimes. As previously mentioned, pressure also has an effect on the combustion mechanism. As a result, the burning rate curve portrayed in Fig. 6 will shift downward and to the right for lower pressures and upwards and to the left for higher pressures [41].

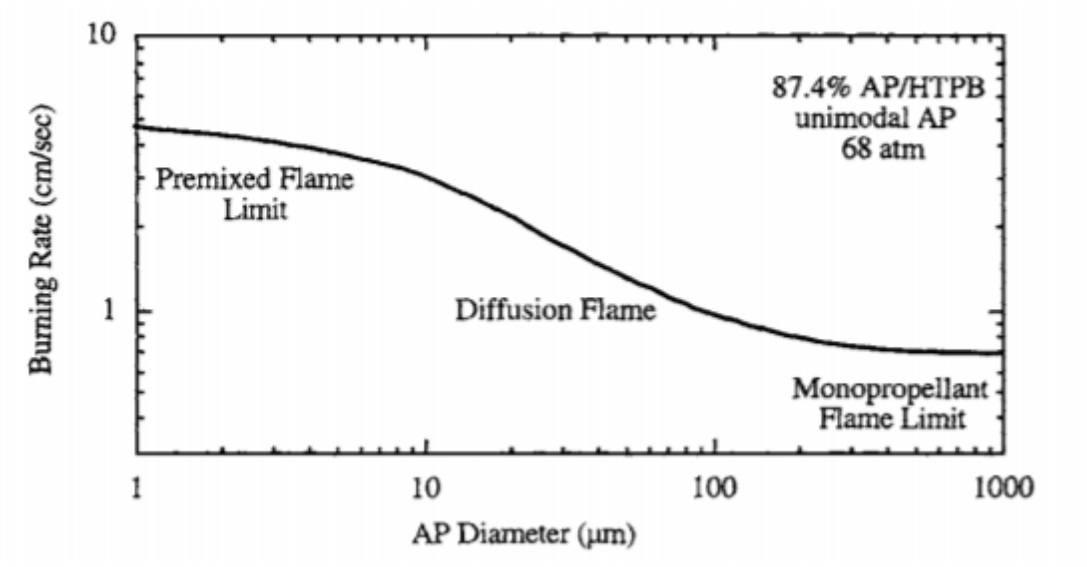

Figure 6. Particle-size dependence of AP burning rate predicted using BDP model. Reprinted from Beckstead [40].

Beckstead and Gross further expanded on this particle size effect by establishing three combustion regions: the AP monopropellant limit, the premixed limit, and the diffusion flame region [59]. As AP particle size is increased, the monopropellant limit is reached around 400 μm. Larger AP particles burn significantly slower than fine particles due to the surface heat flux coming primarily from the cooler AP monopropellant flame rather than the hotter primary and diffusion flames, which are limited by the smaller AP/binder contact surface area [60].

For finer particles, the premixed flame limit is approached around 10 μm. In this region, the AP decomposition products are allowed to completely mix with the binder pyrolysis products, forming a premixed flame that reaches the mixture's adiabatic flame temperature [60]. The premixed limit also represents the highest burning rate for a

specific formulation and pressure due to the primary flame covering the entire burning surface, thus producing the maximum surface heat flux.

Intermediate particle size combustion results from a combination of the AP monopropellant flame and premixed flame conditions. The heat flux from the diffusion flame forming close to the surface supplements the lower heat flux from the AP monopropellant flame [60]. These intermediate particle sizes form the third combustion region, the diffusion flame region. The transition from the premixed limit to this region is referred to as the premixed cutoff, which is the largest AP diameter at which an AP/HTPB mixture burns in a premixed manner [60]. Pressure heavily influences this cutoff diameter due to the rates of diffusion and gas-phase reactions. At lower pressures, the reaction rates are slow and decomposition species are allowed to diffuse extensively above the surface. However, gas-phase reaction rates are typically proportional to the pressure squared, so at higher pressures, the kinetics take place so quickly, that fewer decomposition species are allowed to diffuse. As a result, premixed flames form very close to the surface at higher pressures [60].

2.2.3 Aluminized AP/HTPB-Based Solid Propellants

Aluminum has been used as a performance booster in solid propellants for decades due to its desirable high density, high heat release during oxidation (which leads to higher theoretical flame temperatures), low cost, and relative safety. Despite the reaction product of aluminum (Al_2O_3) being in a liquid state during combustion, better combustion fluids are produced by the oxidation of aluminum, which reduces the

oxidizer vapors (H_2O and CO_2) to H_2 and CO [61]. This result allows, in combination with the high heat release during combustion, for specific impulse increases of roughly 10% and a propellant mass fraction net gain of typically 15% [61]. Combustion instabilities are also suppressed by the inclusion of aluminum. However, there are down sides to including aluminum, particularly, the agglomeration of aluminum particles at the burning surface which can retard the burning rate and never completely combust.

During combustion, aluminum typically does not vaporize, but rather tends to stick to the binder melt layer, forming agglomerations. These agglomerations can then coalesce into large, condensed particles which leave the surface and burn in the gas-phase flow field [61]. In real combustion, however, these aluminum particles never completely combust, but rather detach from the surface and only partially burn in the gas-phase flow field. Aluminum combustion is also inhibited by the oxide coatings on the particle surfaces produced during manufacturing. Extensive research has been conducted on aluminum particle agglomerations, including efforts to experimentally quantify and track aluminum agglomerations during AP composite propellant combustion [62]. Additionally, several reviews have been produced in recent years summarizing the combustion of aluminized solid propellants [61, 63-65].

2.2.4 Effects of Nanometal Catalysts in AP/HTPB-Based Solid Propellants

Nanocatalysts have been used for years to enhance propellant burning rates by altering the combustion characteristics of AP and HTPB. By changing the thermal conductivity, energy barrier of thermolysis, heat of reaction, and gas-phase reaction

mechanisms of the AP and HPTB, these nanocatalysts have the potential to increase the decomposition rates, enhance the burning rates, and increasing the combustion efficiency of AP/HTPB composite propellants [66]. Yan et al. provide an extensive review of catalytic additives and proposed catalytic mechanisms [66].

Two common nanocatalysts are metal oxides, iron oxide (Fe_2O_3) and titania (TiO_2). Nano-iron oxide is an excellent catalyst due to its high specific surface area, surface area per unit mass, and a large number of atoms and vacancies on its surface [66]. The thermal decomposition of AP has been shown to increase with the addition of nFe_2O_3 due to the iron oxide lowering the peak decomposition temperature of AP [67]. Similarly, TiO_2 also decreased the AP peak decomposition temperature due to its high specific area and was also shown to affect the frequency factor of AP decomposition [68]. Both the catalytic effects of Fe_2O_3 and TiO_2 are dependent on their morphology, with certain phases producing higher burning rate increases than others. Additionally, TiO_2 can also be used in its anatase phase to produce plateau burning rates at higher pressures.

Regardless of their morphology, particle agglomerations in the propellant can reduce the catalytic effectiveness of nanocatalysts by reducing the particle surface area. Reid et al. resolved this issue for TiO_2 by the in-situ synthesis of TiO_2 nanoparticles in a solution containing HTPB [69-72]. The in-situ method results in uniform, homogeneous, dispersion of $nTiO_2$ in HTPB, drastically reducing particle agglomeration and maximizing particle specific surface area. Compared to the traditional methods of incorporating $nTiO_2$ which can produce a 34-59% increase in burning rate depending on

the incorporation method, the in-situ TiO_2 has been shown to increase baseline AP/HTPB propellant burning rates by 101% [69-72].

2.3 High-Pressure Studies

Many strand burner facilities are capable of determining composite propellant burning rates, but most only test regularly up to about 15.5 MPa (2250 psi). Few burning rate data exist for higher pressures and almost none for pressures exceeding 34.5 MPa (5000 psi). As a result, most studies fail to capture the exponent break phenomenon. While some very-high-pressure testing has been conducted in some past efforts, most of these studies either investigated the deflagration characteristics of pure AP only or AP-based propellants with binders other than HTPB [3-15]. Almost no studies exist that evaluate the burning rates of AP/HTPB-based propellants. Table 1 provides a summary of existing high-pressure studies relevant to this proposal. This section reviews these studies in detail.

Table 1. Survey of previous high-pressure studies utilizing pure AP or AP-based composite propellants [3-15].

Study	Propellant Type	Maximum Pressure Tested
Friedman & Nugent (1955)	Pressed AP Pellets	7250 psi (~50 MPa)
Levy & Friedman (1962)	Pressed AP Pellets (asbestos wrapped)	6000 psi (~41.4 MPa)
Glaskova (1963)	Pressed AP Pellets	14,500 psi (~100 MPa)
Irwin, et al. (1963)	Pressed AP Pellets (plioband inhibited, asbestos wrapped)	23,000 psi (~158.6 MPa)
Bobolev et al. (1964)	Pressed AP Pellets (clear)	10,000 psi (~68.9 MPa)
Boggs (1970)	Single AP Crystals	6000 psi (~41.4 MPa)
Atwood et al. (1999)	Pressed AP Pellets and Single AP Crystals	51,300 psi (~354 MPa)
Petersen et al. (2019)	Pressed AP Pellets	6500 psi (~44.8 MPa)
Cole et al. (1962)	AP/Polysulfide and AP/PBAA-based composite propellants	20,000 psi (~137.9 MPa)
Cole (1966)	AP/Nitrocellulose and AP/CTPB-based composite propellants	20,000 psi (~137.9 MPa)
Glascoe & Tan (2010)	AP/HTPB-based propellants with aluminum	44,000 psi (~300 MPa)
Kanelbaum et al. (2011)	AP/HTPB-based composite propellant grains with Fe_2O_3 and silicone carbide	8500 psi (~58.6 MPa)
Atwood et al. (2013)	AP/HTPB- based composite propellants containing various AP particle sizes, μm-Al, Fe_2O_3, and Dioctyl Adipate (DOA) or Dioctyl Sebacate (DOS) plasticizers	50,000 psi (~345 MPa)

2.3.1 Pure AP

The first very-high pressure study on AP was conducted by Friedman and Nugent in 1955 who studied the effects of pressure, temperature, particle-size distribution, and catalysts on the deflagration rates of uninhibited, pressed reagent-grade (≥95% purity) AP pellets [3]. Friedman et al. found that at higher pressures beyond 2200 psi, the AP deflagration rates reached an upper deflagration limit, with rates drastically decreasing at increasing pressures. Friedman et al. later attributed this upper deflagration limit to conductive cooling [4].

Similar to Friedman's initial observations, Glaskova and Bobolev et al. both saw dramatic decreases in AP deflagration rates past 2000 psi when testing pressed AP pellets [5,7]. This dramatic change in deflagration rates at higher pressures was further characterized by Boggs in his study where he determined the deflagration rates of pure AP single crystals for pressures between 300 and 10000 psi and observed four distinct burning rate regimes as seen in Fig. 7 [8]. The first two regimes, 300-800 and 1000-2000 psi, are characterized by increasing burning rates with varying pressure exponents. Between 2000 and 4000 psi, the burning rates are negative, falling as low as 0.1 in/s. Past 4000 psi, in the fourth regime, the burning rates begin to increase again and continue to increase out to 10000 psi. In addition to determining the burning rates for all four regimes, Boggs also quenched deflagrating crystals in each pressure regime to observe the surface characteristics. At the lower pressures, frothy layers formed of decomposition gases trapped in condensed phase products were observed. As the pressure increased, this frothy layer gradually disappeared. In a later study, Atwood

repeated the same experiments with pure AP single crystals and verified the four distinct burning rate regimes [9]. More recently, Petersen et al. repeated similar studies with pressed AP pellets and observed similar burning rate regimes but with higher deflagration rates in the third and fourth regimes [10].

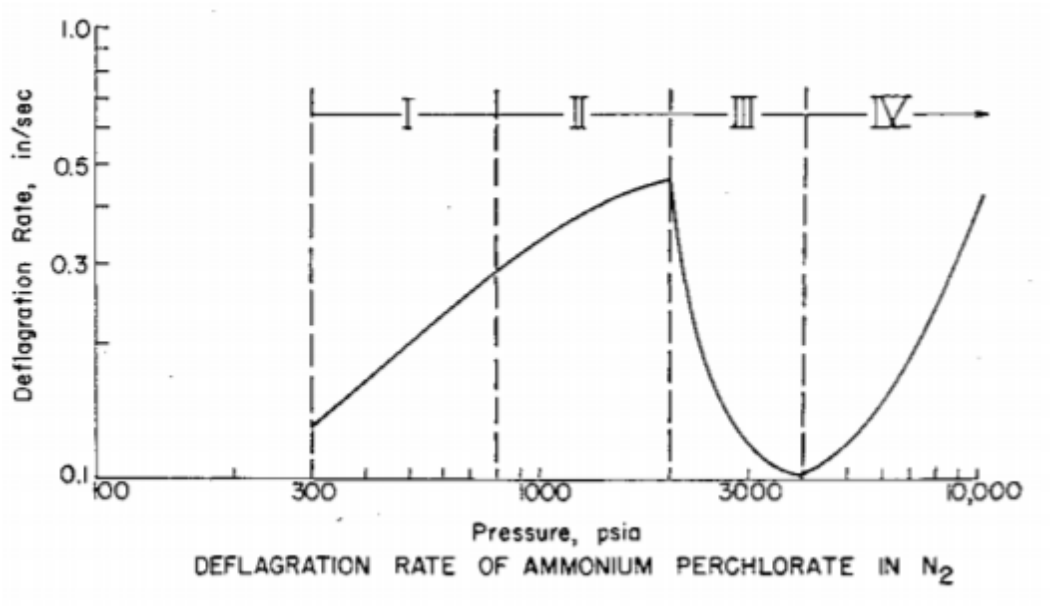

Figure 7. Four distinct deflagration rate regimes of pure AP as determined by Boggs. Reprinted from Boggs [8].

In addition to the aforementioned studies, Irwin et al. also measured the AP deflagration rate for pressures between 1000 and 20000 psi using pliobond restricting coated and asbestos-insulated pure AP cylindrical strands [6]. Unlike Boggs, they did not observe four distinct burning rate regimes, but rather one single drastic increase in slope around 5000 psi, where the pressure exponent went from 0.251 to 1.75 as seen in Fig. 8. This dramatic pressure exponent increase is indicative of the exponent break feature in AP/HTPB composite propellants.

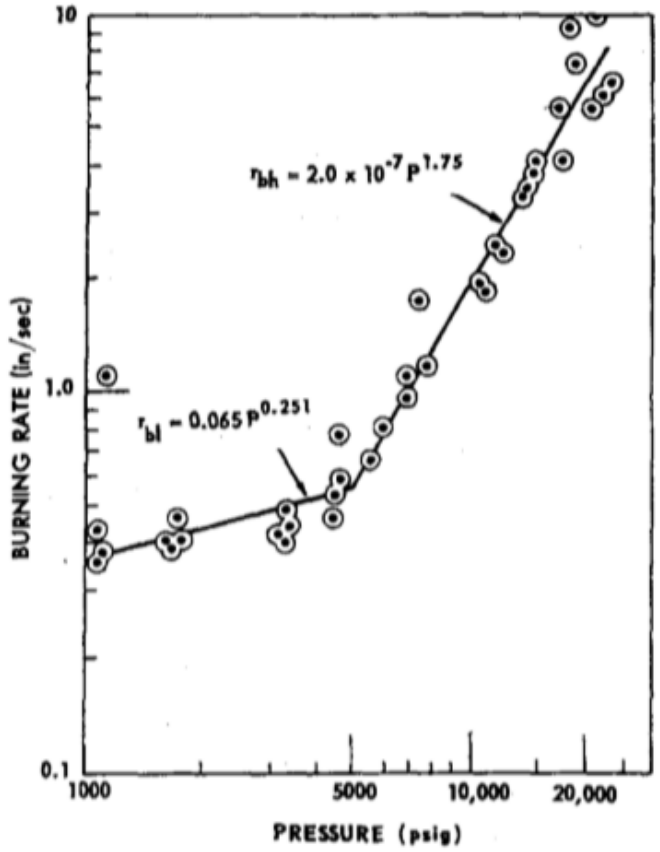

Figure 8. AP deflagration curve produced by Irwin et al. Reprinted from Irwin et al. [6].

2.3.2 AP-Based Propellants

Several studies have been conducted on AP-based propellants with non-HTPB binders. The first study was conducted by Cole et al. who tested AP/Polysulfide and AP/PBAA-based composite propellants with varying AP distributions, concentrations, and AP particle sizes out to pressures of 20,000 psi [11]. All six formulations displayed an exponent break with pressure exponents equal to or greater than one for pressures above 5000 psi. Regardless of AP distribution or concentration, the burning rates merged and became identical for pressures between 10,000 and 20,000 psi [11]. The

formulations with fine AP burned slightly higher than those with coarse AP, but only barely. From these results, Cole et al. concluded that binder type has no effect at high pressures since the burning rates merged at the higher pressures.

In a subsequent study, Cole looked at the effects of very-high pressures on CTPB (carboxyl-terminated polybutadiene)/AP and NC (nitrocellulose)/AP-based propellants [12]. He varied the AP particle size and concentration for each binder and also included catalytic additives and micron aluminum for several of the formulations. Regardless of the AP characteristics, inclusion or catalysts or aluminum, all formulations for both binders exhibited some form of exponent break in the form of a pressure exponent transition regime. For both the CTPB and NC/AP-based formulations, he again observed a decrease in AP particle size effect at the higher pressures. However, instead of appearing to merge at the high pressures, the burning rates formed an envelope of sorts, with linear, parallel burning rates even out to 20,000 psi.

With regards to varying AP concentration, the burning rates for neither binder merged at higher pressures. Similar to the AP particle sizes, the effect of AP concentration diminished at higher pressures regardless of binder. The burning rates for the NC/AP formulations remained linear and parallel, with the higher AP concentration burning slightly faster. The CTPB/AP burning rates did not remain completely parallel and appeared to begin to converge around 20,000 psi [12].

The effects of aluminum on the high-pressure burning rate behavior varied depending on the binder. For the CTPB/AP formulations, the burning rates merged as pressure increased. Contrastingly, the NC/AP burning rates crossed around 8000 psi, but

did not converge. The inclusion of aluminum in the NC/AP propellants also caused the pressure exponent at higher pressures to decrease [12]. The catalyst effects were negated at the higher pressures regardless of binder.

2.3.3 AP/HTPB Propellants

The few existing very-high-pressure AP/HTPB-based propellant studies focus on application-specific formulations and investigate the effect of multiple variables simultaneously including metal content; plasticizer and binder types; catalysts; and oxidizer particle size [13-15]. Glascoe and Tan do not provide the formulation specifics other than mentioning that two of the formulations contain aluminum [13]. The third formulation is a proprietary mixture that they were contracted to test out to very-high pressures. Both the aluminized formulations exhibited an exponent break around 4000 psi, whereas the third formulation did not exhibit a slope break but rather maintained a constant pressure exponent out to 43,000 psi. Kanelbaum et al. tested AP/HPTB-composite propellant grains containing Fe_2O_3 and silicon carbide [14]. They also saw a slope change around 4200 psi, where the pressure exponent went from 0.55 to 0.845.

In Atwood et al.'s study investigating the burning rates of AP/HTPB-based composite propellant formulations containing various additives, AP particle sizes, distributions, and plasticizers, the exponent break feature is apparent regardless of formulation details [15]. Similar to Cole's study with CTPB/AP and NC/AP-based propellants, any catalytic effect was lost at the high pressures, as the burning rates converged around 14,000 psi [12]. Unlike Cole's study, however, where the AP particle

size still had a minimized effect on the burning rates at high pressures, any particle size effects were negated after the pressure exponent break. It is difficult to tell the importance, if any, of altering these formulation variables since the Atwood et al. study was more application-specific and altered multiple values at once.

Although several overarching trends were observed, the studies ultimately resulted in confounding variables and did not resolve the need for a fundamental, systematic study of the AP/HTPB-combustion mechanism at very-high pressures.

2.4 AP Barrier

A common theme in the aforementioned studies is the apparent dominating influence of AP decomposition at high pressures. This dominance has led to the introduction and hypothesis of an "AP barrier", where the AP deflagration rate serves as a lower burning rate limit at both low and high pressures for all AP-containing formulations [11-12,15-16]. Atwood et al. also noted an apparent pressure exponent limit imposed by the pure AP deflagration rate for AP/HTPB-based propellants with varying oxidizer and additive characteristics [15]. However, since the formulations in Atwood's study included multiple variables at once, it is difficult to determine if the observed pressure exponent limit is formulation-specific or an innate feature of AP/HTPB-based propellants.

2.5 Pressure Exponent Break Mechanisms

Although few experimental data exist at very-high pressures, several mechanisms have nonetheless been proposed to explain this exponent break feature. The most prominent of these are AP-driven. Irwin, Atwood, and Glick et al. all suggest that above the characteristic pressure, P*, the contribution of AP to the combustion process dominates, thus the burning rates are controlled by the AP decomposition flame [6,15,17,73]. Irwin et al. proposed that the increase in burning rates at very-high pressures is due to an increased AP surface area as a result of cracks or pores forming and/or expanding in the AP crystals due to thermal stress induced by the steep temperature gradient n the solid phase at these pressures [6,73]. They developed a geometric model based on this theory which agreed well with their high-pressure AP strand burning rates [73]. As part of a study on high-pressure burning rates, Cole later investigated this theory by thermally shocking large AP particles using liquid nitrogen and toluene baths [12]. The thermally shocked AP particles exhibited multiple fine-AP fragments, experimentally confirming that steep temperature gradients can produce large enough stresses to fracture AP particles and that AP particles in solid composite propellants could potentially crack given suitable deflagration-wave temperature gradients [12].

In the same high-pressure study, Cole proposed the concept of "series-burning" to qualitatively explain the exponent break phenomenon [12]. The "series-burning" refers to the AP particles burning significantly faster than the binder in a composite propellant, leaving small craters or holes in the surrounding binder. As a result, this thin

layer of binder must react before additional AP particles are exposed and begin to burn, hence the “series-burning”. Additionally, the binder regression rate becomes the burning rate limiter.

The remaining exponent break models and theories in the literature are those proposed by Glick and Hermance [17, 75-76]. Glick showed that the granular diffusion flame model can be used to qualitatively describe the exponent break theory by incorporating experimentally determined burning rates and pressures [17]. Hermance proposed that the pressure exponent increase is a result of the onset of turbulence in the previously laminar fuel-oxidant flame rather than the AP decomposition flame [75-76]. Although each explanation holds merit, further research is required to determine the fundamental mechanism driving the exponent break and resulting characteristic pressure.

CHAPTER III

EXPERIMENTAL METHODOLOGY

3.1 Sample Preparation and Testing

In this study, a total of sixteen composite propellant formulations were mixed and tested out to 10,000 psi. Seven of these formulations were baselines (AP/HTPB only), two were aluminized, and the remaining seven contained various metal additives. In each formulation, ammonium perchlorate (AP) was used as the crystalline oxidizer; R45-M hydroxyl-terminated polybutadiene (HTPB), the fuel-binder; and isophorone diisocyantate (IPDI) as the curative. The baseline formulations contained a variety of average AP particle sizes ranging from 46 to 210 μm, concentrations (80 and 85%), and distributions (monomodal, bimodal, and trimodal). All of the AP, aside from the 138.9-μm which was off-the-shelf 145-μm AP from American Pacific (AMPAC), was sieved in a Resodyn Laboratory Resonant Acoustic Mixer (LabRAM) using a series of sieves. The resulting average particle sizes and distributions were measured with a Beckman Coulter LS 13 320 XR Laser Diffraction Particle Size Analyzer and are shown in Fig. 9. The respective CDF curves are located in the Supplemental Material.

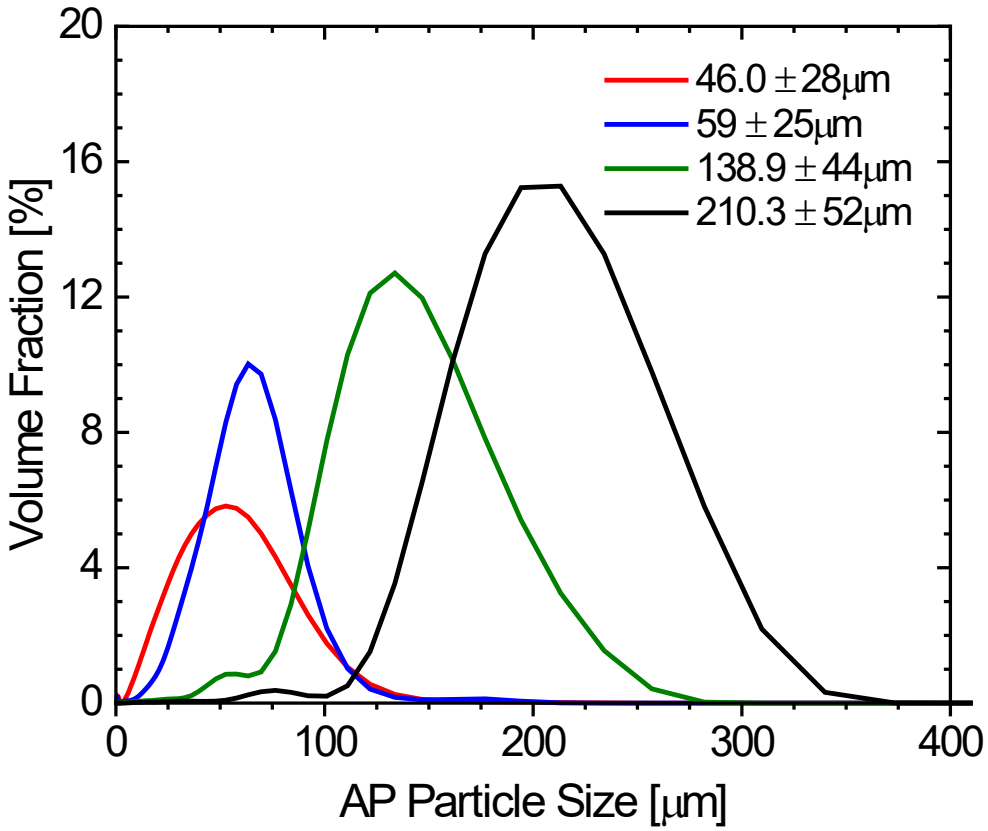

Figure 9. Particle size distributions for AP used in this study.

Micron aluminum, 400 Mesh, from Firefox Enterprises LLC was incorporated into the aluminized formulations and either Mach I nano-iron oxide (Fe_2O_3), Mach I nano-titania (TiO_2), or *in-situ* titania, to the propellants containing additives. Both of the MACH I additives are nano-sized at 15-20 nm and 3-5 nm for the titania and iron oxide, respectively. The spherical titania particles have a surface area of 96-m^2/g and the amorphous iron oxide particles, 269 m^2/g. The *in-situ* titania particles were produced by Helicon Chemical Company using techniques described by Reid et al. [71]. Unlike the MACH I additives which are dry powders, the *in-situ* titania particles are synthesized directly in the HTPB binder at a nominal particle size of 20 nm. This unique synthesis

method reduces particle agglomerations and improves particle dispersion, both of which increase its catalytic efficiency. As a result, these particles have been shown to significantly increase AP/HTPB-based propellant burning rates [71-72,77-79]. Table 2 provides the complete propellant composition details.

Table 2. Propellant formulation details for this study.

Formulation Name	Solids Loading* (mass %)	AP Distribution	AP Particle Size (μm)	Additive	Additive Mass %
1	80	Monomodal	46.0 ± 28	-	-
2	80	Monomodal	59.0 ± 25	-	-
3	80	Monomodal	138.9 ± 44	-	-
4	80	Monomodal	210.3 ± 52	-	-
5	85	Monomodal	210.3 ± 52	-	-
6	85	Bimodal	210/20 (70:30)	-	-
7	85	Trimodal	400/210/20 (4:2:1)	-	-
8	83	Monomodal	210.3 ± 52	Aluminum	8
9	83	Monomodal	210.3 ± 52	Aluminum	16
10	80	Monomodal	46.0 ± 28	MACH I TiO_2	1
11	80	Monomodal	46.0 ± 28	MACH I Fe_2O_3	1
12	80	Monomodal	210.3 ± 52	MACH I TiO_2	1
13	80	Monomodal	210.3 ± 52	MACH I Fe_2O_3	1
14	85	Monomodal	210.3 ± 52	MACH I Fe_2O_3	1
15	85	Trimodal	400/210/20 (4:2:1)	MACH I Fe_2O_3	1
16	80	Monomodal	138.9 ± 44	*In-situ* TiO_2	0.50

*Solids loading includes both the AP and additive mass percentages. Remaining mass is HTPB and IPDI with a cure ratio of 10.44:1.

The propellant samples were produced using techniques developed by Stephens et al. [80] where each ingredient is hand-mixed together with intermediate vacuuming. The final propellant mixture is extruded into Teflon tubing and cut into 1-in-long and

0.1875-in-diameter samples. These extruded samples are then placed in an oven to cure at 63°C for one week. Prior to testing, the cured propellant samples are removed from the Teflon tubing and inhibited with HTPB to ensure linear burns. The ends of each propellant sample are also removed to ensure a homogeneous propellant throughout. To verify the densities, the mass and length of each sample are also measured before inhibiting.

A minimum of ten samples were burned for each formulation between pressures of 1000 and 10000 psi in two, constant-volume pressure vessels. Ignition is achieved by running a current across a nichrome wire attached to two metal leads on the sample holder. Pressures up to 5000 psi are tested in the high-pressure facility described by Carro et al. and Kreitz et al. [81-82]. Higher pressures are tested in the very-high pressure strand burner facility developed and characterized at Texas A&M University as described by Dillier et al. [83]. Both vessels are pressurized using inert nitrogen gas, with pressures above 5000 psi achieved using an air-supplied Haskel AG-75 gas booster. Figure 10 shows each vessel along with a propellant sample holder.

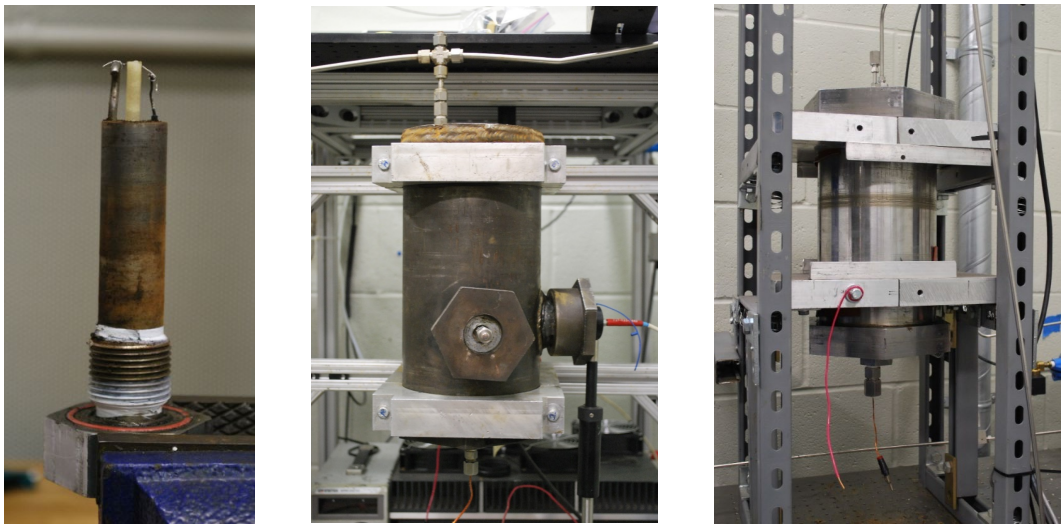

Figure 10. Left: Propellant sample holder. Center: High-pressure strand burner used to test up to 5000 psi. Right: Very-high pressure strand burner used to test up to 10000 psi.

3.2 Data Analysis

The burning rate is experimentally determined using the initial sample length and burn time as indicated by the clear inflection points from the measured pressure trace indicating the start and end of combustion. An example pressure and light trace for the high-pressure facility is shown in Fig. 11. The light trace is only used to verify the beginning and end of combustion. As seen in Fig. 11, the pressure increases during combustion. This increase ranges from approximately 9% of the initial pressure at low pressures and 5% of the initial pressure at very-high pressures. The test pressure, therefore, is taken as the average of the initial and final pressures during combustion. Although the very-high pressure strand burner does not have optical ports and therefore no light trace is recorded during combustion, the pressure traces are similar to those

produced using the high-pressure facility as proven by Dillier et al [83]. The characteristic pressure, P*, was taken as the numerically-solved intersection point between the burning rate curves above and below the exponent break as seen in Eq. (5) and Figure 12. A_1 and n_1 and a_2 and n_2 the experimentally determined burning rate coefficient and pressure exponent for the burning rate curve below P* and above P*, respectively.

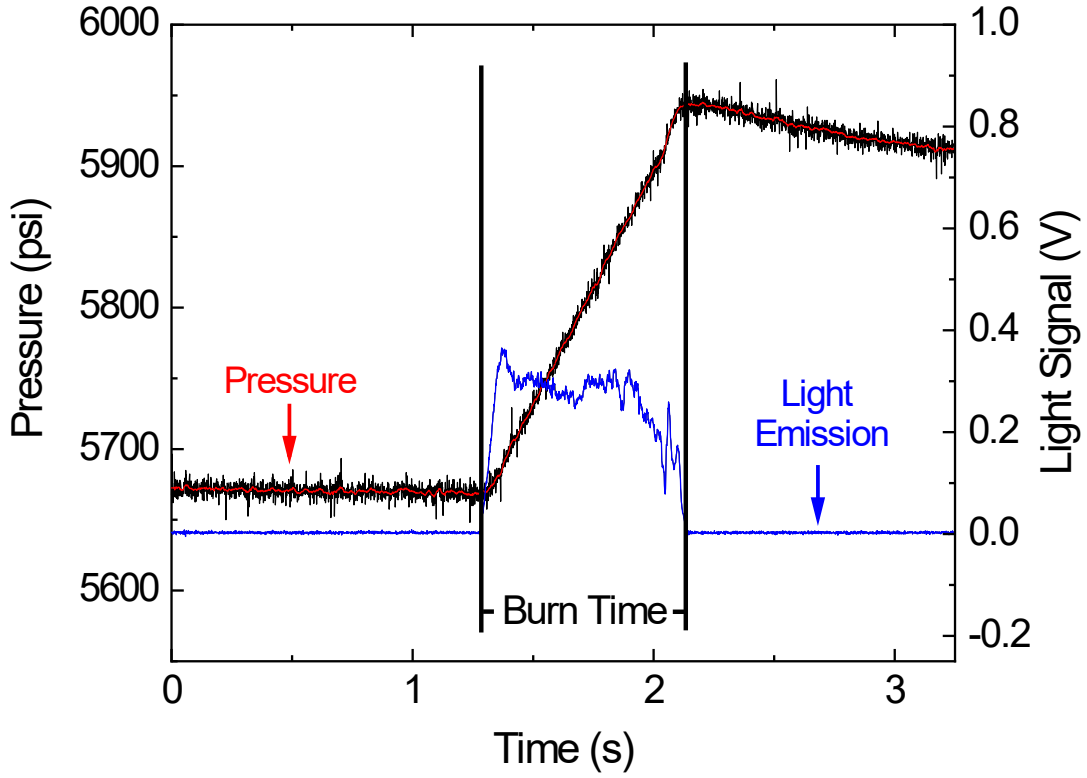

Figure 11. Example pressure and light trace used to determine the burn time.

$$P^* = \left(\frac{a_1}{a_2}\right)^{\left(\frac{1}{n_2 - n_1}\right)} \tag{5}$$

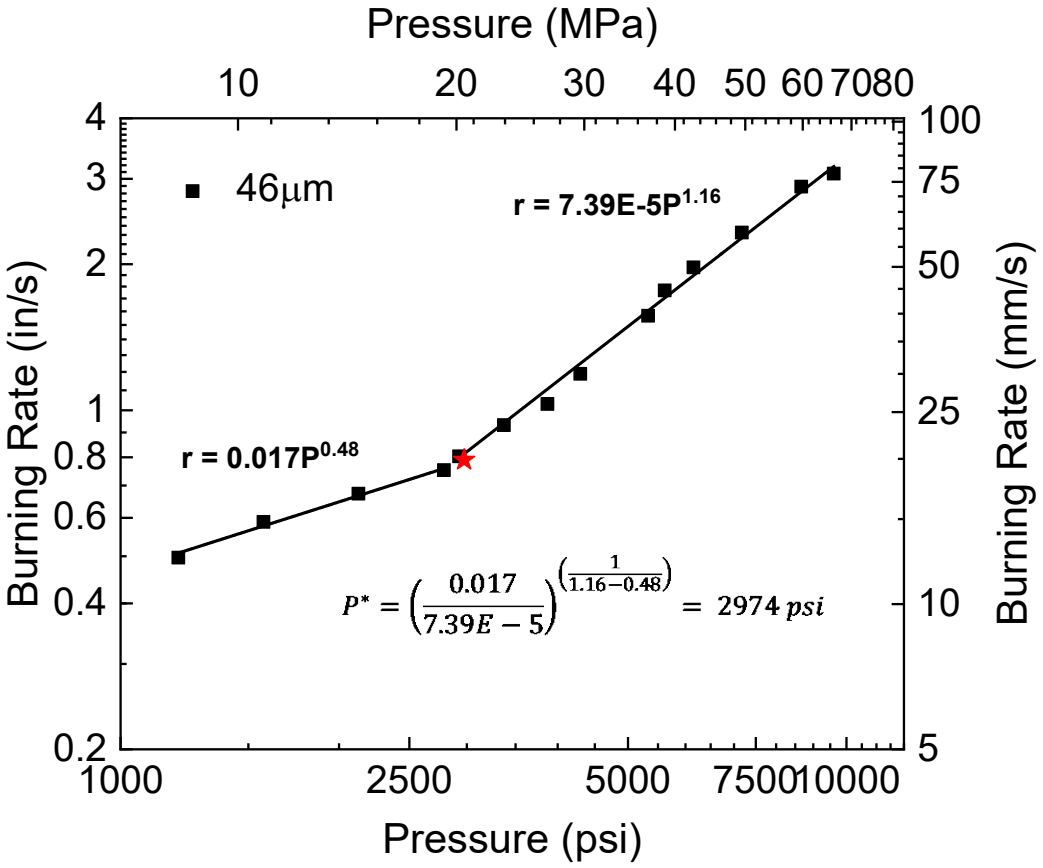

Figure 12. Example of P* calculation. P* is indicated by the red star on the plot.

3.3 Uncertainty

The uncertainty in this study is primarily related to the experimental burning rate results. Demonstrative 11.5 % uncertainty bars are included for the lowest and highest pressures tested on all of the burning rate result plots in this study, representing the maximum data scatter. This uncertainty is principally due to natural combustion fluctuations and measurement precision, both of which are common with composite propellant testing. The tolerances in sample mass, length, and pressure measurements

were ± 0.01 g, ± 0.0005 in, and 0.15% of the test pressure, respectively. The largest source of and variation in uncertainty is in defining the burn time, which was determined from the measured pressure trace. While the propellant burn ends with a distinct peak in the pressure trace, the beginning is more gradual, producing a slight curve, or transient portion in the pressure trace. The maximum uncertainty in the burn time, therefore, is taken as this transient amount and ranges from approximately ±0.25 to ±0.06 seconds at the lowest and highest pressures, respectively. The resulting overall burning rate uncertainty, including uncertainty due to measurement precision, burning rate analysis, and propellant variation, ranged from 1.6-14.5%.

The burning rates at the lowest and highest pressures have the highest uncertainties. At lower pressures, the propellant is more sensitive to combustion fluctuations since the flame has a greater standoff distance. Additionally, it takes longer for the propellant to fully ignite at lower pressures, thus increasing the initial transient portion of the pressure trace. Contrastingly, although the propellant fully ignites quickly at higher pressures, reducing the burn time uncertainty, the total burn time is extremely short, typically 0.5 seconds or less, resulting in a mathematically higher overall burning rate uncertainty. The average scatter in the data presented herein is lower, however, ranging from 0.001-11.5%, with an average of 2.92%. The scatter is lower than the uncertainty because the intersection between the linear slope of the pressure trace and the initial pressure is used as the ignition point to calculate the ideal burning rates.

CHAPTER IV

HIGH-PRESSURE BURNING RATES

4.1 Baseline Formulations with Varying AP Characteristics

The fitted burning rate trends in the form of Eqn. 1 and characteristic pressure for every formulation tested herein are provided in Table 3. The burning rate results for formulations one through four containing various AP particle sizes ranging from 46 to 210.3 μm are plotted in Fig. 13. As previously mentioned, all four of these formulations, regardless of AP particle size, displayed an exponent break. The formulations with the smallest particle sizes, 46 and 59 μm, showed higher burning rates than either the 138.9- or 210.3-μm batches at both the lower and higher pressures. This result was expected since it is commonly known that finer AP particles burn faster than larger particles due to their increased surface area. While the 59-μm formulation appears to burn faster than the 46-μm batch, the burning rates are actually within scatter of each other. This is not uncharacteristic since the average particle sizes are very close as opposed to the 138.9- and 210.3-μm batches, which have vastly different average particle sizes and subsequently significantly different burning rates.

Table 3. Burning rate characteristics for the propellant formulations used in this study.

Formulation Name	Characteristic Pressure, P* (psi)	Below P*			Above P*		
		Burning Rate at 1000 psi (in/s)	Burning Rate Coefficients		Burning Rate at 10000 psi (in/s)	Burning Rate Coefficients	
			a	n		a	n
1	2974	0.47	0.017	0.48	3.23	7.39×10^{-5}	1.16
2	3056	0.49	0.022	0.45	2.93	1.40×10^{-4}	1.08
3	4061	0.43	0.050	0.31	2.56	2.34×10^{-6}	1.51
4	3676	0.30	0.010	0.49	2.20	7.29×10^{-6}	1.37
5	3852	0.33	0.003	0.68	2.47	6.19×10^{-5}	1.15
6	5415	0.36	0.004	0.65	2.49	7.52×10^{-6}	1.38
7	3415	0.22	0.001	0.78	2.48	8.23×10^{-6}	1.37
8	4170	0.31	0.008	0.53	2.93	4.65×10^{-7}	1.70
9	3542	0.27	0.005	0.58	2.42	6.67×10^{-6}	1.39
10	-	0.72	0.014	0.57	2.67	0.014	0.57
11	4643	0.71	0.042	0.41	2.65	7.30×10^{-4}	0.89
12	5517	0.49	0.011	0.55	2.38	1.25×10^{-4}	1.07
13	4883	0.55	0.065	0.31	2.40	8.70×10^{-6}	1.36
14	4477	0.53	0.027	0.43	2.49	7.51×10^{-5}	1.13
15	4288	0.53	0.047	0.35	2.25	8.16×10^{-5}	1.11
16	-	0.62	0.007	0.65	2.79	0.007	0.65

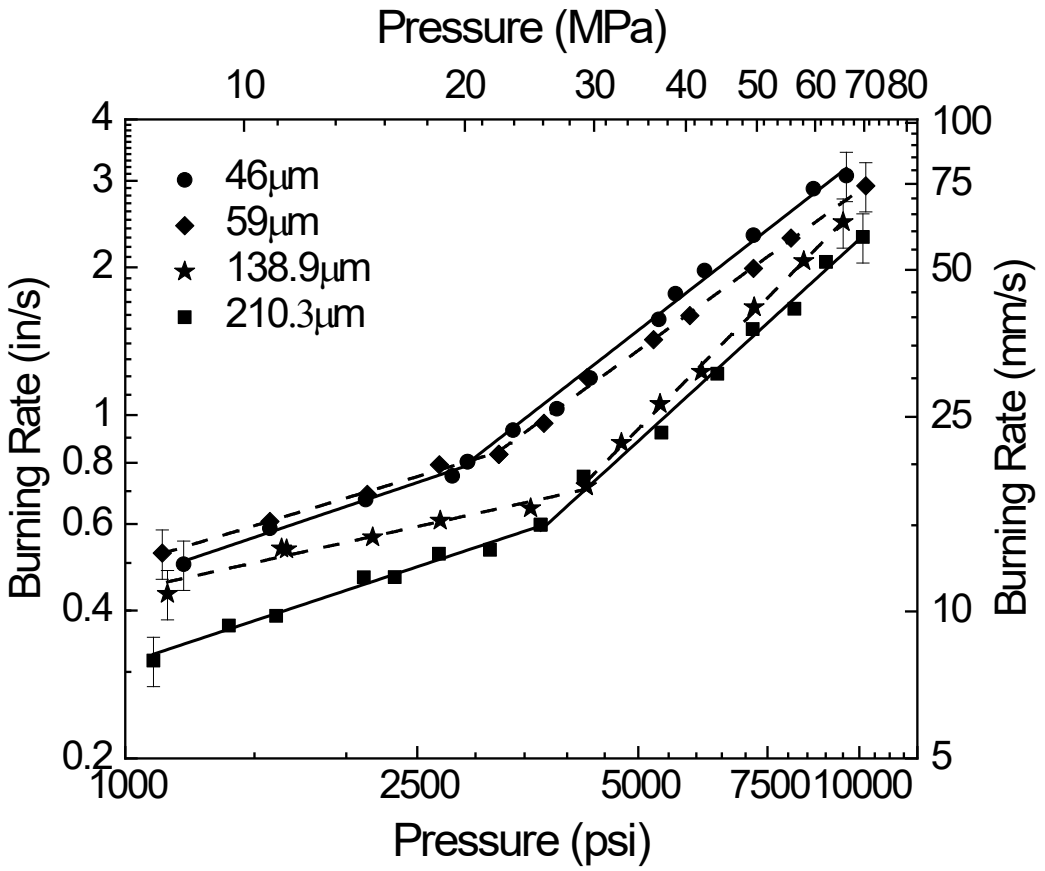

Figure 13. Burning rate results for baseline formulations with varying average AP particle sizes and 80% solids loading.

In terms of pressure exponents, the batches with 46-, 59-, and 210.3-μm AP all have similar pressure exponents ranging from 0.45-0.49 at the low pressures below their respective characteristic pressures, P*. Formulation three with 138.- μm AP however, has a noticeably lower pressure exponent at 0.31 below the exponent break as seen in Table 3 and Fig. 13. This difference could be attributed to the AP particle size distribution since it is slightly skewed towards the finer AP as seen in Fig. 9. While it does not impact the overarching results of the current study, it does advocate for the

testing of additional particle sizes and distributions to fully characterize the exponent break feature.

The burning rates, regardless of average AP particle size, remain relatively parallel at the higher pressures above the exponent breaks. The pressure exponents for the 46- and 59-μm batches are similar at 1.16 and 1.08, respectively; while the pressure exponents for the larger AP particle size batches are slightly higher at 1.51 and 1.37 for the 138.9- and 210.3-μm batches, respectively. Further testing of additional particle sizes is necessary to determine if or how the average particle size affects the pressure exponent above the characteristic pressure, P*. Regardless, it is evident that the average AP particle size affects the exponent break in terms of the characteristic pressure, P*, where it occurs. As seen in Fig. 13, both of the smaller AP particle sizes, 46 and 59 μm, exhibit lower characteristic pressures at 2974 and 3056 psi, respectively, compared to the formulations with 138.9- and 210.3-μm AP at 4061 and 3676 psi, respectively.

Figure 14 displays the burning rate results for the three formulations (5-7) with varying AP distributions. All three formulations show an exponent break, with the characteristic pressure appearing to increase with burning rate. As expected based on the AP particle sizes in each formulation, the bimodal formulation has the highest burning rate below the exponent break due to part of the 210.3-μm AP being replaced with finer 20-μm AP; and the trimodal, the lowest, due to the 400-μm AP. This effect is negated, however, above the exponent break as the burning rates for all three formulations begin to converge around 7500 psi. Unlike the AP particle size, the AP distribution does not have a clear effect on the exponent break feature. The characteristic pressure appears to

increase with burning rate from 3415 to 3852 and finally to 5415 psi for the trimodal, monomodal, and bimodal formulations, respectively. Additionally, the pressure exponent above the characteristic pressure is significantly lower for the monomodal batch at 1.15 than the bimodal or trimodal, which have pressure exponents of 1.38 and 1.37, respectively.

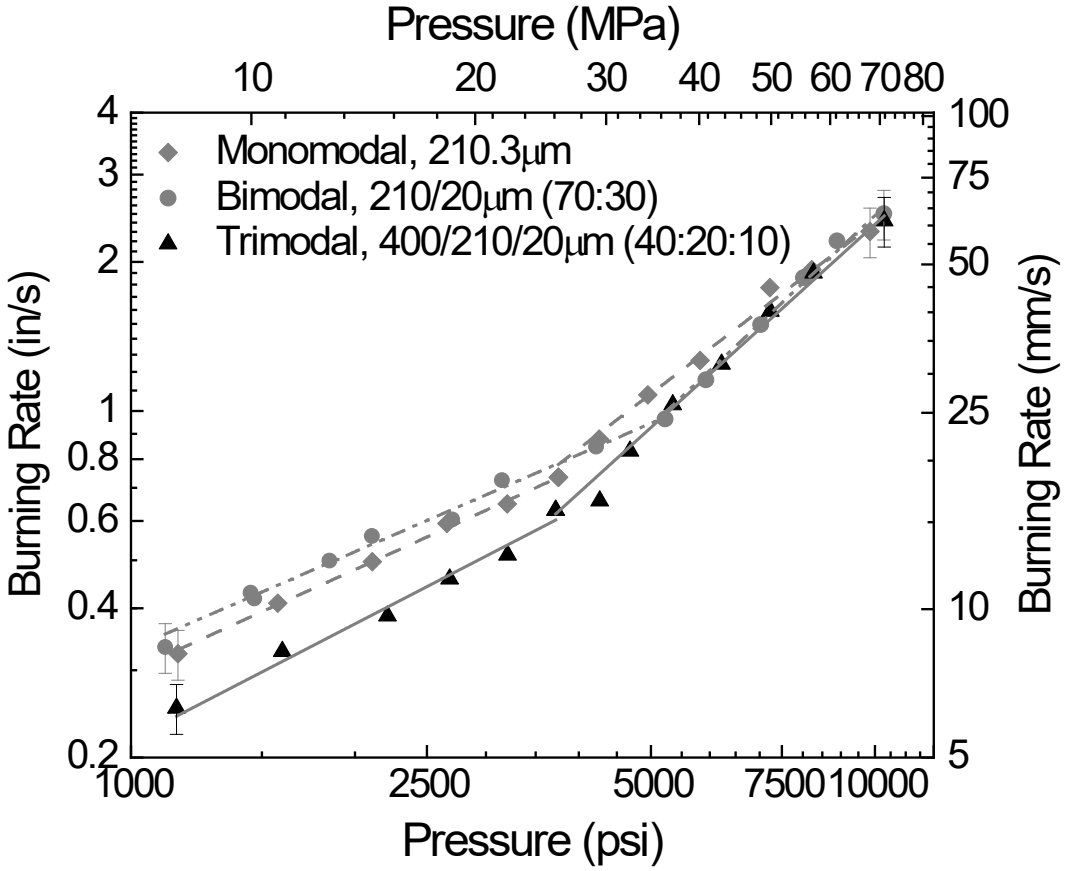

Figure 14. Burning rate results for baseline formulations with varying AP distributions and 85% solids loading.

As seen in Fig. 15, the burning rate results for formulations 4 and 5 are re-plotted together to assess the effect of AP concentration on the exponent break feature. The

increase in AP concentration produces an increase in burning rate at both the low- and high-pressures, with the burning rates eventually converging around 10000 psi. While the 5%-increase in AP concentration does not significantly affect the characteristic pressure, it does influence the pressure exponent, both below and above the characteristic pressure, P*. The increase in AP concentration increases the pressure exponent from 0.49 to 0.68 below P* and decreases it from 1.37 to 1.15, producing a more gradual slope change.

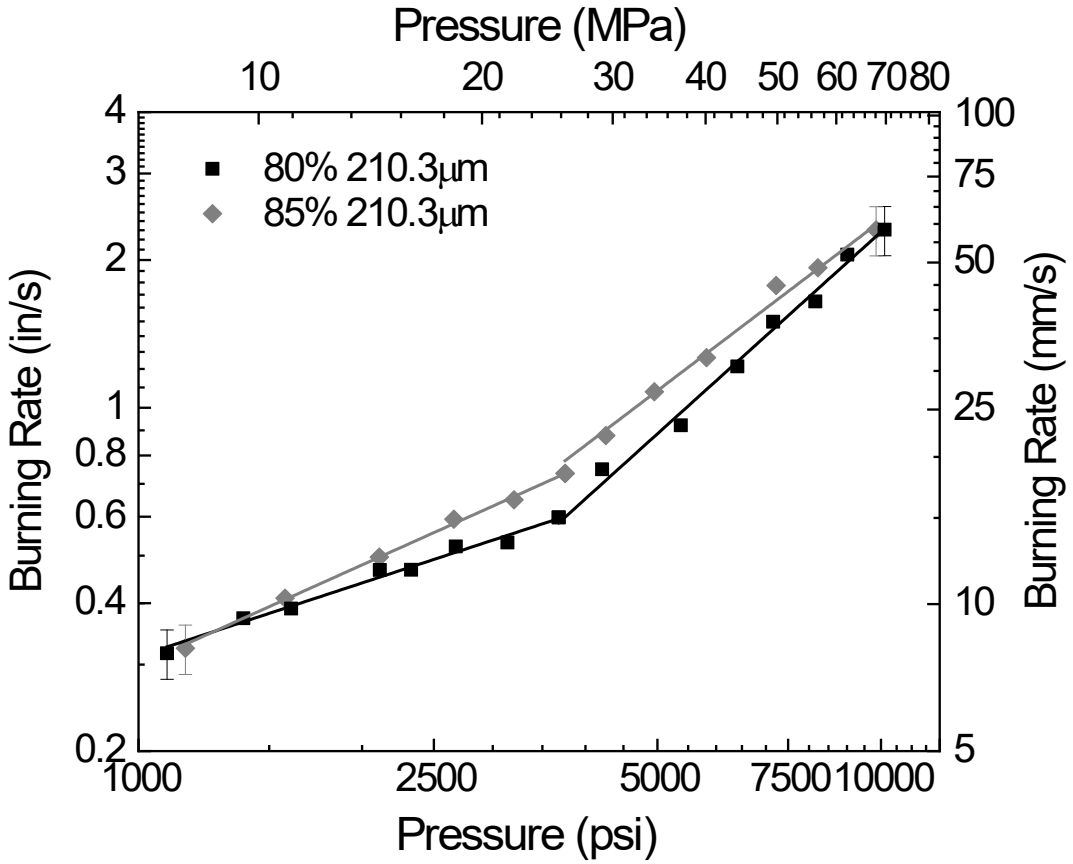

Figure 15. Burning rate results for baseline formulations containing different AP concentrations.

To further evaluate both the AP-concentration and particle-size burning rates further, the results were compared to a recent correlation paper from the Petersen Research Group as seen in Figs. 16-17 [84]. While the correlation created by Thomas et al. agrees relatively well with the 210.3-µm formulation and the burning rate magnitude for the 138.9-µm formulation, it over-predicts the 46- and 59-µm burning rate results as well as the pressure exponent for the 138.9-µm batch. The discrepancies for the 59- and 138.9-µm formulations can most likely be attributed to the differences in AP distribution between those used herein and the batches used to create the correlation since it only accounts for average particle size and concentration. In addition to the average particle size, it is well-known that the AP particle size distribution can significantly affect the propellant burning rates [84]. The discrepancy between the 46-µm formulation and the correlation, however, indicates a potential issue with the batch since the correlation agrees well with other fine-AP batches at similar sizes and distributions [84]. Further analysis on the data and propellant samples is necessary to evaluate this difference.

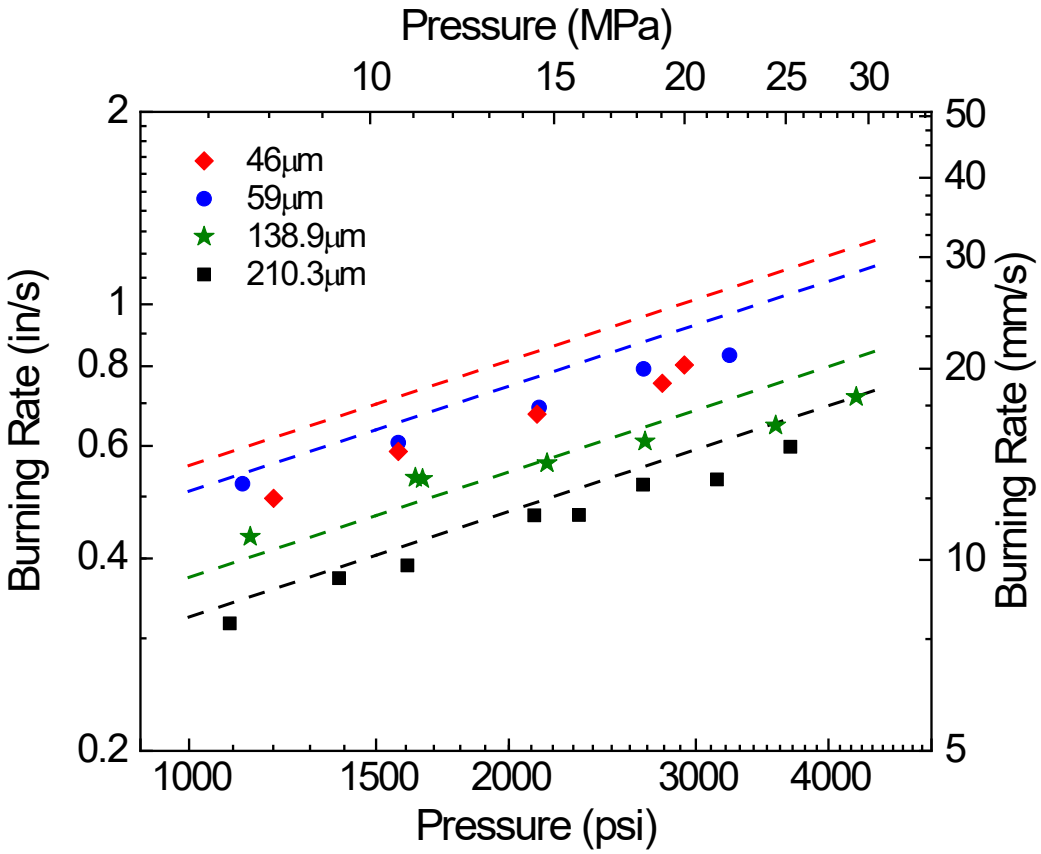

Figure 16. Burning rates for formulations containing varying AP particle sizes compared to burning rates predicted by the Thomas et al. correlation [84].

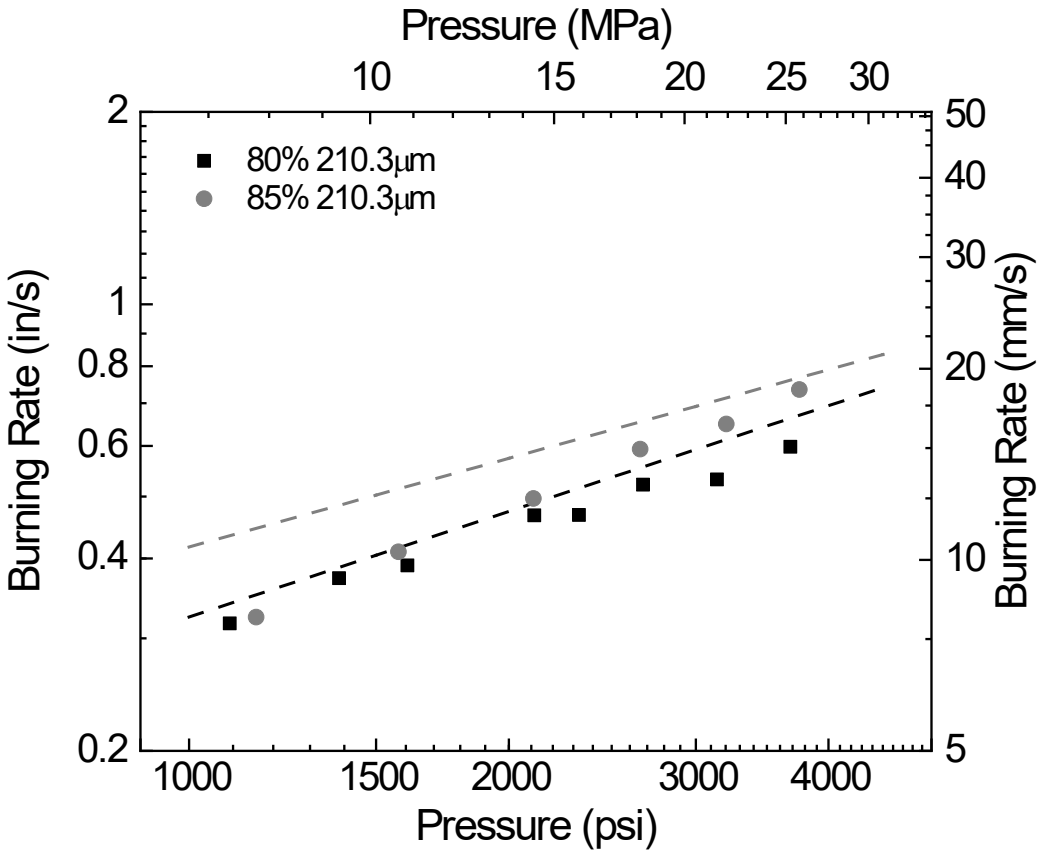

Figure 17. Burning rates for formulations containing varying AP concentrations compared to burning rates predicted by the Thomas et al. correlation [84].

As seen in Fig. 17, the Thomas et al. correlation overpredicts the burning rates and underpredicts the pressure exponent for the 85%-solids loading formulation. This discrepancy is not unexpected as the correlation overpredicts the higher AP concentration-formulations and underpredicts the pressure exponents for the data presented in Thomas et al. [84]. Regardless, the correlation does a good job predicting low-pressure burning rates with varying AP sizes and concentrations that are in relative agreement with experimental results. Figure 18 provides a scatter plot of correlation

burning rate predictions for the data in the current study as well as data from Thomas et al., King, and Foster et al. [47,50,84]. As seen in Fig. 18, the correlation accurately predicts the majority of the burning rates within ±10%. The high-pressure burning rates were not compared to the correlation since it is limited to pressures below the exponent break feature.

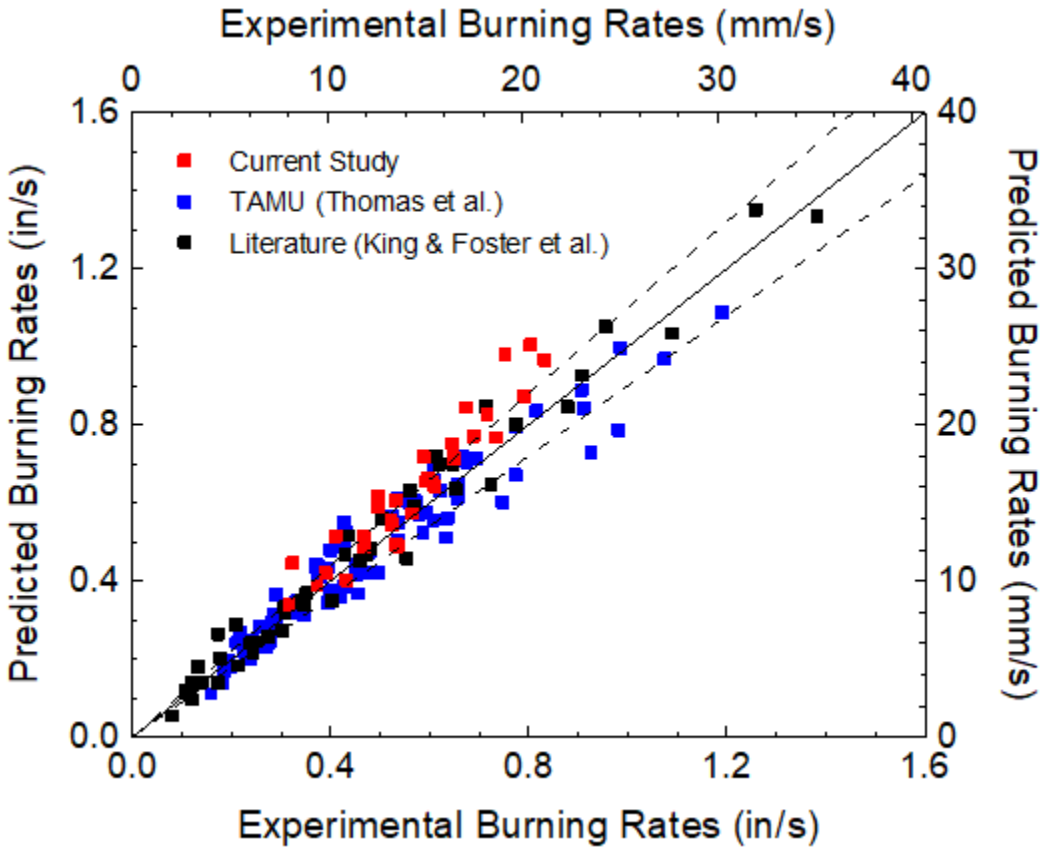

Figure 18. Scatter plot of correlation burning rate predictions for data from the current study, Thomas et al. [84], King [50], and Foster et al. [47].

4.2 Aluminized Formulations

Figure 19 provides the burning rate results for the two formulations containing 400-mesh (24 µm) micron-sized aluminum. As with the previous formulations, both aluminized propellants exhibited an exponent break. The aluminum concentration appears to affect both the characteristic pressure and pressure exponent above P*. Increasing the aluminum concentration from 8% to 16% decreases the characteristic pressure from 4170 psi to 3542 psi and the pressure exponent from 1.70 to 1.39. The aluminum concentration has little to no effect on the pressure exponent below P*, as the pressure exponents for the 8% and 16% aluminized formulations are extremely close at 0.53 and 0.58, respectively.

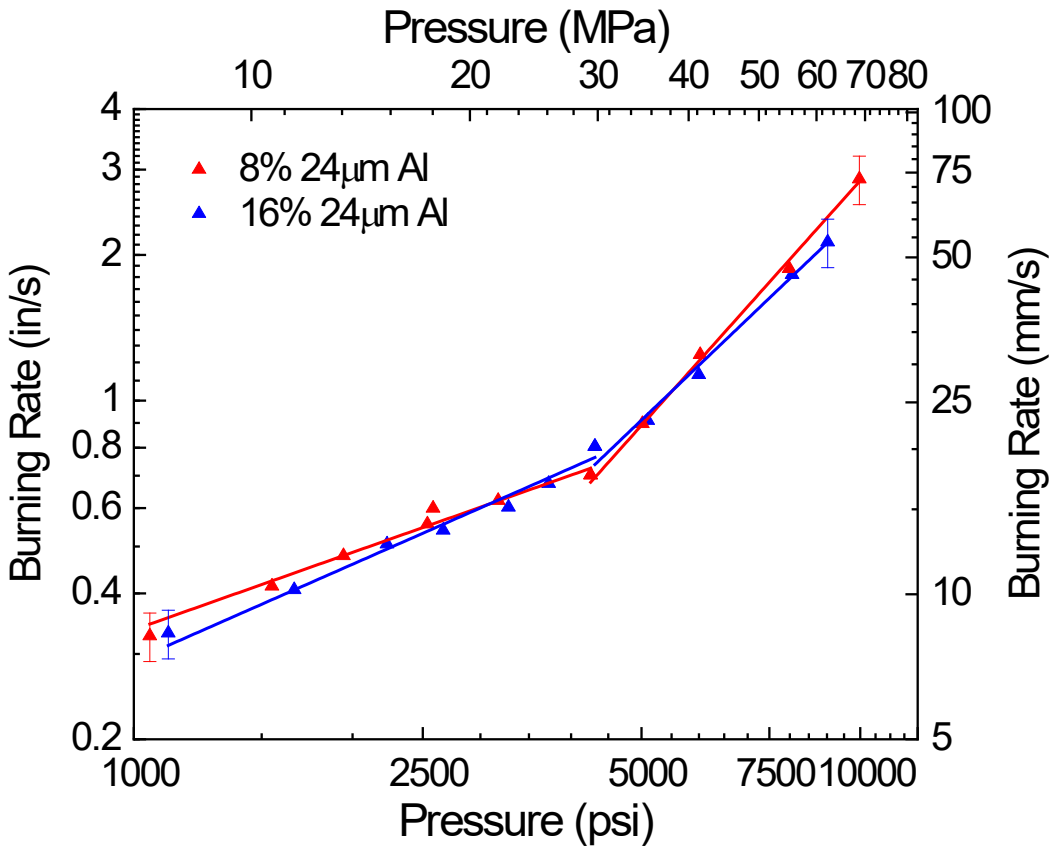

Figure 19. Burning rate results for 8% and 16%-wt aluminized formulations.

4.3 Catalytic Additive Formulations

To evaluate the effects of additives, particularly catalytic metal additives, seven formulations with either MACH I titania, MACH I iron oxide, or *in-situ* titania were tested with various AP particle sizes and distributions. All of the formulations with the exception of two exhibited an exponent break between 4200 and 5600 psi. The burning rates for the first two of these, formulations 10 and 11, with MACH I titania, MACH I iron oxide, and 46-µm AP are shown compared to their respective baseline, formulation 1, in Fig. 20. Both the 46-µm baseline and formulation including iron oxide exhibit an exponent break, with the addition of iron oxide pushing the exponent break out to 4883 psi. The inclusion of MACH I titania eliminated the exponent break altogether within the range of pressures tested. Similar to some of the baseline formulations which converged at the higher pressures, the batches with MACH I titania and iron oxide also appear to converge around 10000 psi. The baseline burning rate at 10000 psi is slightly higher but within scatter of the titania batch. As expected, both additives increased the low-pressure burning rates. The titania also increased the pressure exponent below the characteristic pressure, while the iron oxide decreased it.

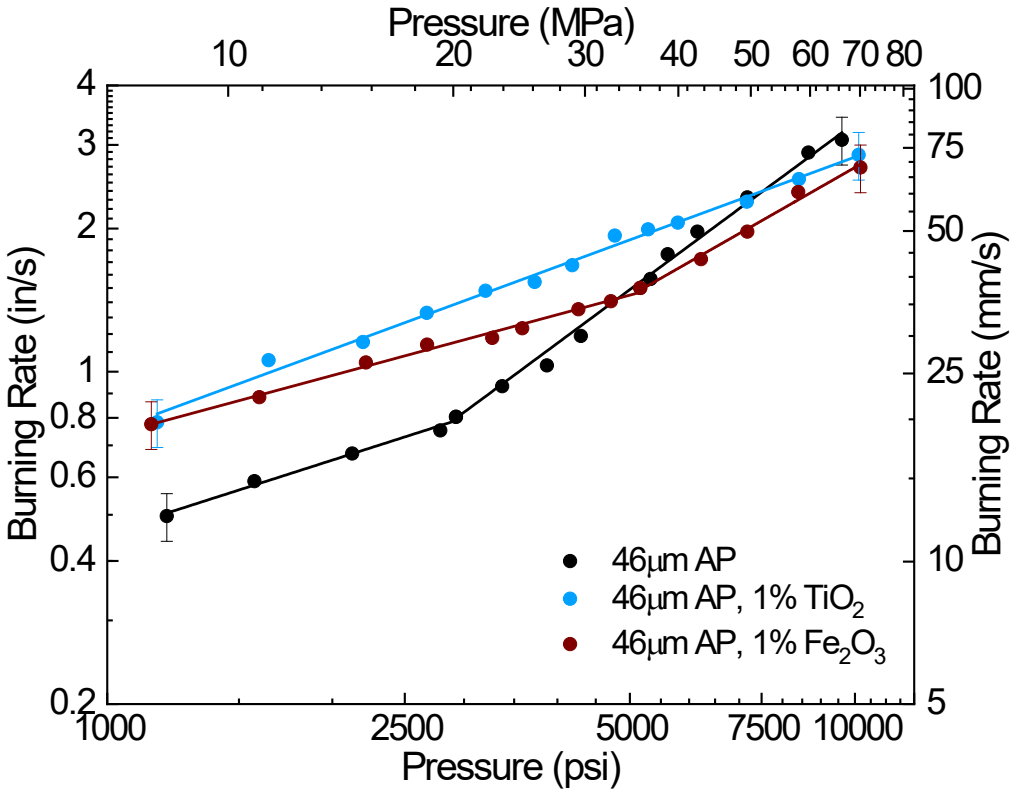

Figure 20. Burning rates for 46-μm AP and MACH I TiO_2 and MACH I Fe_2O_3.

Figure 21 presents the burning rates for formulations 12 and 13 containing the MACH I additives and 210.3-μm AP compared to their respective baseline, formulation 5. The low-pressure burning rates increased with the addition of both titania and iron oxide as anticipated. Similar to the previous results seen in Fig. 20, the titania again increased the pressure exponent below the characteristic pressure, while the iron oxide decreased it. Unlike the previous results, however, where only the batches with additives converged at higher pressures, all three formulations containing 210.3-μm AP started to converge right after their respective exponent breaks. Furthermore, the exponent breaks of the batches containing titania and iron oxide occurred where their respective burning

rate curves intersected with the baseline burning rate curve. Since the titania increased both the burning rate and pressure exponent below P* greater than the iron oxide, it subsequently also increased the characteristic pressure more as well, 5517 psi compared to 4883 psi. The exponent break occurring at the intersection point between the baseline and formulations containing additives is a trend that also appears in the next two sets of data with iron oxide and varying AP concentrations and distributions.

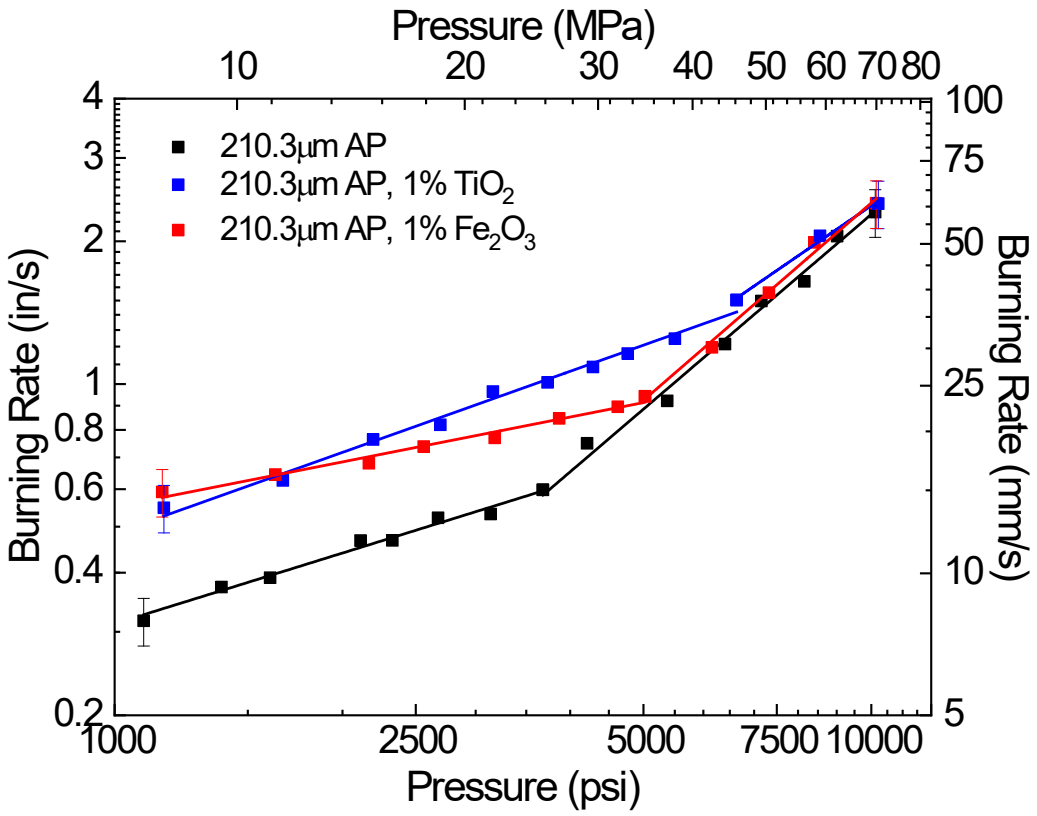

Figure 21. Burning rate results for 210-µm AP and MACH I TiO_2 and MACH I Fe_2O_3.

The next set of results focuses on the effect of iron oxide and AP concentration on the exponent break. As expected, the inclusion of iron oxide increased the low-

pressure burning rates. Similar to the baseline formulations with varying AP concentrations, the batch with iron oxide and 85% solids loading had a greater pressure exponent above and smaller pressure exponent below the exponent break than the batch with iron oxide and 80% solids loading. The addition of iron oxide decreased the pressure exponent below the characteristic pressure for both solids loadings formulations, but had no significant effect on the pressure exponent above the characteristic pressure. Since the iron oxide increased the burning rates for both batches, it also increased the characteristic pressure from 3676 to 4883 psi and 3852 to 4477 psi for the 80% and 85% solids loading formulations, respectively. As with the previous batches containing catalytic additives, the burning rates of the batches containing iron oxide converged with their respective baselines at the higher pressures beyond the exponent break feature as seen in Fig. 22, with all four batches eventually converging around 10000 psi.

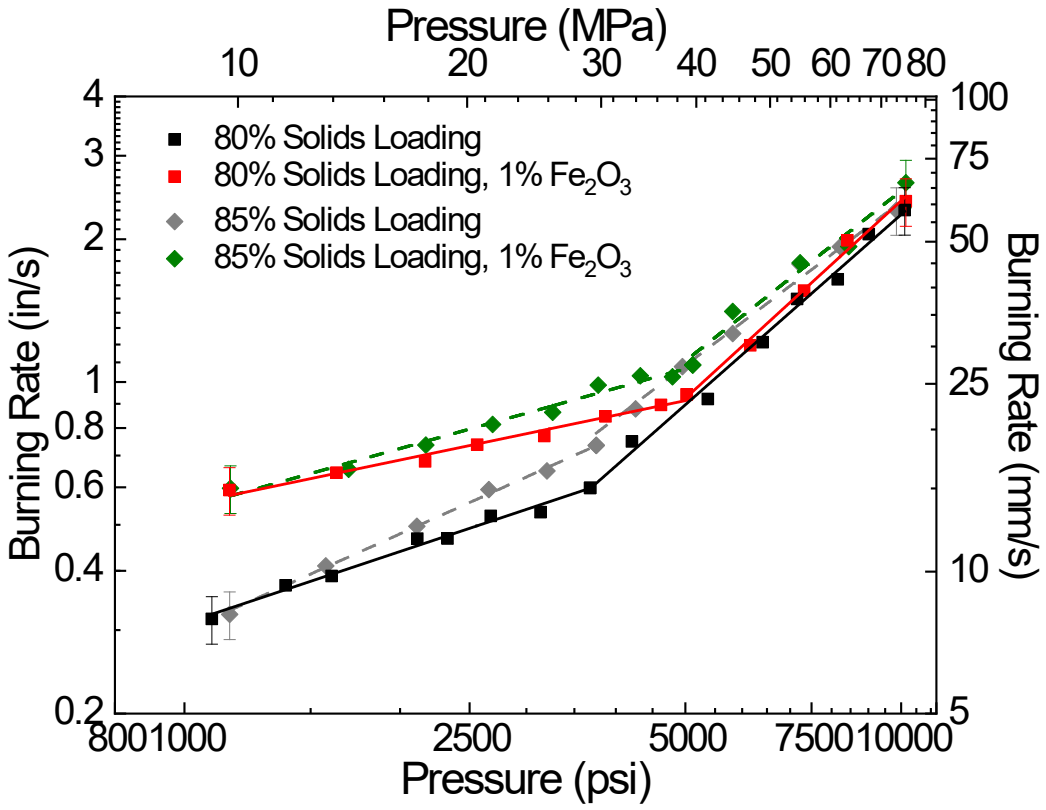

Figure 22. Burning rate results for formulations with MACH I Fe_2O_3 and varying AP concentrations.

The burning rate results containing iron oxide and monomodal and trimodal AP distributions are provided in Fig. 23. As seen in Fig. 23, unlike the monomodal and trimodal baselines where there is a distinct decrease in burning rate with the inclusion of additional AP particle sizes, the two formulations containing iron oxide have almost identical burning rates. The addition of iron oxide eliminates this AP distribution effect by increasing the burning rates to the maximum threshold possible with these formulations. Similar to the iron oxide and varying AP particle size formulations, the iron oxide decreased the pressure exponent below the characteristic pressure. Additional trends observed throughout the additive burning rate results and seen here, are the

exponent break for both formulations with iron oxide occurring at the pressure where their burning rate curves intersect with their respective baseline burning rate curves and the convergence of burning rates for all four formulations at the high pressures. Since the formulations containing iron oxide have similar low-pressure pressure exponents and burning rate magnitudes, they also have similar characteristic pressures of 4477 psi and 4288 psi for the monomodal and trimodal formulations, respectively.

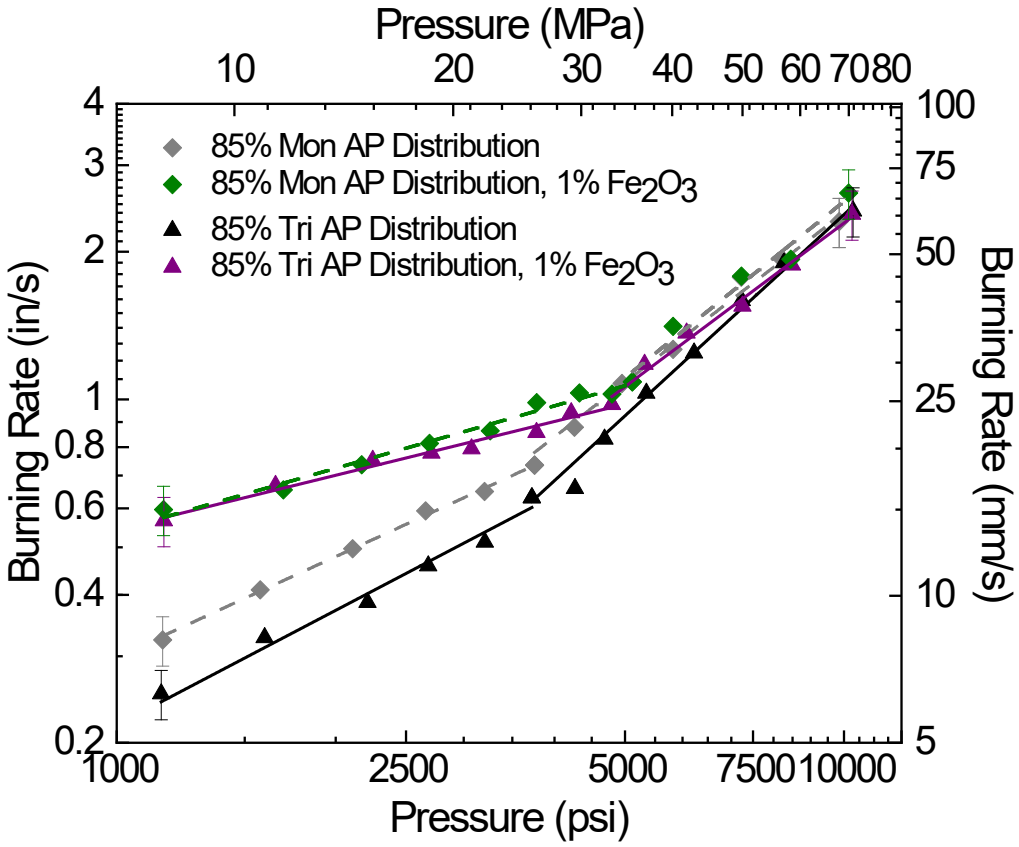

Figure 23. Burning rate results for formulations containing MACH I Fe_2O_3 and varying AP distributions.

Figure 24 presents the final set of burning rates for formulation 16 containing 0.50% *in-situ* titania and 138.9-µm AP. This formulation was specifically chosen and designed to dramatically increase the burning rates enough to eliminate the exponent break. As seen in Fig. 24, the exponent break feature was indeed eliminated as planned within the pressure range tested. Since the *in-situ* titania burning rate curve intersects with its respective baseline at 10000 psi, further testing at higher pressures is necessary to determine if it will follow the previous additive burning rate trends and experience an exponent break at this intersection point.

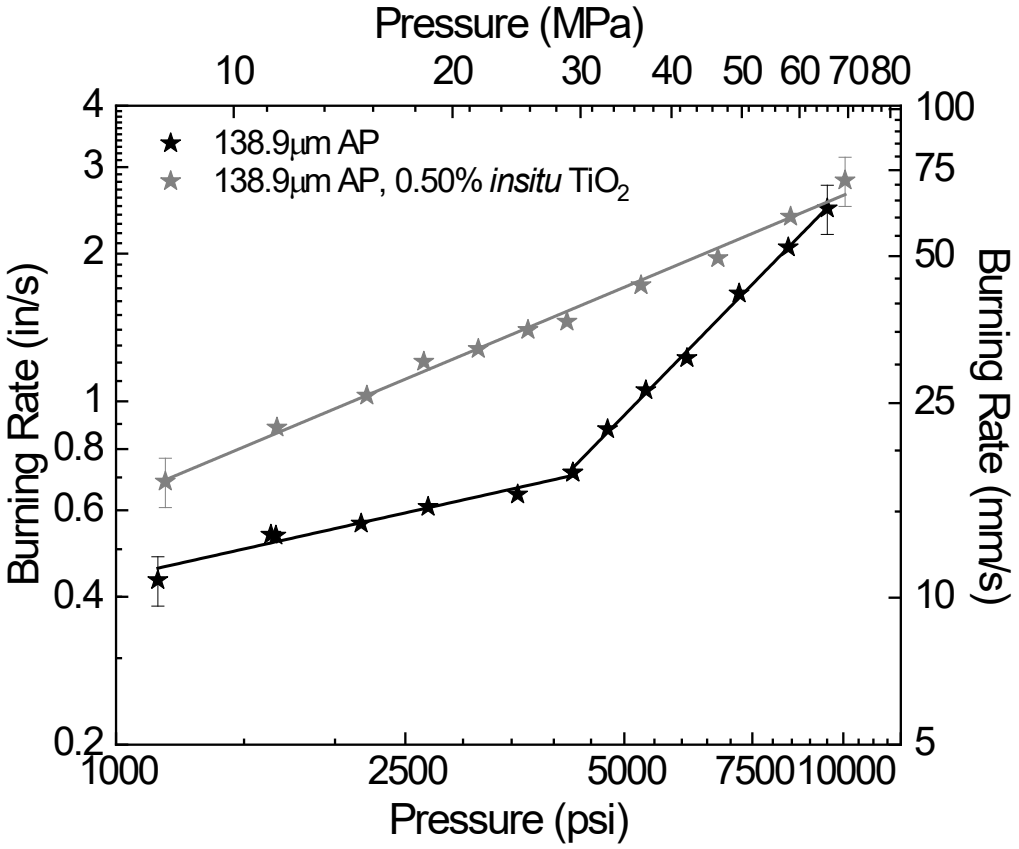

Figure 24. Burning rate results for 0.50% *insitu* TiO_2 and 138.9-µm AP.

CHAPTER V

EFFECT OF FORMULATION DETAILS ON THE EXPONENT BREAK FEATURE

5.1 AP Characteristics

As mentioned in a preceding section, several AP-based propellant formulations using non-HTPB binders and a variety of AP characteristics have previously been tested out to very-high pressures [11-12]. The effects of AP characteristics on the exponent break in these studies varied based on the binder used. With AP/polysulfide-based propellants, the effect of AP particle size was completely negated at the high pressures. However, in a subsequent study, it was observed that the AP particle size still had an effect on the burning rates of AP/carboxyl-terminated polybutadiene (CTPB)- and AP/nitrocellulose-based propellants at high pressures, producing parallel burning rates analogous to those in the current study as seen in Fig. 25 [12]. In the same study with AP/CTPB-based propellants, the characteristic pressure, P*, also increased with AP particle size until reaching 175 μm, where it began to decrease [12]. Although the current study does not have an AP size between 138 and 210.3 μm, a similar trend was still observed where P* increased with particle size up to 138 μm, and then decreased for 210.3 μm. These trends suggest that the exponent break feature is directly influenced by the AP size and related combustion mechanism.

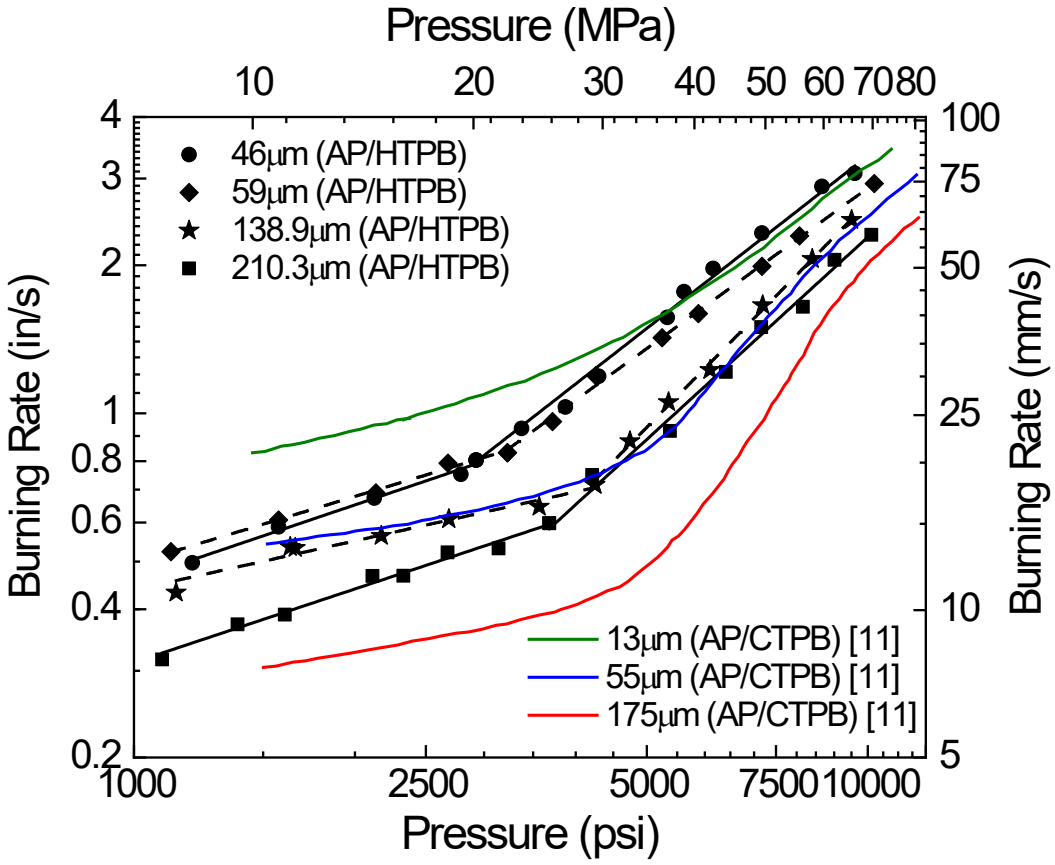

Figure 25. Effect of AP particle size on the exponent break feature of AP/HTPB- and AP/CTPB-based propellants [12].

At 1000 psi, the smallest AP sizes, 46 and 59 μm, are closer to the premixed limit of 10 μm for AP-HTPB combustion as suggested by Gross et al. [59-60]. This premixed limit represents the maximum burning rate for a specific formulation and pressure since the maximum surface heat flux is produced as a result of the primary flame covering the entire burning surface. As particle size decreases, this primary flame becomes a premixed flame that reaches the mixture's adiabatic flame temperature and is formed from the AP decomposition products completely mixing with those from the

binder pyrolysis [60]. The 138.9-µm AP, however, burns primarily as a diffusion flame at 1000 psi, and the 210.3-µm AP as a mixture of diffusion and AP monopropellant flames. As AP particle size increases, AP combustion becomes a combination of diffusion and AP-monopropellant flame conditions, where the lower heat flux from the AP monopropellant flame is supplemented by the diffusion flame forming close to the burning surface [60].

The upper particle size limits for each of the premixed, diffusion, and monopropellant flame conditions decrease with increasing pressure as described by Gross et al. [85]. Smaller particles which previously burned as premixed flames, subsequently burn as diffusion flames at high pressures, and large particles, as monopropellant flames. This effect of pressure on AP combustion behavior, together with the characteristic pressure decreasing with particle size, suggests that the flame structure and specifically diffusion flame kinetics potentially play an important role in the exponent break feature mechanism. The varying-AP-distribution burning rate results further support this possible dependence on flame structure since both formulations containing 20-µm AP, the bimodal and trimodal, exhibited similar pressure exponents above P* at 1.36 and 1.37, respectively. The monomodal formulation which only included 210.3-µm AP, on the other hand, had a significantly lower pressure exponent above P* at 1.15. Although the concentrations of 20-µm AP in the bimodal and trimodal are different, the similar increase in n suggests that the 20-µm AP, which burns principally as a diffusion flame at higher pressures, directly influences the pressure exponent above P*. Furthermore, the bimodal formulation burning rates converge with

those of the trimodal post-exponent break, which appears to occur when its burning rate intersects with that of the trimodal formulation, similar to what was observed with the formulations containing additives.

As with the varying AP sizes, similar very-high pressure AP concentration effects were observed in the above-mentioned study with AP/CTPB-based formulations, where the effect of AP concentration on the burning rates also decreased at very-high pressures. Contrastingly, however, the AP/CTPB-burning rates did not converge at high pressures as they do in the present study, but rather formed an envelope of parallel burning rates similar to the formulations with varying AP sizes. Cole et al. also noticed that dissimilar to the AP size burning rate results in the present study, the effect of AP particle size is effectively negated at high pressures for AP/polysulfide-composite propellants [11]. These differing results suggest that binder type is relevant and that both the AP and binder type impact the exponent break mechanism, further supporting the idea of flame structure and diffusion flame kinetics playing a role in the exponent break mechanism.

5.2 Micron-Aluminum

As seen in Fig. 19, increasing the micron-aluminum concentration appears to have only a slight effect on the high-pressure pressure exponents and characteristic pressure. This similar result is not unexpected since micron-aluminum typically does not affect the burning rates at all or if it does, it slightly decreases them, depending on the concentration. Its primary purpose in composite propellants is to increase the energy

density. However, compared to formulations 4 and 5, which contain 80% and 85% 210.3μm-AP, respectively, the inclusion of 8% 24μm-Al appears to increase both the characteristic pressure and pressure exponent after the break. This potential effect is negated however, as the aluminum content is increased, reducing the characteristic pressure and high-pressure pressure exponent to values comparable to those of the 80% monomodal baseline (formulation 4). An 83% 210.3μm-AP baseline is required to further evaluate the effect of the micron-aluminum.

5.3 Catalytic Additives

Several overarching trends were observed amongst the burning rate results for the formulations with additives. The first is the convergence of the additive-containing burning rate curves with their respective baselines. All of the additive-containing burning rate curves, with the exception of two, started to converge with their respective baselines as the pressure increased towards 10000 psi. The two that did not converge were the formulations containing 46-μm AP and either MACH I titania or iron oxide. Instead of converging with their baselines, these formulations converged with each other at 10000 psi and fell slightly below the corresponding 46-μm baseline. Without testing additional formulations with similar AP particle sizes and additives, it is difficult to determine whether this difference is due to the AP or the additive. Regardless, the overall trend of convergence at higher pressures indicates that the AP decomposition has a dominating role in the exponent break combustion mechanism.

The second trend observed and additional evidence of the AP decomposition dominating at high pressures is the occurrence of the exponent break at the point of intersection between the additive-containing burning rate curves and their respective baselines. At some pressure, the additive burning rate curves intersect with their respective baselines as seen in Figs. 20-23. Immediately past this pressure, the pressure exponent drastically increases regardless of additive type, AP particle size, concentration, or distribution. In most cases, the burning rates also converge with their baselines as previously described. Ultimately, the catalytic effects of the additives and the effects of AP concentration and distribution on the burning rates are all negated as the pressure approaches 10000 psi. These features that would typically be used to tailor propellant burning rates are now irrelevant beyond the exponent break.

Figure 26 illustrates the additional negation of the AP particle size effect at high pressures due to the addition of the catalytic additives. The burning rates of all five formulations containing additives and various AP particle sizes appear to converge at a pressure slightly higher than 10000 psi rather than forming an envelope of parallel burning rates, as previously seen in the baseline results. Although additional testing at higher pressures is required to confirm the convergence, similar trends have been observed in other studies including AP-based propellants [12]. Cole et al. observed that the catalytic effects of ferrocene and CuO_2O_2 decreased at higher pressures when incorporated into AP/CTPB-based propellants [12]. Similarly, in Atwood et al.'s study of AP/HTPB-composite propellants with varying AP distributions, particle sizes, aluminum concentrations, and catalysts, the effects of particle size and catalysts on the

burning rates vanished at pressures above the exponent break for all of their formulations [15]. Unfortunately, it is difficult to determine the importance, if any, of altering each ingredient since the study was more application-specific and varied multiple ingredient concentrations at once.

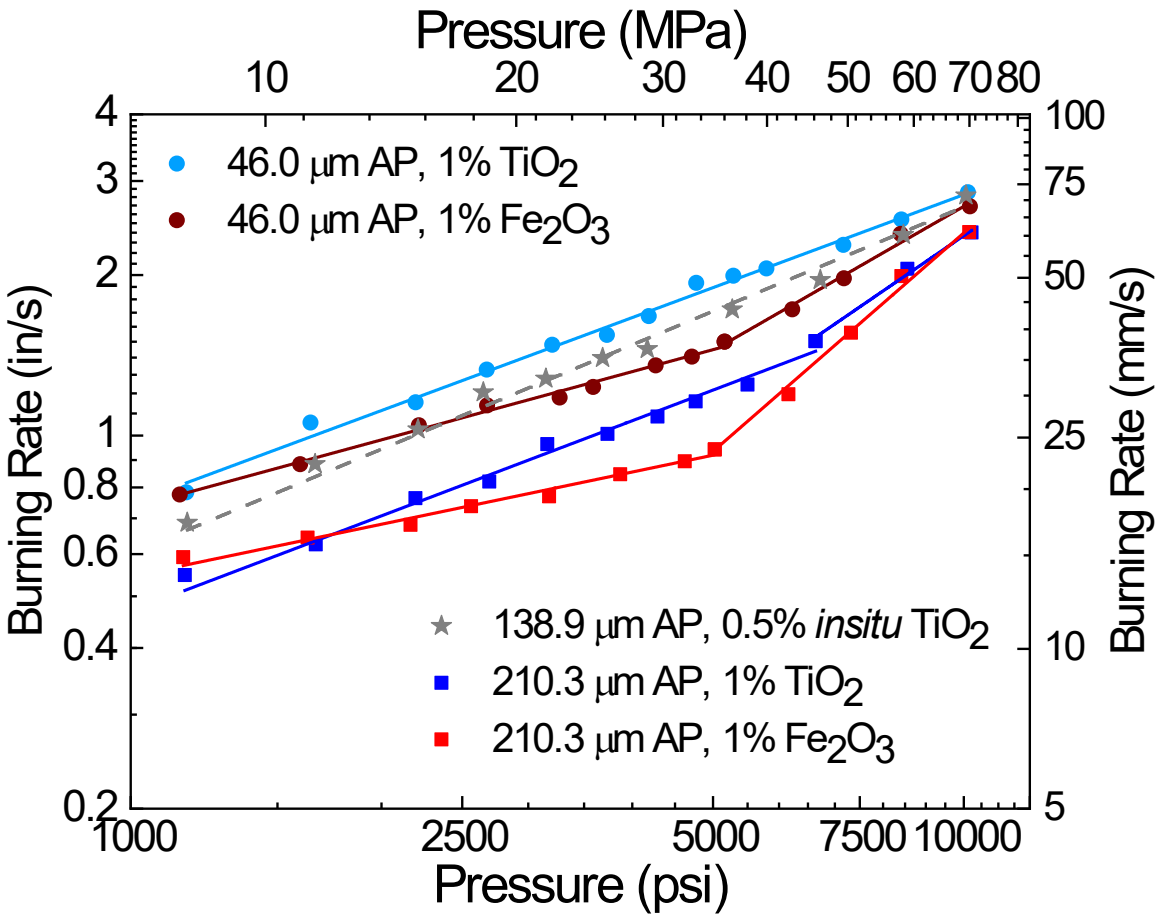

Figure 26. Effect of AP particle size and additives on the exponent break feature.

CHAPTER VI

EXPONENT BREAK MECHANISM

6.1 AP-Driven

As previously mentioned, Irwin, Atwood, and Glick et al. all suggest that above the characteristic pressure, P*, the contribution of AP to the combustion process dominates, thus the burning rates are controlled by the AP decomposition flame [6,15,17,73]. This hypothesis is supported by Bastress' observation that at higher pressures, the AP surface regresses below the fuel surface [74]. Atwood et al.'s study further supports this hypothesis since all of the composite propellant formulations tested approached an "AP barrier", the high-pressure exponent region of pure AP, regardless of the AP particle size, modality, micron-aluminum concentration, burning rate catalyst (Fe_2O_3), or plasticizer used [15]. Although few experimental data exist at very-high pressures, it is evident from the data in the literature and herein that the exponent break feature is indeed primarily AP-driven as all AP-based formulations, regardless of binder type (including inert or energetic), exhibit this characteristic [11-12, 14-16]. The role of AP in the exponent break feature is emphasized when the data from the present study are compared to the AP deflagration curve presented by Boggs and as seen in Figs. 27 and 28 [8].

Material within this chapter has been previously published and is reprinted with permission from "Very-High-Pressure Burning Rates of Aluminized and Non-Aluminized AP/HTPB-Composite Propellants" by C. A. M. Dillier, E. D. Petersen, T. Sammet, and E. L. Petersen, 2021. *Journal of Propulsion and Power*, In Print, Copyright 2021 by authors.

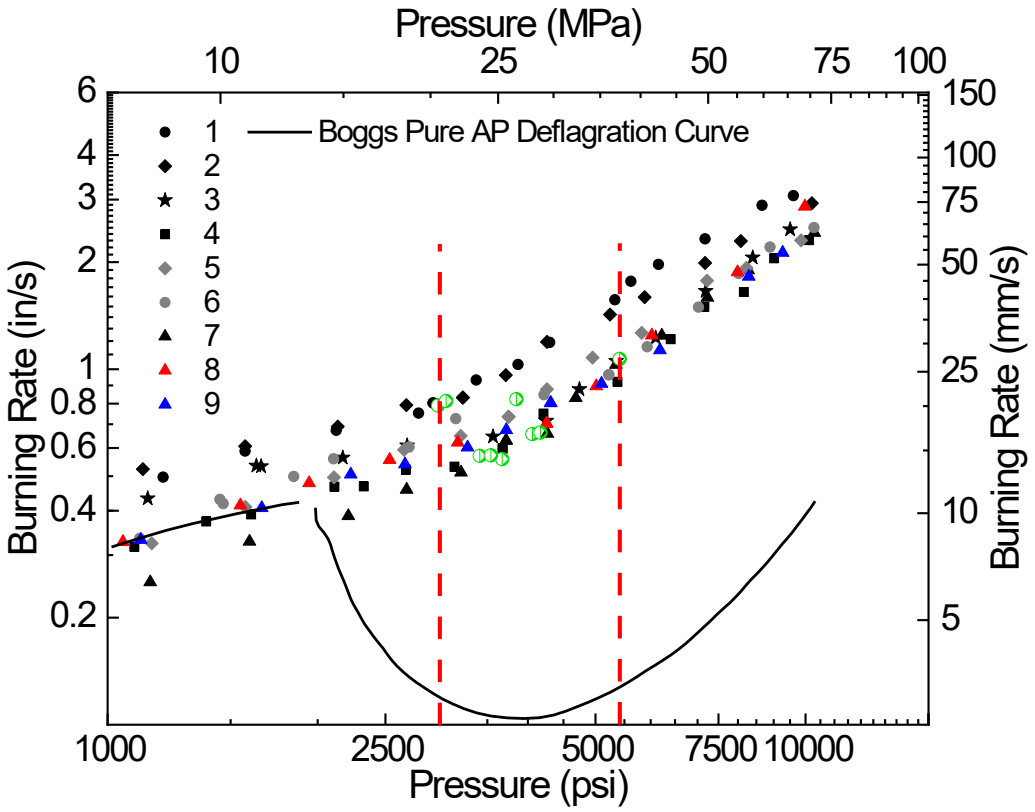

Figure 27. Comparison of baseline and aluminized data from current study to the pure AP deflagration burning rate curve produced by Boggs [8]. The red lines indicate the characteristic pressure range.

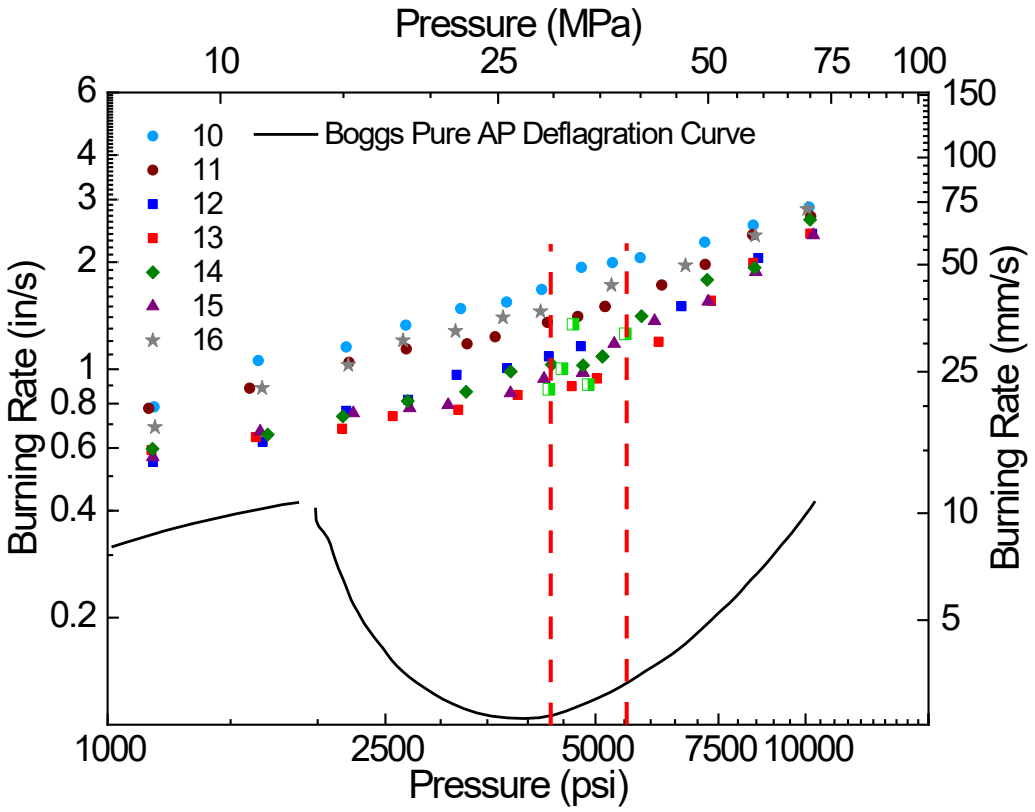

Figure 28. Comparison of data from current study containing catalytic additives to the pure AP deflagration burning rate curve produced by Boggs [8]. The red lines indicate the characteristic pressure range.

Boggs describes four distinct AP deflagration burning rate regimes. In the first two regimes, 300-800 psi and 1000-2000 psi, the deflagration behavior is characterized by positive pressure exponents and increasing burning rates. Past 2000 psi, in the third regime between 2000-4000 psi, the pressure exponent becomes negative, and the burning rates drastically decrease to as low as 0.1 in/s. Around 4000 psi, the burning rates turn positive again and increase out to 10000 psi, the highest pressure tested. As seen in Figs. 27 and 28, the exponent break feature in the current study occurs in the transition between the third and fourth AP deflagration regimes, between pressures of

about 2974 psi and 5517 psi. This location of the exponent break pressure is also true for other AP-based formulations where the exponent break occurs between 2600 and 5100 psi [11-15].

Boggs suggests that two distinct mechanisms are responsible for AP deflagration, one at the lower pressures up to 2000 psi and another for high pressures above 4000 psi [8]. He saw evidence of this change in the surface structures of the single crystals that were thermally quenched in each burning rate regime [8]. As pressure increased, the surface structure transitioned from ridges and valleys to needle-like arrays, clearly indicating a shift in the physical burning mechanism. From Figs. 27 and 28, it can be reasonably concluded that the same two mechanisms also hold true for AP/HPTB composite propellant combustion, and the transition between them is related to the exponent break feature. In his high-pressure study on AP-based propellants, Cole also suggested that two distinct burning rate mechanisms, one for low pressures and a secondary competing mechanism for high pressures [12]. While the dominant physical (or chemical) mechanism is still unknown, it is evident that the fundamental AP decomposition mechanism is altered in a similar manner for all AP/HTPB-composite propellants regardless of AP size, distribution, concentration, or catalytic additive. The existence of an "AP barrier" further supports this as described further in the subsequent section.

6.2 AP Barrier

As previously mentioned in Chapter II, Atwood et al. introduced the concept of an "AP barrier", where the AP deflagration rate serves as a lower burning rate limit at low and high pressures for all AP-containing formulations [11-12,15-16]. This concept holds true for all of the previously mentioned non-HTPB/AP studies, as Cole determined that all of the burning rates fell above the AP deflagration rate as determined by Irwin et al. [6,16]. The existence of the AP barrier for AP/HTPB-composite propellants is also supported by the current results as demonstrated in Fig. 29. This figure compares all of the burning rate results from the present study to Irwin et al.'s AP deflagration curve [6].

Although some of the burning rates appear to fall below the AP deflagration rate at low pressures, all of the burning rates regardless of formulation details remain above the AP deflagration rate at higher pressures. These results agree with those of Atwood et al. who also noted an apparent pressure exponent limit imposed by the pure AP deflagration rate for AP/HTPB-based propellants [15]. In Atwood et al., all of the composite propellant formulations tested approached the high-pressure exponent region of pure AP, regardless of the AP particle size, modality, micron-aluminum concentration, burning rate catalyst (Fe_2O_3), or plasticizer used [15]. Additionally, any exponent breaks observed occurred at pressures less than or equal to the AP monopropellant burning rate [15].

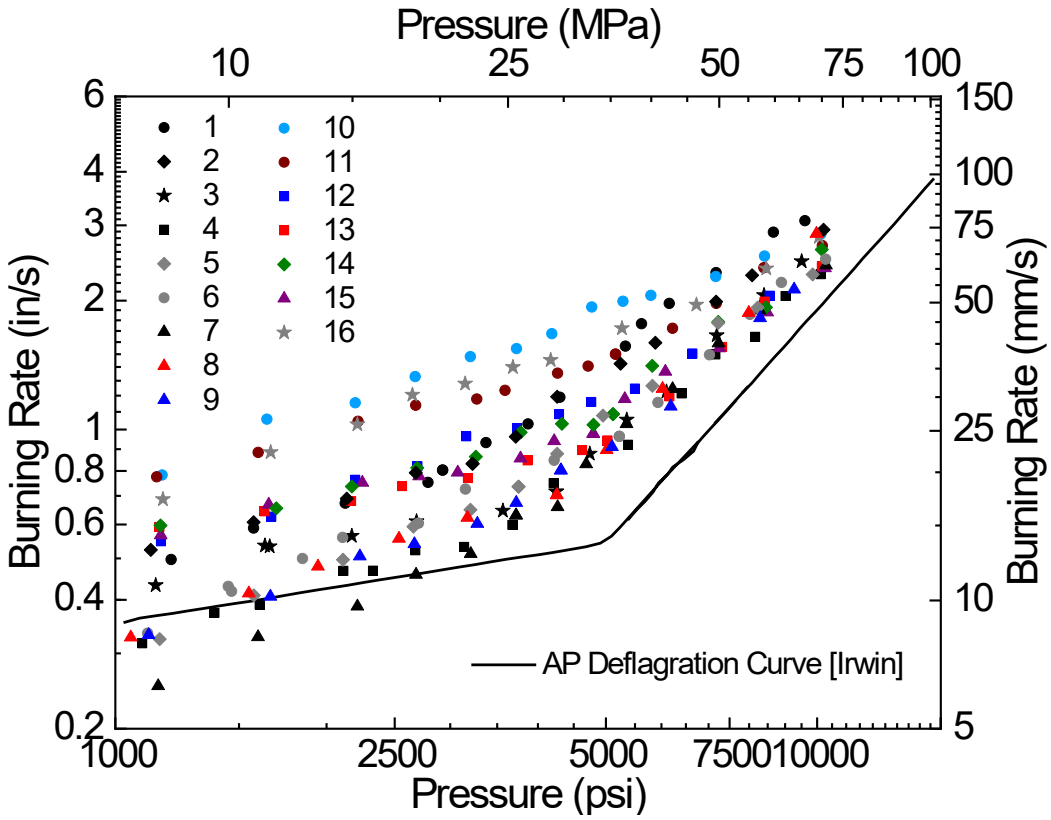

Figure 29. Burning rates from this study plotted against Irwin's pure AP deflagration curve [6]. The pure AP deflagration curve acts as an "AP Barrier", the minimum burning rate boundary for AP-containing propellants.

CHAPTER VII

EVALUATION OF EXISTING THEORIES AND MODELS

7.1 AP Cracking or Pores Forming

Although the exact physiochemical exponent break mechanism is still unknown, several theories and models have been presented in the literature. As previously described in Chapter II, one of these is Irwin et al.'s suggestion that the increase in burning rate at very-high pressures is due to an increased AP surface area as a result of cracks or pores forming and/or expanding in the AP crystals due to thermal stresses induced by steep thermal gradients [6,73]. Based on this this theory, Irwin et al. created a geometric model for the high-pressure burning rates and validated it using their experimental high-pressure AP strand burning rates [6]. To evaluate this model and potential exponent break mechanism further, it was applied to the current baseline data presented in Chapter IV.

Irwin et al.'s model combines a geometric model of the change in surface area with Eyring's crack propagation theory, which relates creep and fracture to material properties. Surface shearing occurs due to steep thermal gradients in the solid phase, leading to existing cracks or pores either expanding or new ones forming. These cracks then form into conically shaped burning surfaces due to penetrating gases. Figure 30 provides a schematic of Irwin et al.'s model. Irwin et al. combined equations for the changing surface area and Eyring's crack propagation theory to yield Eq. (5), where α and β are constants and P is the pressure. The constants α and β in Eq. (5) can be

estimated from the experimental high-pressure burning rates by fitting a best-fit exponential equation as seen in Fig. 31. Although this model originally related the crack-inducing shear stress to the pressure directly instead of the pressure-dependent thermal gradient, the model is essentially unaffected since the thermal stress is nearly linear for pressures greater than 5000 psi [73].

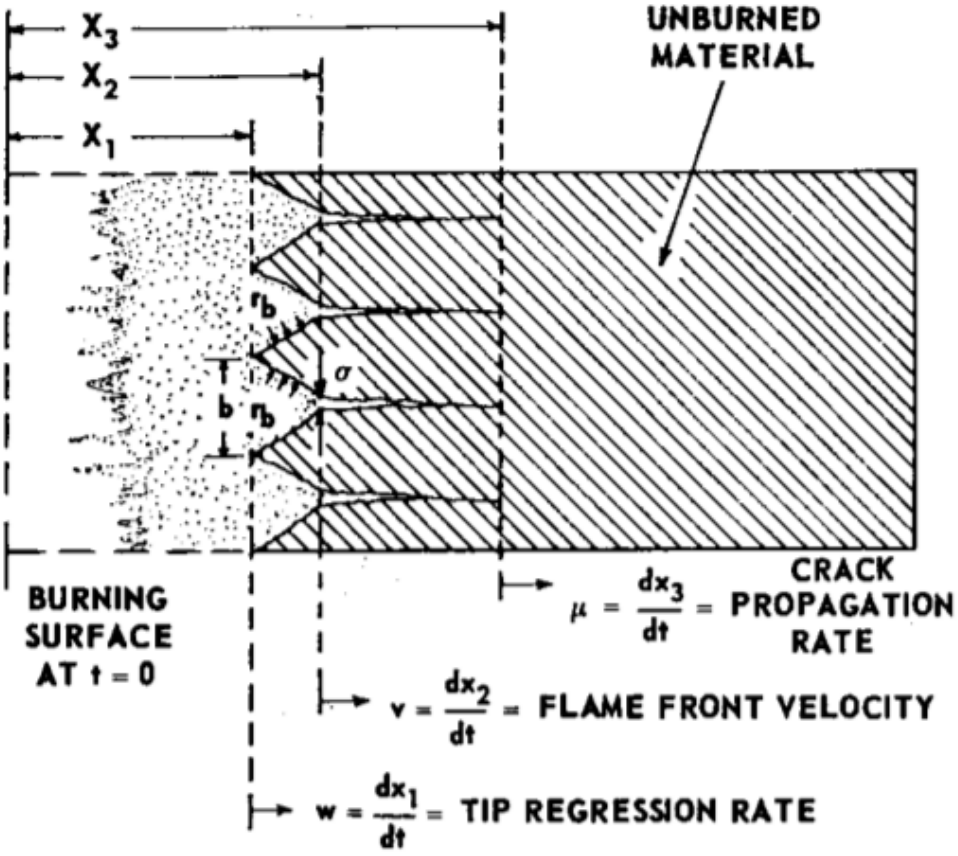

Figure 30. Schematic of Irwin et al.'s geometric model describing cracks growing or forming in the AP surface, producing accelerated burning rates. Reprinted from Irwin et al. [6].

$$v \cong 2\alpha \sinh \beta P \tag{5}$$

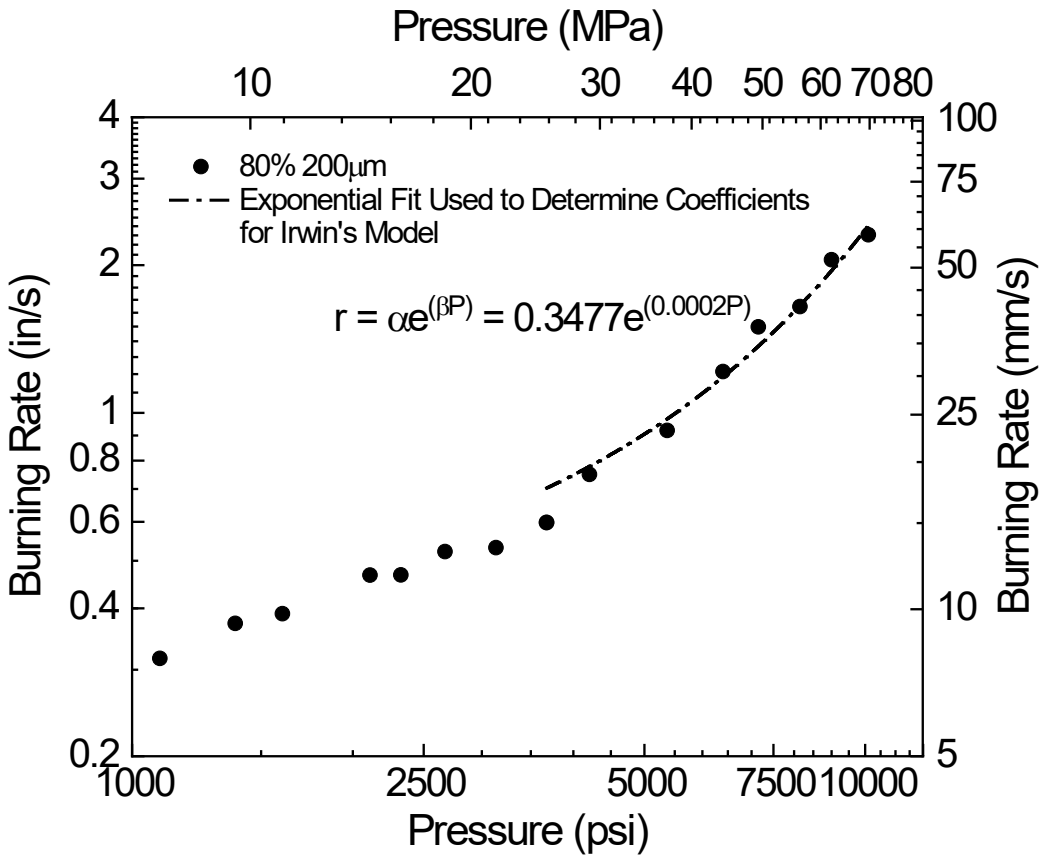

Figure 31. Example of determining the coefficients, α and β, used in Irwin et al.'s geometric model [6, 73].

Although Irwin et al. based the model on the geometry of a solid AP strand, rather than a composite propellant with binder surrounding the AP crystals as seen in Fig. 30, this model can still prove useful in defining the exponent break mechanism as Cole et al. observed cracking in AP particles due to steep thermal gradients in his high-pressure AP composite propellant study [12]. Therefore, this model was evaluated using the current study's burning rate data as a possible explanation for the exponent break feature. As described and illustrated in Fig. 31, best exponential-fits were applied to all

of the baseline high-pressure burning rate data to determine α and β for each baseline formulation. These constants were then combined with Eqn. 5 and the resulting lines plotted against the experimental burning rate data as seen in Figs. 32-34.

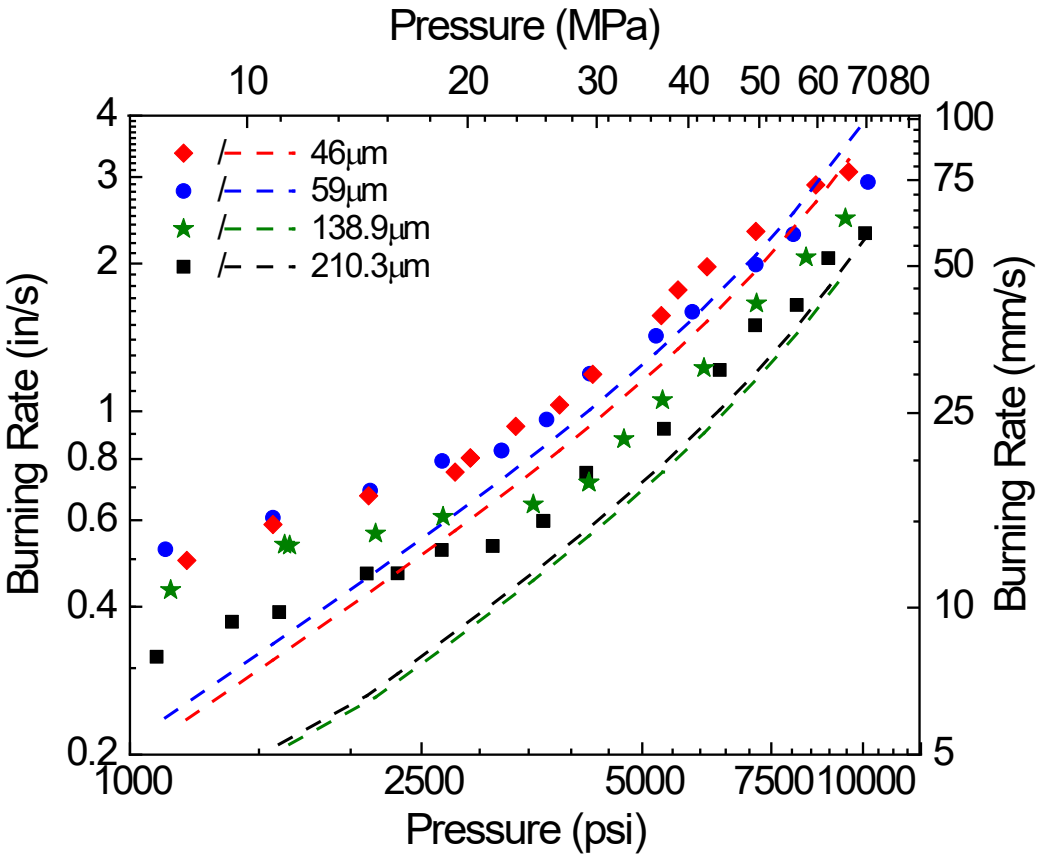

Figure 32. Irwin et al.'s predicted burning rates compared to the experimental burning rate data for different AP particle sizes.

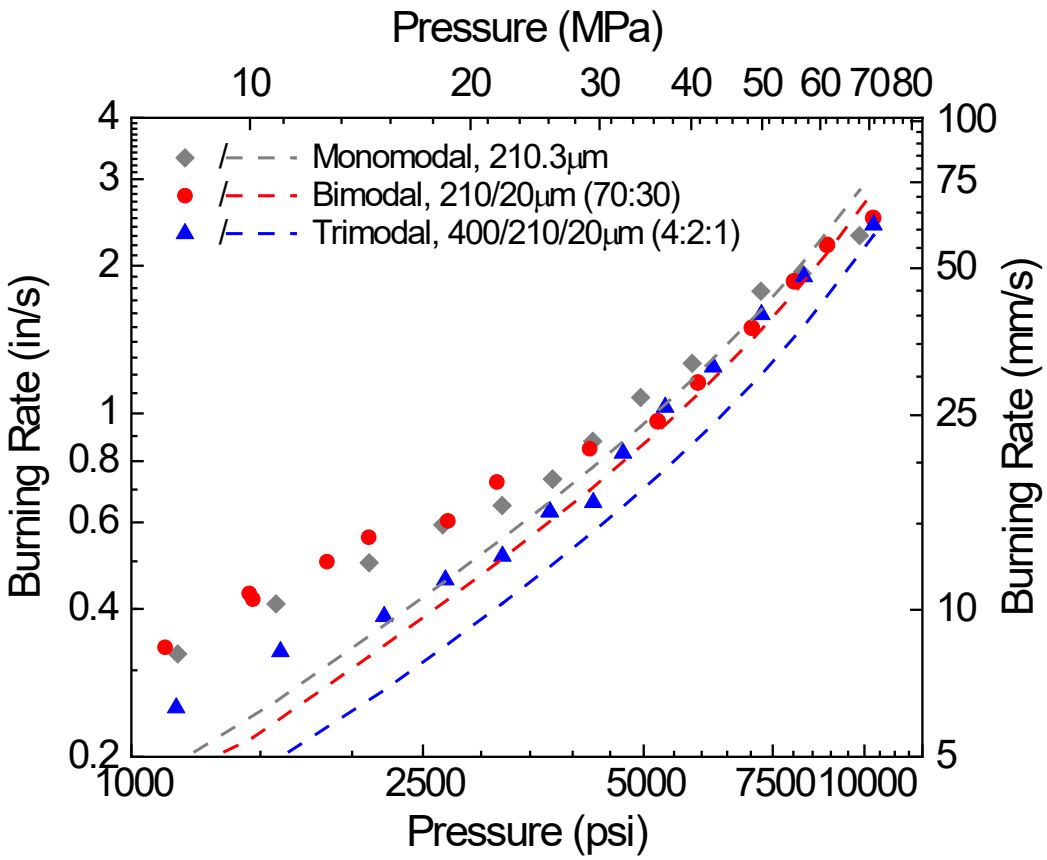

Figure 33. Irwin et al.'s burning rate predictions compared to experimental burning rate results for varying AP distributions.

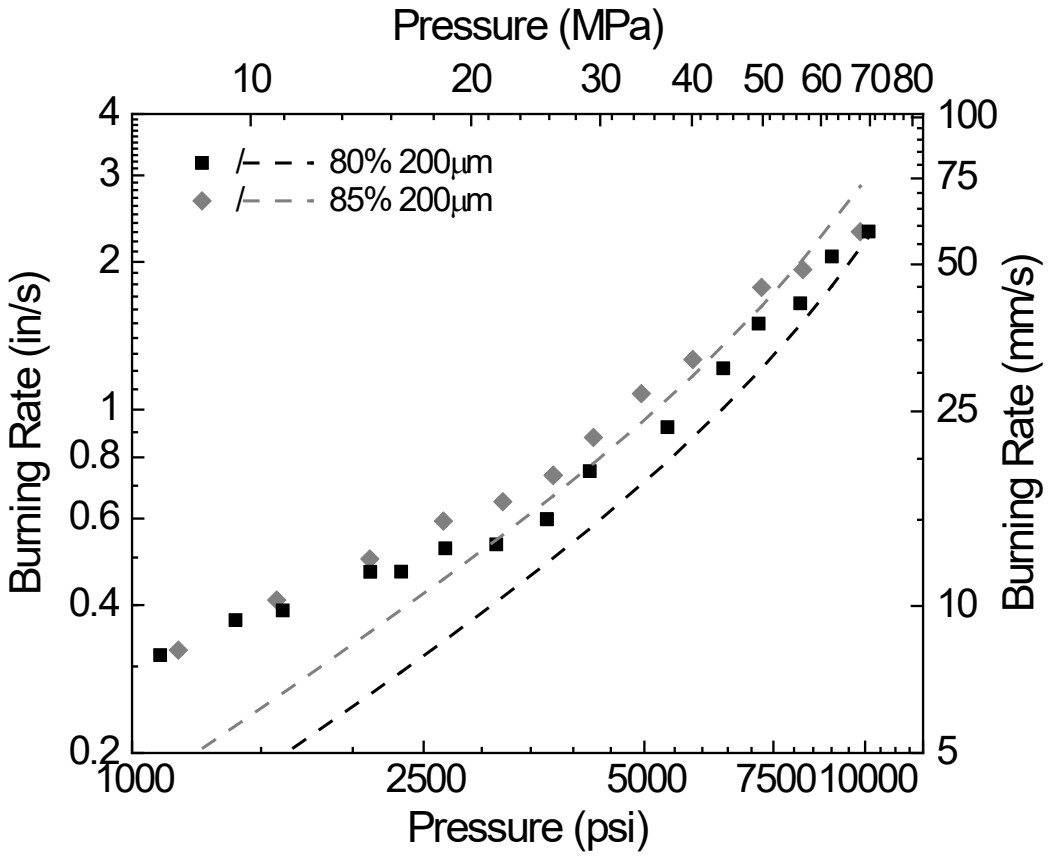

Figure 34. Irwin et al.'s predicted burning rates compared to the experimental burning rates for varying AP concentrations.

As seen in Figs. 32-34, the burning rate magnitudes for each batch are underpredicted to varying degrees by Irwin et al.'s geometric model, which in turn causes the characteristic pressure to be overpredicted as seen in Fig. 35. This trend is the most evident for the 80%-AP batches with varying particle sizes as not only are the predicted burning rates too low, the burning rate trends are also incorrect. The 59-µm batch is predicted to burn faster than the 46-µm formulation, and the 210.3-µm faster than the 138.9-µm. This breakdown in the model makes sense as the geometric model

was created based on solid AP strands, not composite propellants. The 80%-formulations contain more binder than the 85%-AP propellants, thus the role of the binder plays a greater role which is not captured in the pure-AP model. This observation is also the reason why the model does a better job predicting the burning rates for the various distributions, since they contain a higher AP content, and thus resemble a solid AP strand more closely.

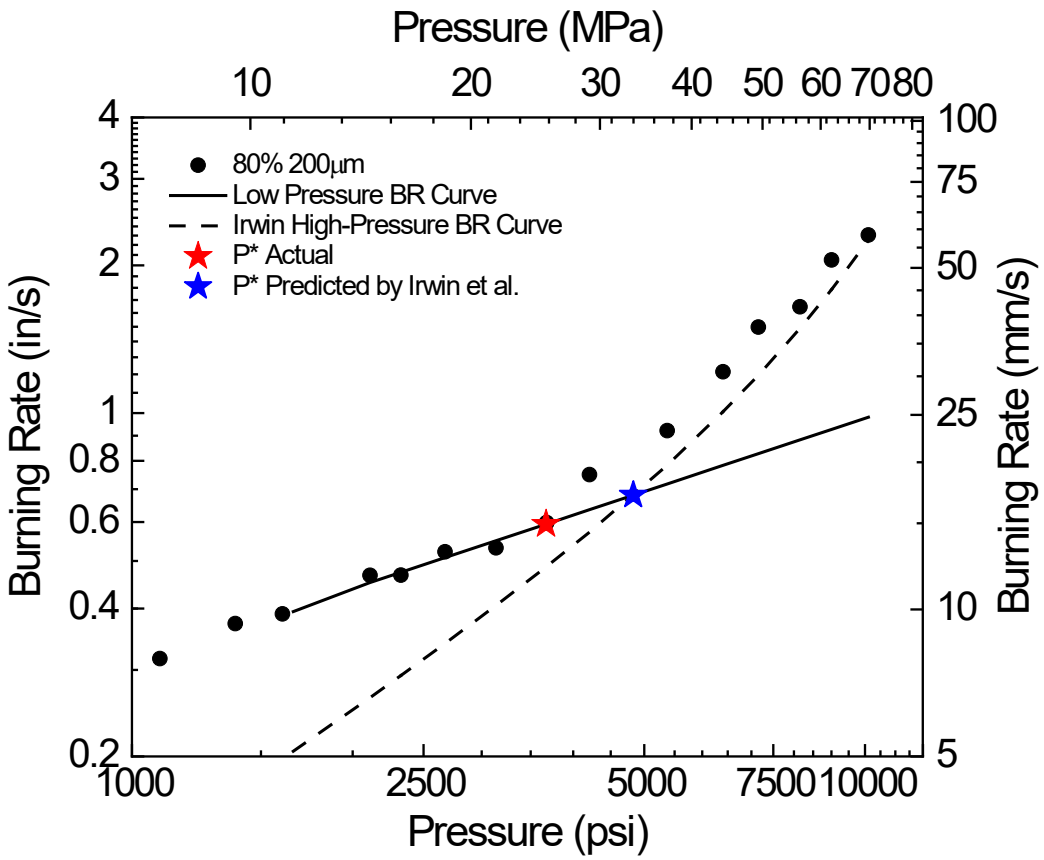

Figure 35. Comparison of actual characteristic pressure compared to that predicted by Irwin et al.'s geometric model. The red star indicates the characteristic pressure determined experimentally.

The most impressive aspect of the model predictions is the capture of the steep pressure exponents. As seen in Figs. 32-34, although the burning rate magnitudes are underpredicted, the slopes are extremely close. This similarity in slopes suggests that cracks either propagating or forming potentially relate directly to the drastic increase in pressure exponent. The increase in burning rate could be a secondary artifact of the increased burn surface. This mechanism also suggests the possibility of convective combustion or isothermal decomposition occurring due to the potential formation of cracks or pores.

Since monopropellants, assuming a 2nd-order global reaction, are expected to have pressure exponents of unity, the increase in pressure exponent to greater than unity could suggest that some form of convective combustion is occurring, possibly due to large AP particles cracking. This cracking could be caused by either physical stresses placed on the AP particles due to the high pressure or due to internal stresses resulting from pores forming within the AP particles as shown recently by Kalman et al. [89]. Kalman et al. demonstrated that as large AP particles are isothermally heated, pores within the particles begin to form, trapping decomposed gases within [89]. Assuming equilibrium conditions, the internal pore pressures could hypothetically rise up to as high as 10-100 MPa (1450-14500 psi), ultimately causing stress-induced dislocations to occur within the crystal lattice, which then become nucleation sites that enable further decomposition, reducing the amount of oxidizing gas available [89]. This behavior could also explain why the single-crystal burning rate decreases as shown in the study by Boggs and previously described herein [8]. As seen in Figs. 27 and 28, the exponent

break typically occurs in the pressure range where the single-crystal burning rate transitions from a negative to a positive slope. Therefore, it is possible that the exponent break mechanism is related to pores forming within the AP crystal or the crystal lattice experiencing a phase change from orthorhombic to cubic and should be further investigated.

As previously mentioned, while the theory of cracks propagating or pores forming provides a reasonable explanation for the pure-AP exponent break, it does not account for a variety of composite propellant formulation factors such as oxidizer characteristics or binder type since it was created based on the geometry of an AP strand, not a composite propellant one. Therefore, it cannot be used to fully explain the exponent break or high-pressure burning rate behavior of composite propellants. This limitation is particularly evident in the AP particle size high-pressure burning rates presented in Chapter IV, as the smaller particles exhibited an exponent break at a lower pressure than the larger particles. Smaller AP particles are arguably more crack-resistant, so these results suggest that this theory lacks a physiochemical mechanism involving particle size that could potentially be driving the exponent break. Additionally, the high-pressure burning rate is modeled as a hyperbolic curve, whereas it is clear from the experimental data that the high-pressure burning rates follow the exponential relationship seen in Eq. (1). Although this theory does not fully explain the exponent break mechanism, there is strong evidence that it could play a role in the larger-AP particle combustion at high-pressures and should be considered and potentially

incorporated into future high-pressure ammonium perchlorate composite propellant models.

7.2 Current AP-Composite Propellant Combustion Model

This section provides a brief overview of the ammonium perchlorate composite propellant model used to evaluate the existing exponent break theories and models proposed in the literature. It also provides a sensitivity analysis of the input parameters for this model for both fine and coarse AP particles. A sensitivity analysis was then used to tailor the input parameter values to model the high-pressure burning rates presented in Chapter IV. These model results were then used to comment on the soundness of existing exponent break theories.

7.2.1 Effect of Input Parameters & Sensitivity Analysis

To further evaluate the exponent break theories and models proposed in the literature and obtain additional insight into the exponent break mechanism, a sensitivity analysis was performed on the input parameters of an ammonium perchlorate composite propellant model. The model created by the Petersen Research Group, specifically, Thomas et al., was chosen as it is based on the traditional three-flame model originally proposed by Beckstead et al. (Beckstead-Derr-Price model), but has been updated to include several modifications recently proposed in the literature as well as built-in, variable flame temperatures and combustion product transport properties determined from combustion equilibrium analyses (CEA) [86].

As seen in Fig. 5 (in Section 2.2.1), the model primarily consists of three flames, the AP monopropellant, primary diffusion, and final diffusion flames. Part of the AP reacts below the surface in the condensed phase and the remaining portion reacts in the gas phase at the surface, forming the AP monopropellant flame. At the contact surface between the AP crystal and binder, the AP and fuel decomposition products react together to form the primary diffusion flame. Lastly, any remaining products from the fuel decomposing, primary diffusion flame, and AP monopropellant flame, react to form the final diffusion flame. In the Thomas et al. model, Arrhenius rate equations are used to describe these reaction rates, with the exception of the final diffusion flame, which is not included in the model. Figure 36 provides an illustration of each reaction included in the model as an Arrhenius relationship. The model also includes equations describing the diffusion flame height of the primary flame and propellant surface geometry.

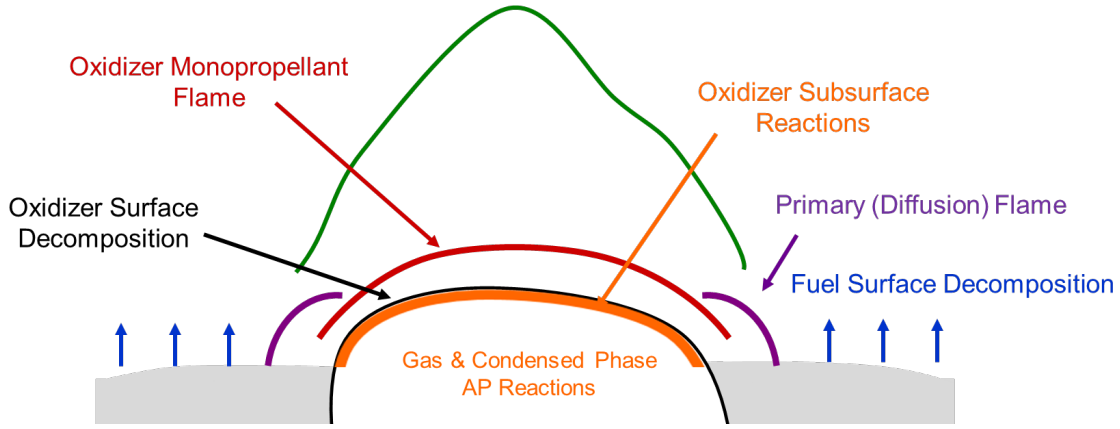

Figure 36. Illustration of reaction rates modeled as Arrhenius equations in the Thomas et al. composite propellant model, based on the BDP model.

Typical composite propellant models, including the Thomas et al. one herein, do not include high-pressure effects as rocket motors operate at lower pressures due to the exponent break feature of composite propellants. As a result, the pressure is only considered when calculating the primary diffusion flame height in the Thomas et al. model [86]. While the model captures AP particle size and concentration effects on the burning rates rather well, it does not predict the exponent break at higher pressures as seen in Fig. 37, which of course is not unexpected. Although this model is not designed for pressures above the exponent break, it can still be used to obtain insight into the exponent break feature primarily through determining which input parameters produce the greatest changes in burning rate magnitude and pressure exponent. These parameters can then be tailored to produce a rough-fit model to the high-pressure burning rate data as a first start in modeling the exponent break feature.

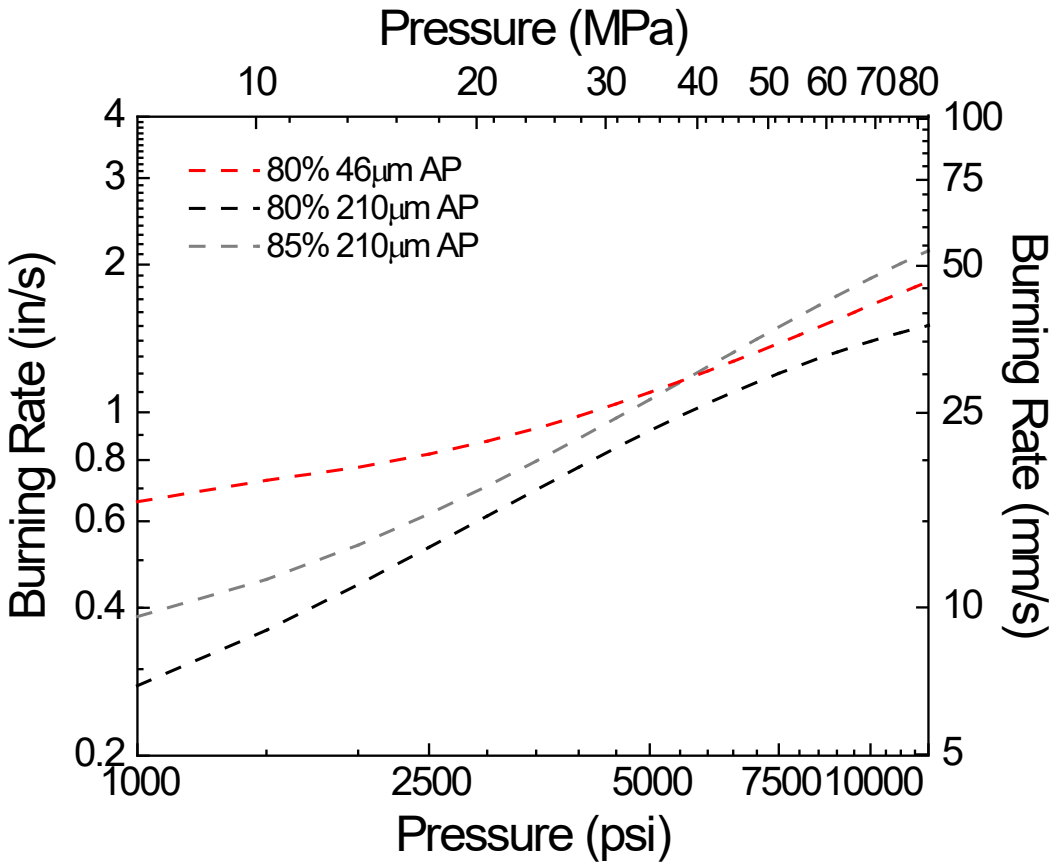

Figure 37. Thomas et al. model [84] burning rate predictions for AP/HTPB-composite propellants containing varying AP particle sizes and concentrations.

Although the Thomas et al. model has a total of thirty input variables, only the ones shown in Table 4 were assessed. All variables relating to physical properties were eliminated as it is unlikely they are changing at the higher pressures. A full list of input parameters is provided in Appendix B along with additional plots describing the effect of each parameter not provided in the main text. As seen in Table 4, the parameters evaluated primarily consist of the kinetic pre-factors and activation energies for each of the reaction rates described by an Arrhenius equation. The other parameter modified was

the average flame height factor, which relates to the primary diffusion flame height over the oxidizer and binder.

All of the parameters were first adjusted within the given ranges in Table 4, which come from various literature resources. Since no range was provided for A_s and E_s, the oxidizer surface decomposition kinetics pre-factor and activation energy, respectively, these values were adjusted using the ranges for the oxidizer subsurface parameters as both are similar in value. As the parameters were adjusted, several limits were found where the model broke down, as seen in Fig. 38. These breaks are explained by looking closer at the model-predicted values for the portion of the AP that reacts in the gas phase, β_P, net heat release at the oxidizer surface, Q_L, net heat release in the AP monopropellant flame, Q_{ox}, and the net heat release in the primary diffusion flame, Q_{PF}, listed in Table 5. As seen in Table 5, the model breaks down for certain parameter values due to unrealistic values calculated for these various heat releases and the amount of AP that reacts in the gas phase.

Table 4. Parameters modified to adjust the burning rates predicted by Thomas et al.'s model for composite propellant combustion.

	Parameter	Range	Value	Units	Reference
	Oxidizer (AP) Parameters				
A_s	Kinetics Pre-factor of Oxidizer Surface Decomposition	-	2.5×10^7	g/cm^2-s	[87]
E_s	Activation Energy of Oxidizer Surface Decomposition	-	30	kcal/mol	[87]
A_{ox}	Kinetics Pre-factor of Oxidizer Subsurface Reactions	$1 \times 10^7 – 1 \times 10^9$	1.56×10^8	g/cm^2-s	[1]
E_{ox}	Activation Energy of Oxidizer Subsurface Reactions	10 – 50	32	kcal/mol	[1]
A_{AP}	Kinetics Pre-factor of Oxidizer Monopropellant Flame Reaction	$1 \times 10^3 – 1 \times 10^5$	5.45×10^4	g/cm^3-s-atm$^{\delta AP}$	[87-88]
E_{AP}	Activation Energy of Oxidizer Monopropellant Flame Reaction	10 – 50	30	kcal/mol	[1]
	Fuel (HTPB) Parameters				
A_f	Kinetics Pre-factor of Fuel Surface Decomposition	$1 \times 10^3 – 1 \times 10^5$	3×10^3	g/cm^2-s	[1]
E_f	Activation Energy of Fuel Surface Decomposition	5 – 30	15	kcal/mol	[1]
	Primary Flame Parameters				
A_{fh}	Average Flame Height Factor with Respect to Oxidizer	0 – 1	0.3	-	[1]
A_{PF}	Kinetics Pre-factor of Primary Flame Reaction	$1 \times 10^3 – 1 \times 10^5$	2.41×10^3	g/cm^3-s-atm$^{\delta PF}$	[87]
E_{PF}	Activation Energy of Primary Flame Reaction	5 – 30	16.9	kcal/mol	[87]

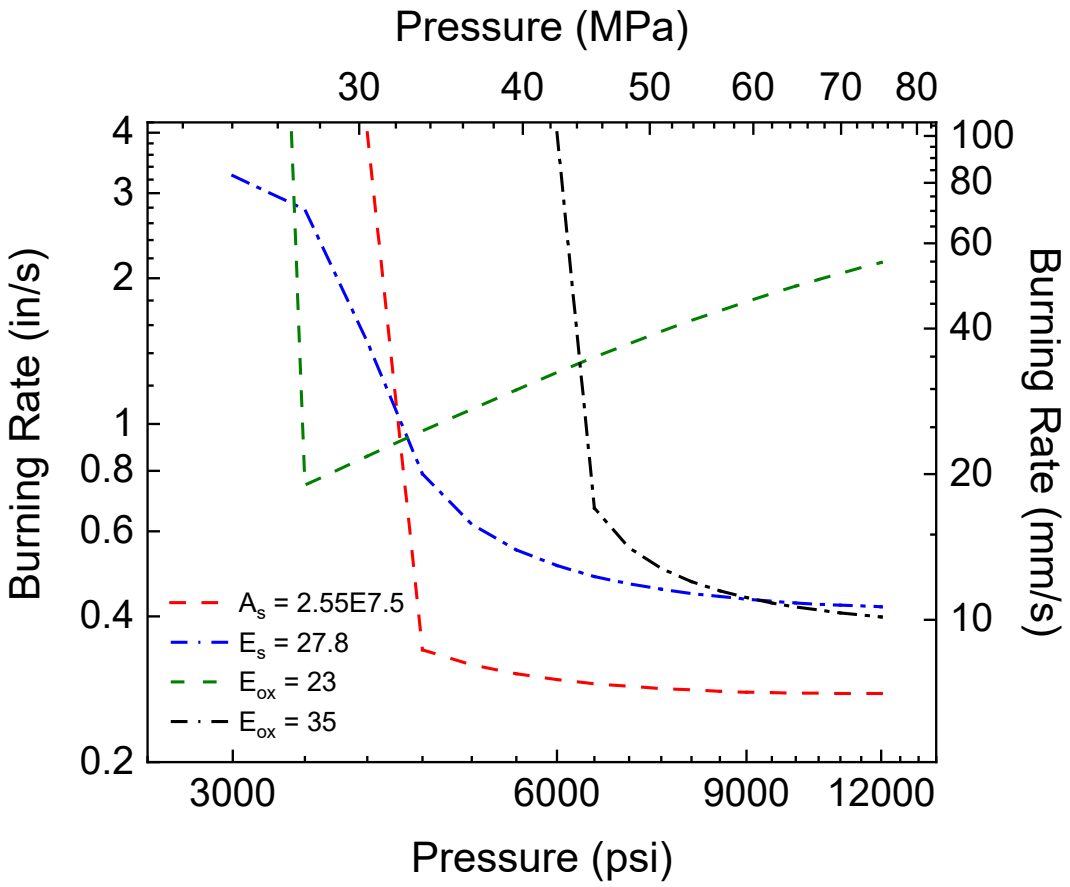

Figure 38. Model parameter values for which the Thomas et al. model breaks down, predicting unrealistic burning rates. Burning rates correspond to an 80% 210.3-μm AP propellant.

Table 5. Model-calculated energy data for an 80% 210.3μm-AP propellant burned at 5000 psi with varying parameters changed. Only the parameter listed was changed, all other parameters were kept constant (baseline values).

	β_P	Q_L	Q_{ox}	Q_{PF}
Baseline	**0.5022**	**-2.09E+05**	**1.83E+06**	**2.48E+06**
A_s = 2.55E7.51	Unrealistic (negative)	Unrealistic (extremely exothermic)	Unrealistic (negative)	Unrealistic (negative)
E_s = 27.8	Unrealistic (negative)	Unrealistic (extremely exothermic)	Unrealistic (negative)	Unrealistic (negative)
E_{ox} = 23	Unrealistic (almost one)	Unrealistic (extremely endothermic)	3.65E+06	3.93E+06
E_{ox} = 35	Unrealistic (negative)	Unrealistic (extremely exothermic)	Unrealistic (negative)	8.21E+05

*Baseline values are listed in Table B1 in Appendix B.

Overall, adjusting the parameters in Table 4 mainly affected the burning rate magnitude, either increasing it or decreasing it as seen in Fig. 39. The pressure exponent either decreased or remained the same for most parameter values. The only exception was decreasing the activation energy of the fuel decomposition reactions, E_f. As seen in Fig. 40, the pressure exponent actually increased with decreasing E_f, eventually reaching a value greater than one for the 80% 210.3μm-formulation when E_f was set to zero. This trend indicates that the fuel regression mechanism is either at its maximum reactivity or changes at pressures near the exponent break. This finding will become important when Cole's series-burning theory is evaluated in the subsequent section.

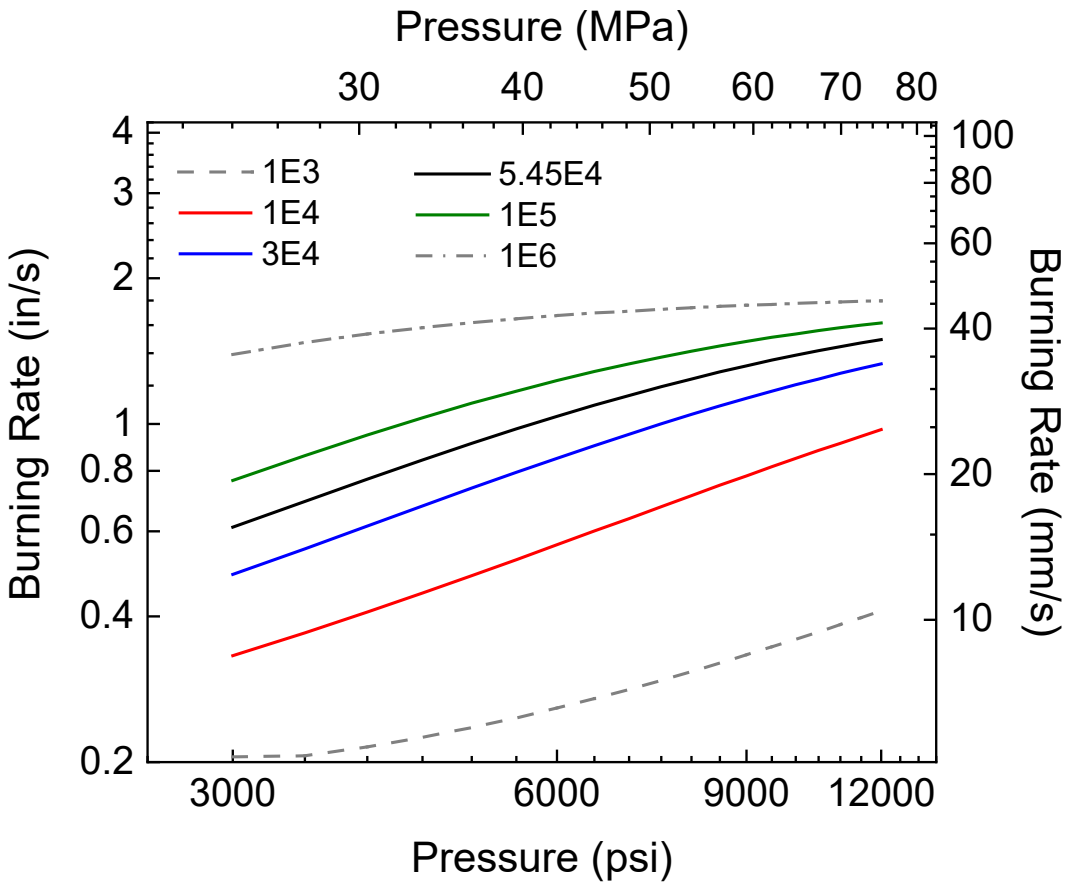

Figure 39. Effect of modifying the kinetics pre-factor of the oxidizer monopropellant flame reaction, A_{AP}, on the burning rate predictions of a formulation containing 80% 210.3-μm AP.

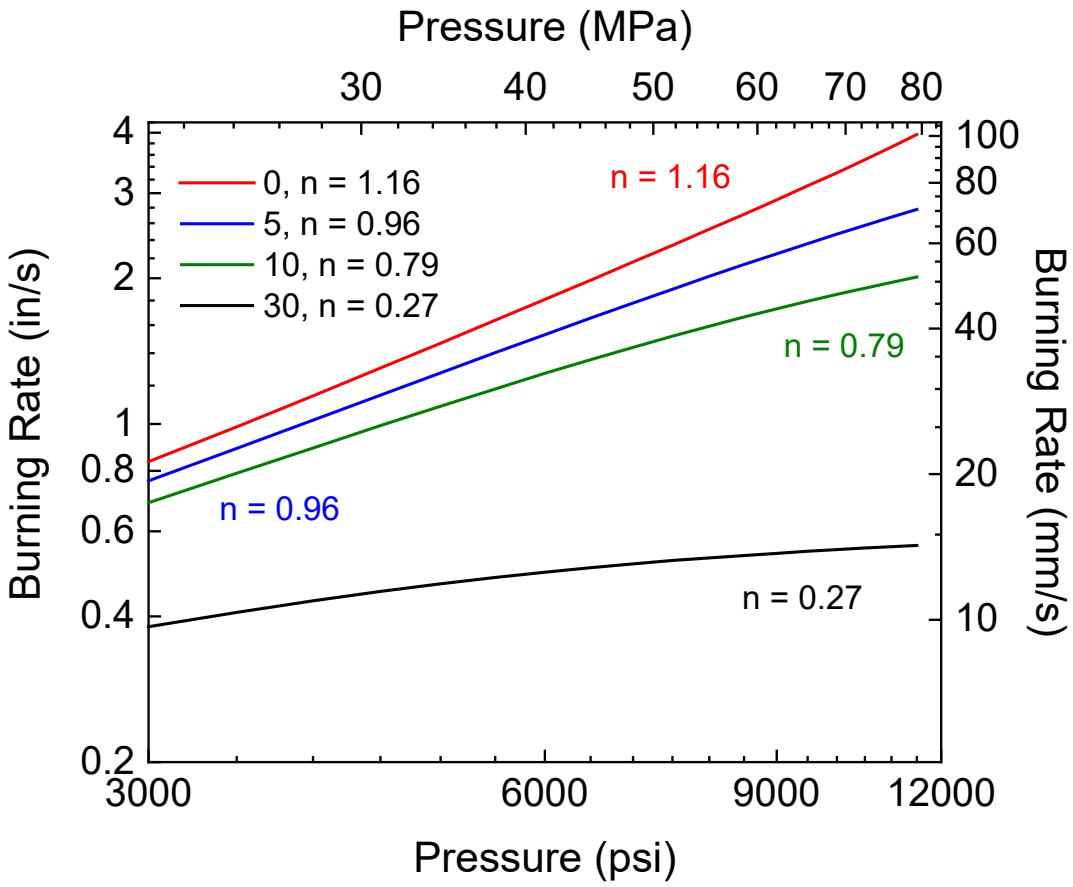

Figure 40. Effect of modifying the activation energy of the fuel surface decomposition, E_f, on the burning rate predictions of an 80% 210.3μm-AP formulation.

As seen in Fig. 41, while E_f equals zero produces pressure exponents greater than one for the 80% 210.3-μm formulation, it does not have the same effect on the finer AP particle sizes. In fact, it actually causes the effects of both particle size and concentration on the burning rates to be reversed, so the larger particles and lower concentrations burn faster than their respective counterparts as seen in Figs. 41 and 42. This feature, along with others as seen in the full sensitivity analyses for each parameter provided in Figs. 43 and 44, appears to have opposite effects on the fine and coarse AP particles,

signifying that a fundamental high-pressure mechanism related to particle size is missing in the model. Currently, the particle diameter is considered only in regards to the surface geometry. This apparent effect of AP particle size at very-high pressure suggests that either the surface geometry is changing, similar to Irwin et al.'s crack propagation theory, or that the particle size plays a greater role in one of the chemical reaction rates at high pressures.

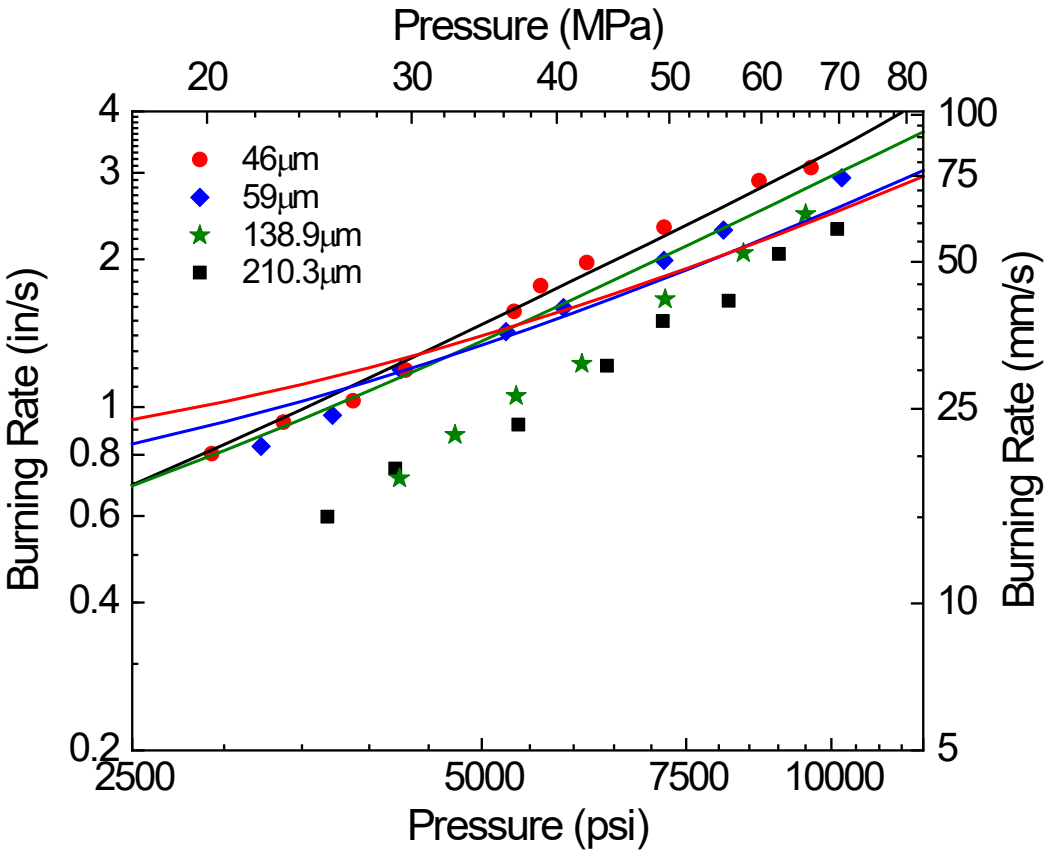

Figure 41. Effect of setting E_f equal to zero reverses the effect of particle size on the burning rates.

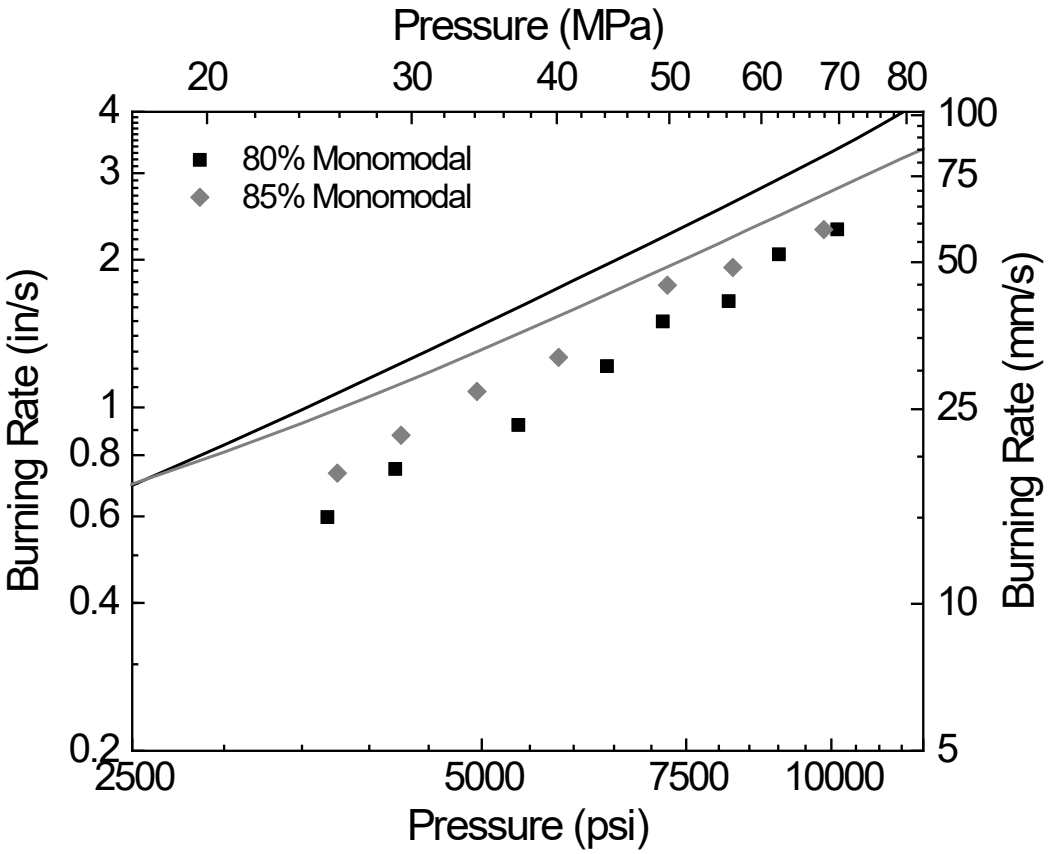

Figure 42. Effect of setting E_f equal to zero reverses the effect of AP concentration on the burning rates; so, an 85% solids loading propellant is predicted to burn slower than an 80% solids loading propellant.

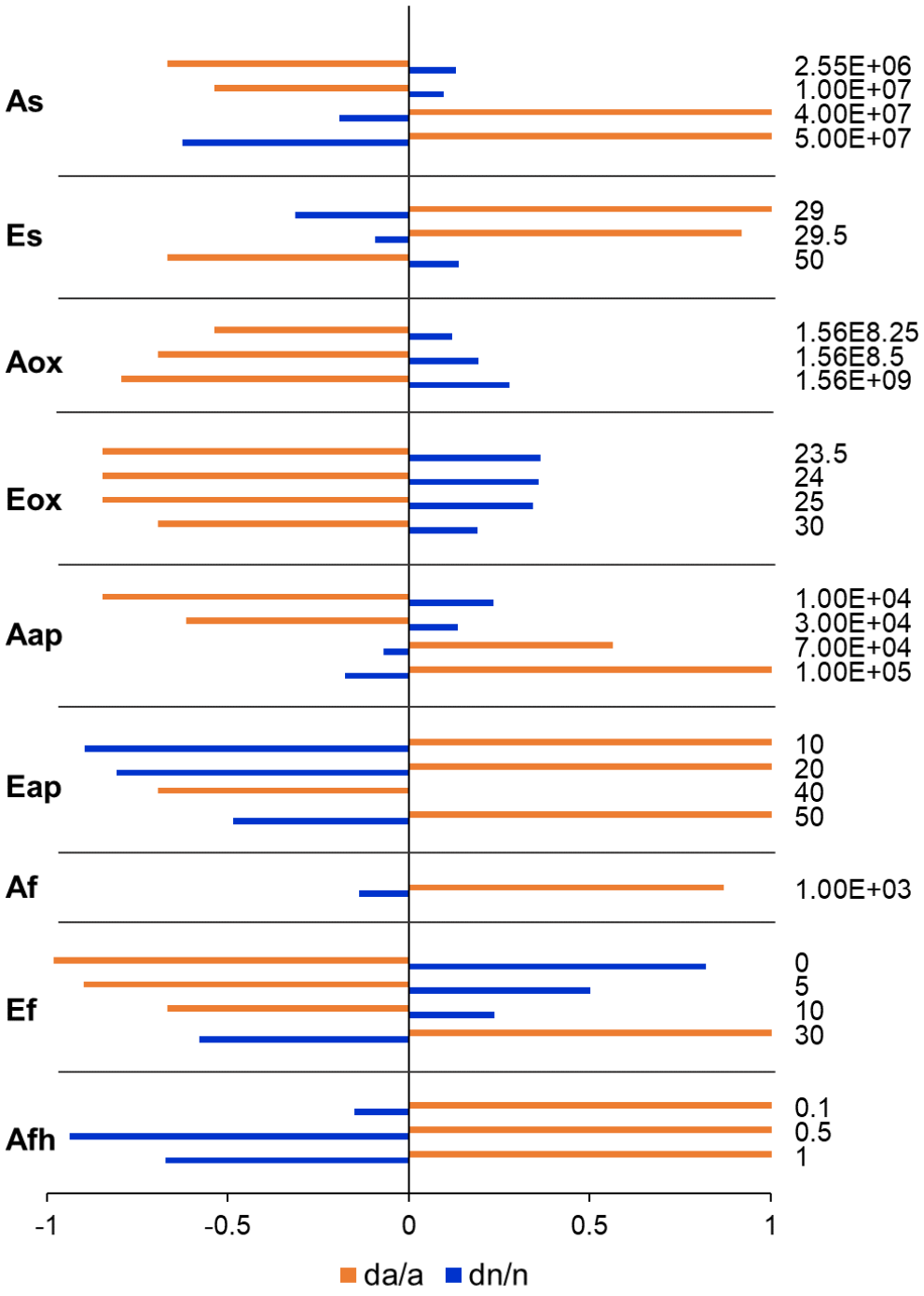

Figure 43. Sensitivity analysis of the parameters listed in Table 4 for an 80% 210.3-μm AP propellant formulation. da/a is the change in burning rate magnitude and dn/n, the change in pressure exponent. Both values are with respect to the original model parameter values seen in Table 4.

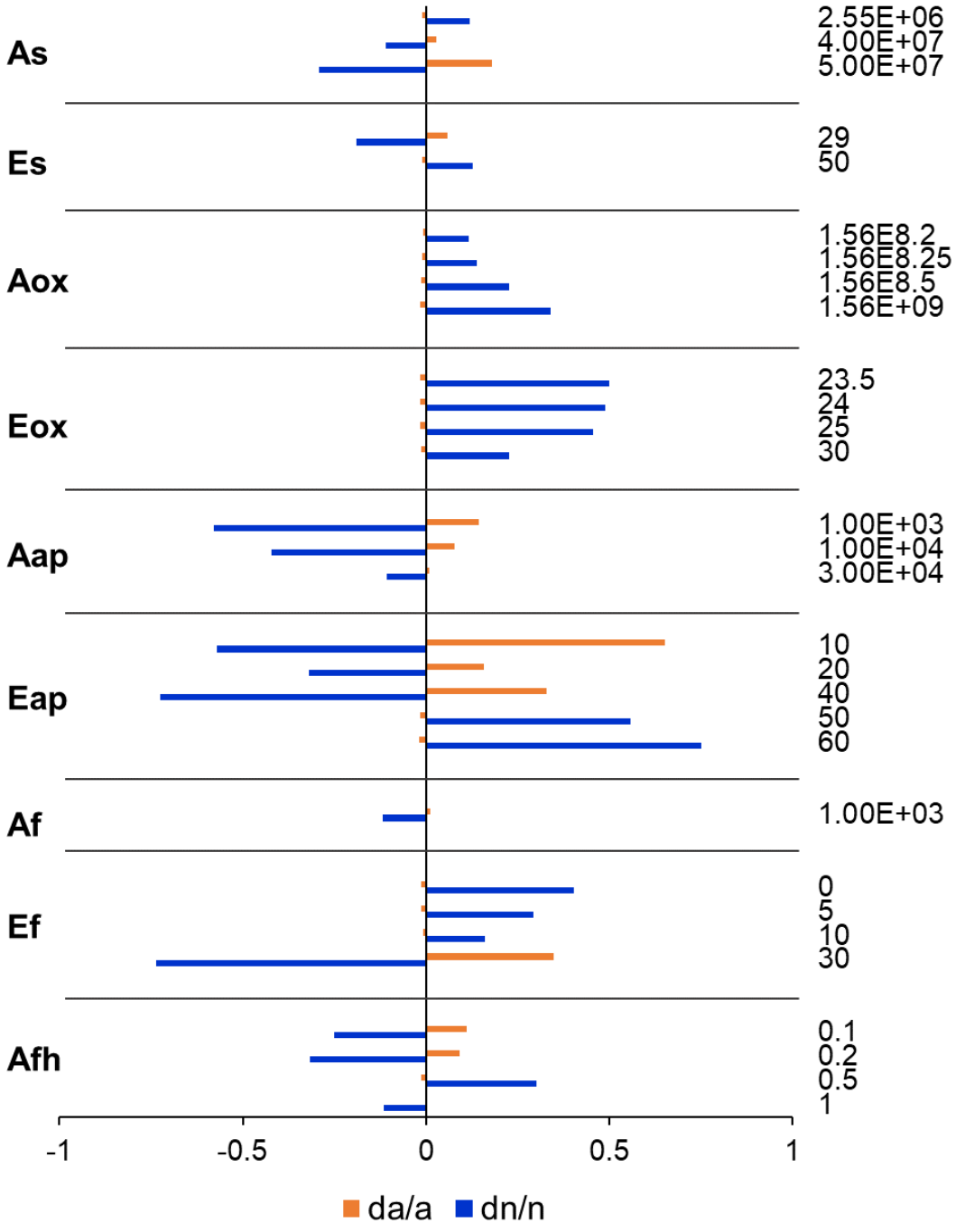

Figure 44. Sensitivity analysis of the parameters listed in Table 4 for an 80% 46-μm AP propellant formulation. da/a is the change in burning rate magnitude and dn/n, the change in pressure exponent. Both values are with respect to the original model parameter values seen in Table 4.

As evident in Figs. 43 and 44, decreasing or increasing each parameter typically has opposite effects on the burning rate magnitude, a, and pressure exponent, n. If one increases, the other decreases. Similarly, altering the parameters tends to affect the burning rate magnitude of the 210.3-µm formulation and the pressure exponent of the 46-µm formulation. As a result, to create a best-fit model for all of the high-pressure burning rates, these effects must be balanced, as changing one parameter typically has the opposite effect on the fine and coarse-AP batches.

7.2.2 High-Pressure Modeling Results

The sensitivity analyses in Figs. 43 and 44 were used to adjust the values of the parameters listed in Table 4 to create a best-fit model for the high-pressure baseline data presented in Chapter IV. To correct for the reverse particle size and concentration burning rate trends while also maintaining an increase in pressure exponent for the 138.9-µm and 210.3-µm AP batches, the average flame height factor, A_{fh}, was drastically decreased from 0.3 to 0.02 as seen in Figs. 45 and 46. This was the only parameter that corrected the burning rate trends while also maximizing the increase in pressure exponent for all of the baseline formulations. While the pressure exponents are below one for all five batches, they are extremely close, ranging from 0.97 to 0.90. Changing additional parameters only affected the burning rate magnitudes, so a maximum threshold was reached for the pressure exponents give the current mechanisms included in the Thomas et al. model. This point supports the idea that a secondary combustion mechanism not currently accounted for in composite propellant models is responsible for the exponent break and increased pressure exponents at high-pressures.

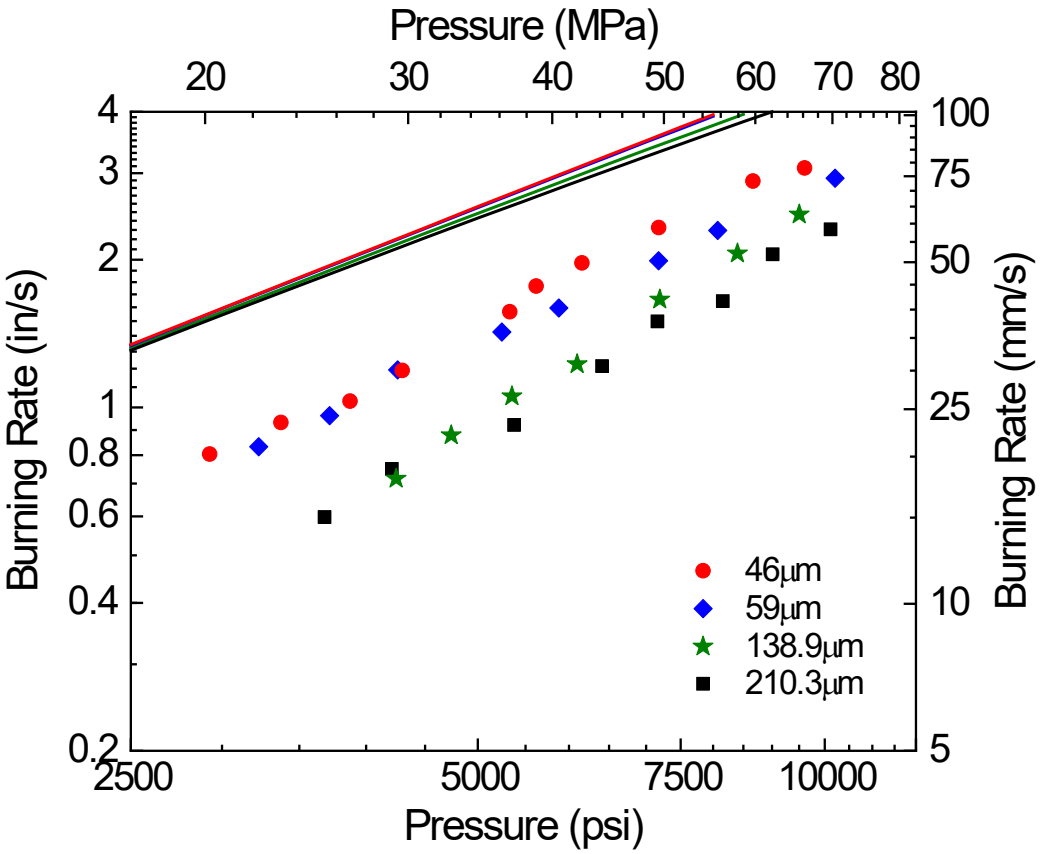

Figure 45. Significantly reducing A_{fh} corrects for the reverse trends generated by setting to zero and decreases the pressure exponents to just below one for all four particle sizes.

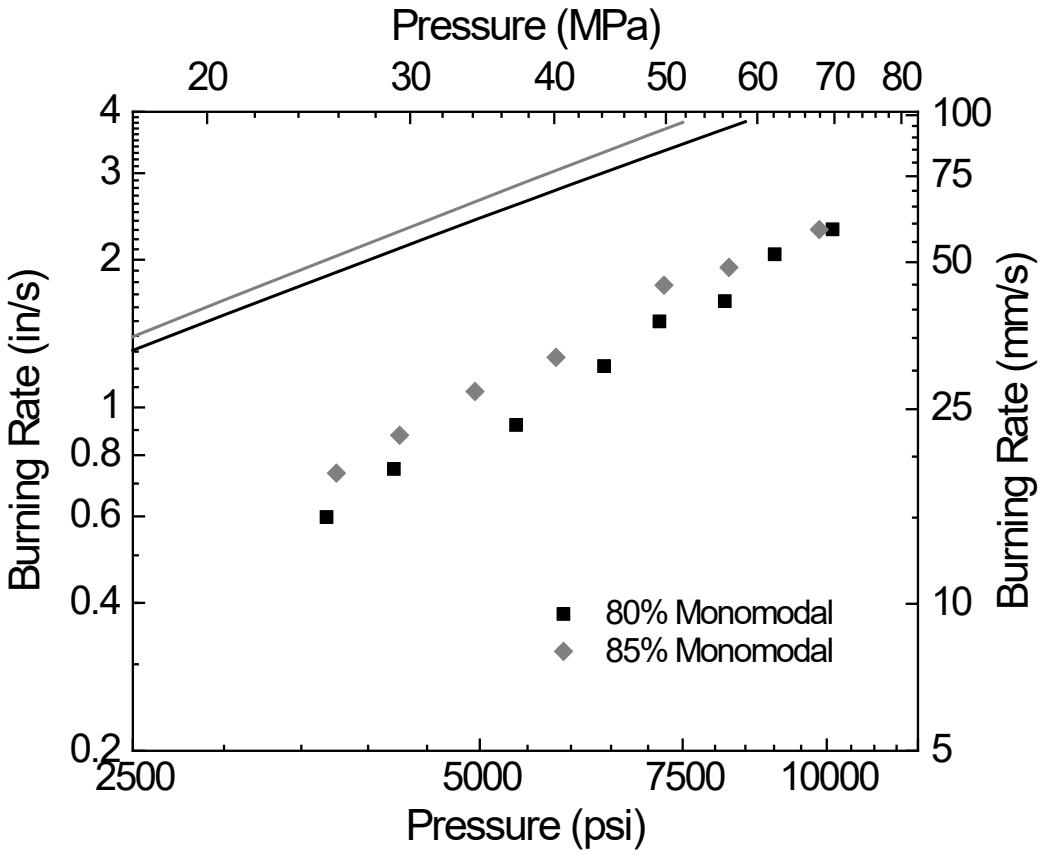

Figure 46. Significantly reducing A_{fh} corrects for the reverse trends generated by setting to zero and decreases the pressure exponents to just below one for both AP concentrations.

To adjust the burning rate magnitudes and maintain the maximum pressure exponents, Aox and E_{AP} were increased from 1.56×10^{8} to $1.56\times10^{8.5}$ and 30 to 32, respectively. A_{AP} was also decreased from 5.56×10^{4} to 1×10^{4}. Altering these parameters produced the "averaged" model predictions seen in Figs. 47 and 48. As shown in Figs. 47 and 48, the best-fit model agrees relatively well with the fine-AP batches, but significantly underpredicts the pressure exponent and moderately overpredicts the burning rate magnitude for the larger-AP particle sizes and higher AP concentration. It is

clear from the sensitivity analyses and these model results that the mechanism responsible for increasing the pressure exponent above one is not in the current composite propellant model. These results emphasize the existence of a secondary, possibly competing, physiochemical mechanism at the very-high pressures.

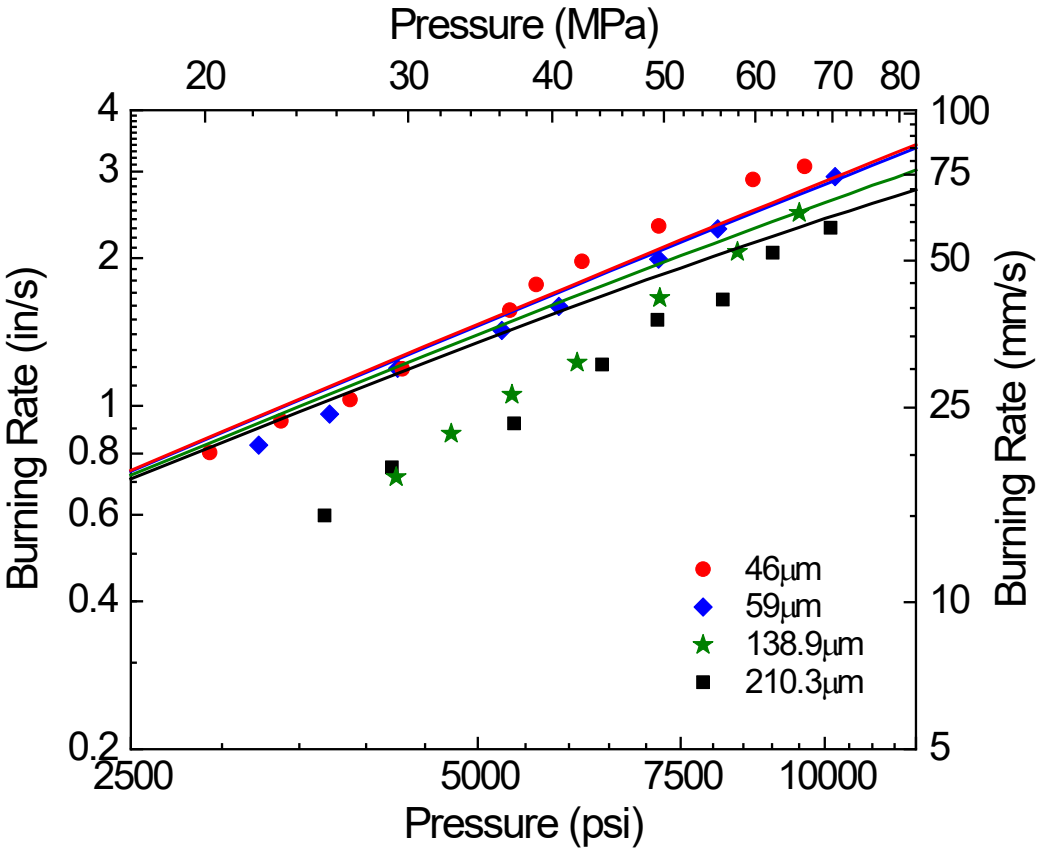

Figure 47. Model predictions with tailored parameter values compared to high-pressure particle size burning rate data. E_f was set equal to zero, A_{fh} reduced to 0.02, A_{ox} and E_{AP} increased to $1.56\times10^{8.5}$ and 32, respectively, and A_{AP} decreased to 1×10^{4} to produce the best-fit trends for all baseline formulations.

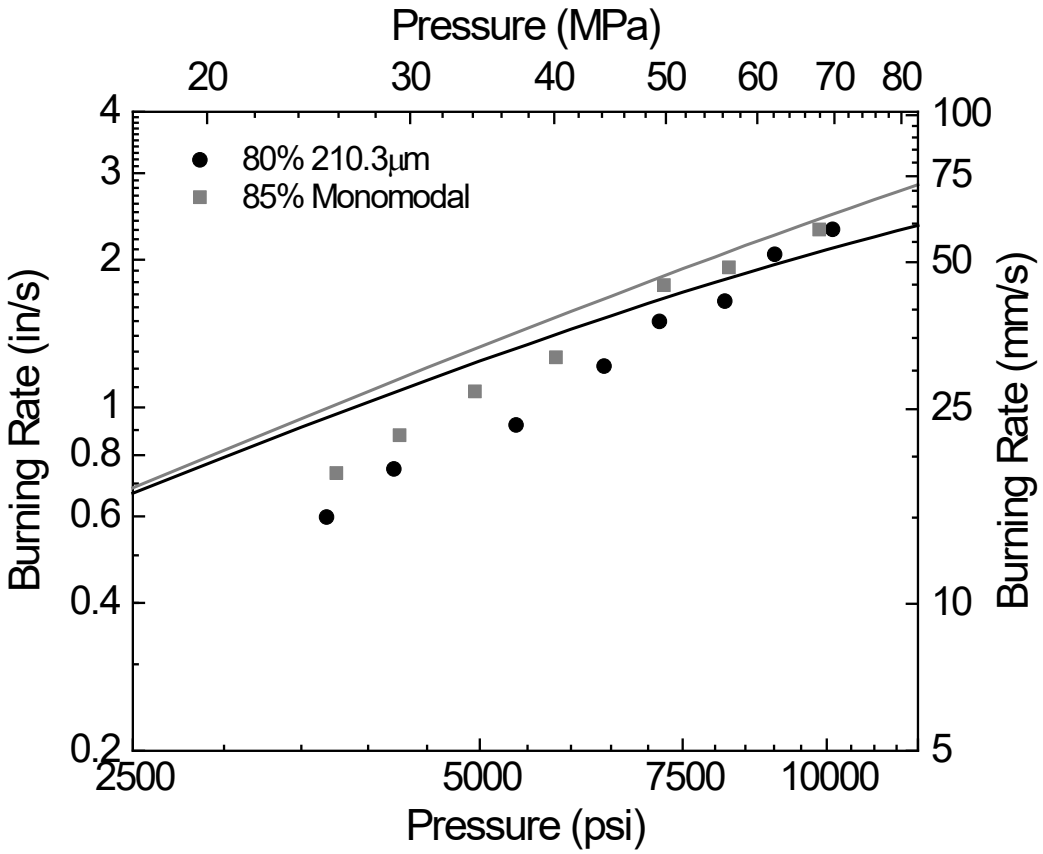

Figure 48. Model predictions with tailored parameter values compared to high-pressure AP concentration burning rate data. E_f was set equal to zero, A_{fh} reduced to 0.02, A_{ox} and E_{AP} increased to $1.56\times10^{8.5}$ and 32, respectively, and A_{AP} decreased to 1×10^{4} to produce the best-fit trends for all baseline formulations.

To represent what a potential combined low- and high-pressure model would look like with the exponent break, the modeling results with the original parameters used by Thomas et al. were combined with the modified model predictions as seen in Figs. 49 and 50 for both the AP particle size and concentration formulations. While the models intersect for the 46-µm, 59-µm, and 138.9-µm AP batches, the resulting predicted characteristic pressures are increasingly underpredicted as the particle size increases.

The predicted high-pressure burning rates do not even intersect with the predicted low-pressure burning rates for the 80% 210.3-µm formulation. The characteristic pressure is also drastically underpredicted for the 85% 210.3-µm batch.

Despite these, however, the model is still an improvement from the original at high-pressures. Both the burning rate magnitudes and pressure exponents are significantly increased, with most of the pressure exponents approaching one. Additionally, the modified model does a good job predicting the burning rates for both the 46-µm and 59-µm batches. The characteristic pressure predicted by the intersection point between the low- and high-pressure models is also close to the actual characteristic pressure, 2944 psi compared to 2974 psi. Overall, while it is evident from these results that additional work and information is needed to model the exponent break feature accurately, these modifications provide a good starting place and insight into the exponent break mechanism.

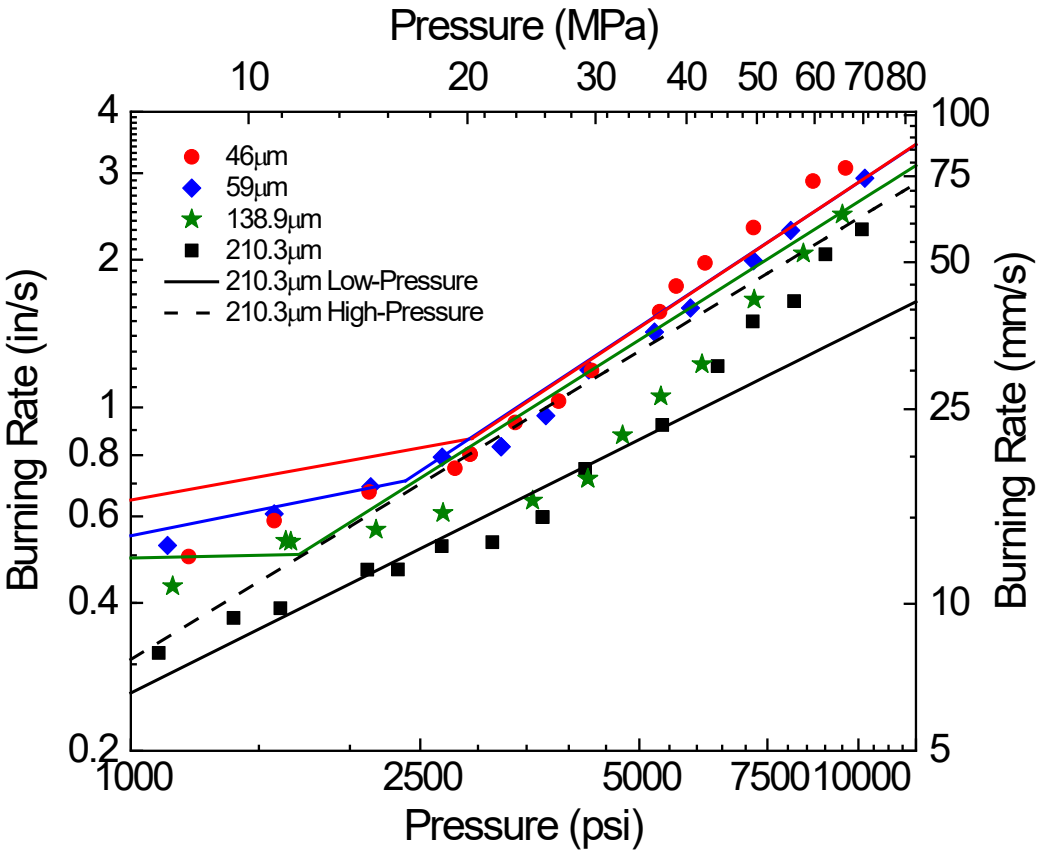

Figure 49. Thomas et al. model burning rate predictions for the propellants containing varying AP particle sizes. Original model parameters were used for the low-pressure burning rates. The model parameters were tailored to best-fit all baseline formulations.

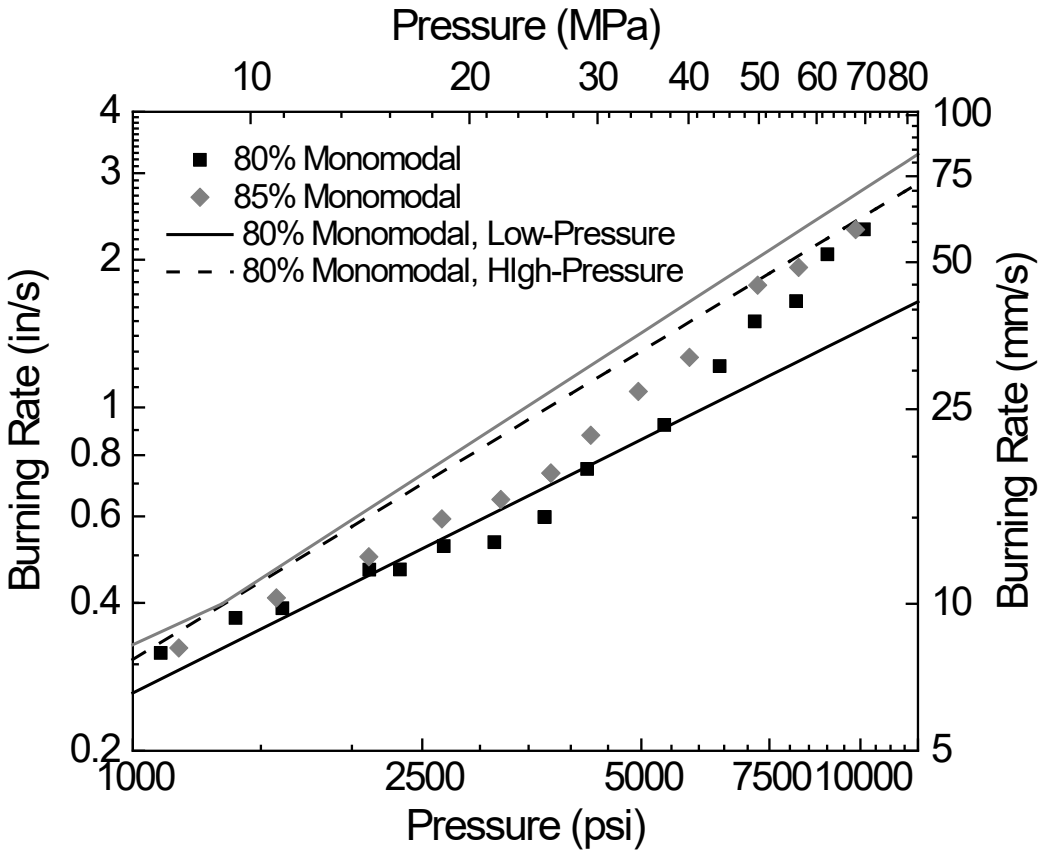

Figure 50. Thomas et al. model burning rate predictions for the propellants containing varying AP concentrations. Original model parameters were used for the low-pressure burning rates. The model parameters were tailored to best-fit all baseline formulations.

7.3 Cole's "Series-Burning"

As mentioned in the previous section, the results from the model parameter sensitivity analyses suggest that Cole's qualitative "series-burning" exponent break mechanism theory holds merit. Cole describes a new combustion mechanism where the AP particles burn out before the binder, leaving small craters and a layer of binder that must regress before the next AP particles are revealed, hence the "series-burning" [12]. As he explains, as pressure increases, the AP particle decomposition becomes more and

more independent of the binder regression. The combination of decreased mass diffusion rates and increasingly faster AP deflagration, as seen in Fig. 7, lead to localized AP decomposition, where the AP burns as a monopropellant and the binder is pyrolyzed independently. As a result, the AP particles burn completely before the binder, and binder regression rate becomes the controlling factor for the propellant burning rate; hence, binder type and reactivity matters as described in Chapter V and illustrated in Fig. 51. The particle size and concentration effects are reduced, as they primarily affect only the surface geometry and layer of remaining binder.

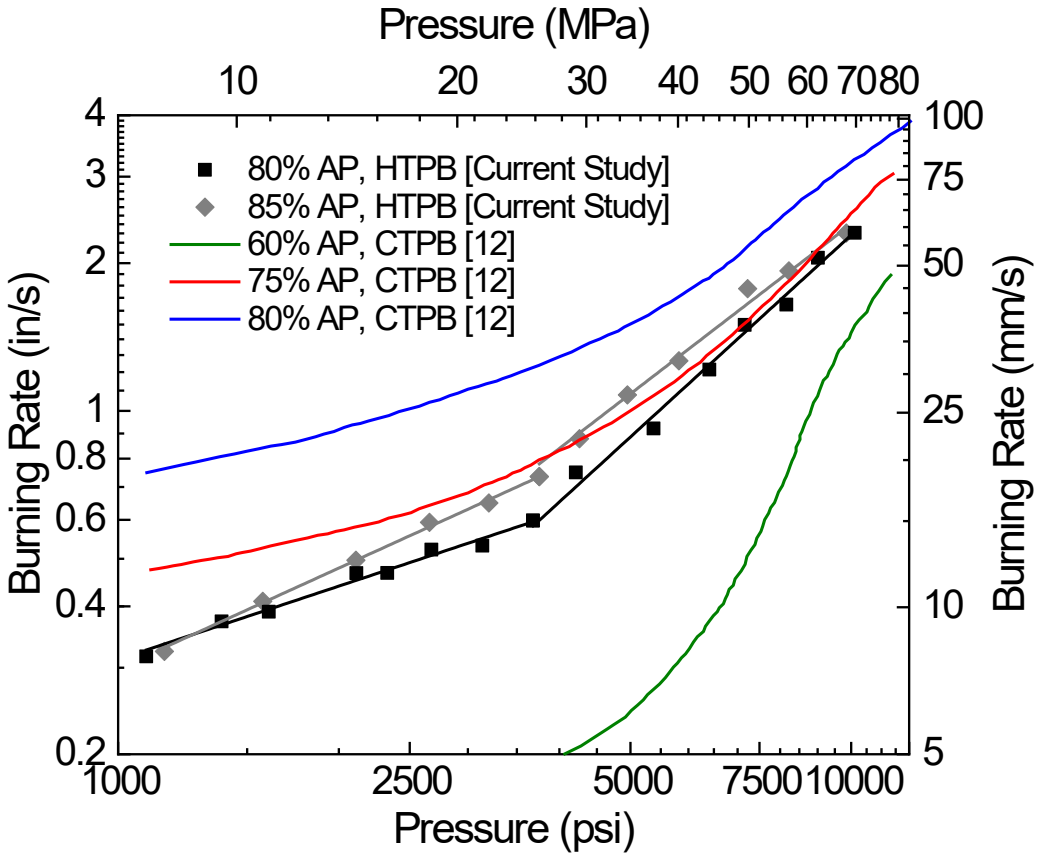

Figure 51. Effect of binder type (HTPB vs. CTPB) on the effect of AP concentration high-pressure burning rates. The CTPB burning rates were re-plotted from Cole [12].

The particle size burning rate results support this concept, as the fine-AP batches still burn faster at the higher-pressures than the coarse-AP formulations. Due to their increased surface area, the fine particles leave a thinner layer of binder behind compared to the larger AP particles after they burn. As a result, the limiting burning rate effect of the binder is reduced as the AP particle size decreases. This could also explain why altering E_f in the Thomas et al. composite propellant model significantly increased the pressure exponent for the larger AP particles, but not the smaller ones. By setting E_f equal to zero, the binder reaction rate is essentially maximized. If the binder regression rate is the controlling factor for the high-pressure burning rates, especially for the larger particles, altering the kinetic pre-factor and activation energy of the fuel reaction rate would affect the larger particles more than the smaller ones. Furthermore, the fine AP particles naturally burn faster than the coarse particles due to their increased surface area and this difference would grow as pressure increases. The fine particles, therefore, exhibit the exponent break earlier because this "series-burning" phenomenon occurs at a lower pressure for the fine particles due to their naturally higher burning rates. The leftover binder would then pyrolyze faster due to increased surface heat transfer.

"Series-burning" can also be used to explain the envelope of AP/CTPB-based formulations with varying concentrations seen in Fig. 51. After the AP particles completely burn, a thinner layer of binder will remain for the higher-AP concentration formulations, hence the increased burning rates at higher-pressures. For the AP/HTPB-based batches with varying AP concentrations, it appears the concept of "series-burning" does not fully explain the effect of AP concentration on the characteristic pressure or

high-pressure burning rates, as the characteristic pressures are extremely close and the burning rates converge around 10,000 psi. Further research is needed on the high-pressure pyrolysis of CTPB and HTPB to determine if this difference is binder or AP-related.

7.4 Other Theories and Models

Other theories previously suggested include Hermance's proposal that the exponent break in composite propellants is due to the onset of turbulence in the previously laminar fuel-oxidant flame rather than the AP decomposition flame [75-76]. Turbulence in the previously laminar fuel-oxidant flame would increase the heat transfer, potentially increasing the oxidizer and fuel reaction rates and the burning rates. This theory, however, was deemed unnecessarily complex by Summerfield due to its inclusion of processes that have not yet been proven [11]. Similarly, although Glick's model which incorporated experimentally determined burning rates and pressures into an existing combustion model, mathematically agreed with the limited amount of existing data at the time, it lacks a physiochemical reason for the exponent break [17].

Although each hypothesis holds merit, further research is still required to determine the fundamental mechanism driving the exponent break and resulting characteristic pressure. When the results herein are combined with the existing limited results from the literature and comparing with pure-AP deflagration, it is likely that the exponent break feature is a combination of physical and chemical effects related directly to a change in the dominant combustion mechanism.

7.5 Future Recommendations

To further identify the exponent break mechanism, both Irwin et al.'s geometric model and Cole's "series-burning" idea should be quantitatively modeled separately first and then potentially together to determine whether or not they can account for the increase in pressure exponent. Instead of using the high-pressure burning rates to calculate the coefficients, α and β, as was done in the current study, Irwin et al.'s model should be incorporated into an existing model that includes propellant temperature gradients and pressure-dependent diffusivities. This would provide further insight as to whether or not Irwin et al.'s model can be used to predict the characteristic pressure and high-pressure burning rates without experimental data. Lastly, as mentioned above, further research should be conducted into the high-pressure pyrolysis of HTPB to further validate or disprove Cole's "series-burning" concept. These results in combination with a model that "switches" between the AP deflagration and binder regression rates, thus simulating the "series-burning" could prove extremely helpful in narrowing down the exponent break mechanism.

CHAPTER VIII

SUMMARY AND CONCLUSIONS

Aluminized and non-aluminized AP/HTPB-composite propellants were tested at very-high pressures, up to 68.9 MPa (10,000 psi). The new data add to the relatively small database of AP-based propellant burning rates above 20 MPa. All formulations regardless of aluminum concentration, AP particle size, or distribution showed a distinct exponent or "slope" break above 20 MPa (2900 psi) and a pressure exponent greater than 1.0 after the exponent break. Decreasing the AP particle size decreased both the characteristic pressure and pressure exponent after the exponent break. The propellants with monomodal and trimodal AP distributions showed similar characteristic pressures, whereas the exponent break occurred at a slightly higher pressure for propellants with a bimodal distribution. The slight increase in AP concentration however had minimal effect on the characteristic pressure. Contrastingly, the increase in aluminum concentration from 8% to 16% significantly lowered both the characteristic pressure and pressure exponent above P*.

Overall, several corollary conclusions can be made about the behavior of AP/HTPB-composite propellant burning rates at high pressures. First and foremost, the exponent feature present in many composite propellant burning rate curves is primarily dependent on the pure-AP deflagration rate which forms an "AP barrier". This AP barrier acts as a burning rate minimum limit for AP-containing composite propellants at high pressures. Regardless of AP particle size, concentration, distribution, or catalytic

additive, the burning rates seem to fall above this AP barrier. The characteristic pressure where the exponent break occurs, however, is dependent on the AP characteristics. The minimum characteristic pressure is dictated by the baseline AP/HPTB burning rate curve and can be tailored by altering the AP particle size, distribution, or concentration. It can be increased by incorporating catalysts which serve to increase the burning rate and/or pressure exponent. This effect, however, is limited by the pressure where the additive formulation burning rate curve intersects with its respective baseline. This intersection point is the characteristic pressure; at higher pressures the catalytic effect is altered or negated entirely and the burning rate curve converges with the baseline burning rate.

In the cases of varying AP distribution and concentration, the catalytic effect is negated entirely as the burning rates all converge. These observations support the theory that AP decomposition dominates in the higher-pressure regime. Furthermore, the burning rates presented in this study corroborate the existence and suggestion in the literature of an "AP barrier", where the pure-AP deflagration rate acts as a minimum burning rate limit. Both Irwin et al.'s AP crack propagation and formation and Cole's series-burning theories regarding the exponent break appear to hold merit based on evaluation using the experimental data. Neither of these, however, fully explains the exponent break mechanism alone. Overall, while the mechanism behind the exponent break and high-pressure behavior for pure AP deflagration appears to be well-established, there are no current explanations that fully resolve the effects of binder, oxidizer characteristics, and catalysts on the exponent break and high-pressure burning

rate behavior of AP/HTPB-composite propellants. More information is required to fully describe and understand AP/HTPB high pressure burning behavior.

Ultimately, this study serves as one of the first fundamental and non-application-specific studies on the exponent break for AP/HTPB-composite propellants and fills in the gap of AP/HTPB-based propellant high-pressure burning rate data. The data herein provide a readily available and detailed set of AP/HTPB-based burning rates over a range of pressures where exponent breaks were observed in every formulation. The resulting P* values for each formulation and the trends with AP size, addition of Al, and AP concentration provide a modern data set that can be used in the ongoing study of the AP exponent break phenomenon, including detailed modeling of the heterogeneous propellant combustion.

REFERENCES

[1] N. Kubota, Survey of rocket propellants and their combustion characteristics, Fundamentals of Solid-Propellant Combustion (1984) 1-52.

[2] G. Sutton, O. Biblarz, Rocket Propulsion Elements, 9th ed., John Wiley & Sons, New York, 2017.

[3] R. Friedman, R.G. Nugent, Deflagration of AP, Proc. Combust. Inst. 5 (1955) 612-18.

[4] J.B. Levy, R. Friedman, Further studies of pure ammonium perchlorate deflagration, Proc. Combust. Inst. 8 (1962) 663-72.

[5] A.P. Glaskova, Effect of pressure on the combustion rate of ammonium perchlorate, Russ. J. Appl. Phys. 5 (1963) 193-202.

[6] O. R. Irwin, P. K. Salzman, W. H. Andersen, Deflagration characteristics of ammonium perchlorate at high pressures, Proc. Combust. Inst 9 (1963) 356-365.

[7] V.K. Bobolev, A.P. Glazkova, A.A. Zenin, O.I. Leypunskii, A study of the temperature distribution in the combustion of ammonium perchlorate, Russ. J. Appl. Phys. 3 (1964) 153-58.

[8] T.L. Boggs, Deflagration rate, surface structure, and subsurface profile of self-deflagrating single crystals of ammonium perchlorate, AIAA J. 8 (1970) 867-73.

[9] A. I. Atwood, T. L. Boggs, P. O. Curran, T. P. Parr, D. M. Hanson-Parr, C. F. Price, J. Wiknich, Burning rate of solid propellant ingredients, part 1: pressure and initial temperature effects, J. Prop. Power 15(6) (1999) 740-747.

[10] E. D. Petersen, F. Rodriguez, C. A. M. Dillier, J. C. Thomas, E. L. Petersen, Combustion behavior of ammonium perchlorate at high pressures, 2019 AIAA Propulsion and Energy 2019 Forum, AIAA Paper 2019-4366 (2019).

[11] K. P. Hall, J. Wenograd, R. Cole, Burning rate control factors in solid propellants, Princeton University, Aeronautical Engineering Report Nos. 445 k&l, 1962.

[12] R. B. Cole, Burning rates of solid composite propellants at pressures up to 20,000 psig (U), Rohm and Hass Company Redstone Arsenal Research Division, 1966.

[13] E. A. Glascoe, N. Tan, High pressure burn rate measurements on an ammonium

perchlorate propellant, Lawrence Livermore National Laboratory, LLNL-TR-428515, (2010).

[14] J. Kanelbaum, H. Apped, S. Dadon, Y. Goldstein, T. Ovadia, J. Shefler, High-Pressure Combustion of Composite Propellants, European Conference for Aeronautics and Space Sciences, 2011.

[15] A.I. Atwood, K.P. Ford, C.J. Wheeler, High-pressure burning rate studies of solid rocket propellants, Prog. Propuls. Phys. 4 (2013) 3-14.

[16] R. B. Cole, Combustion of solid propellants at high pressures – a survey, Report No. S-71, Rohm and Haas Company Redstone Arsenal Research Division, 1965.

[17] R. L. Glick, Exponent breaks in composite solid propellants, J. Spacecraft 12 (3) (1975) 185-187.

[18] E. W. Price, History of solid rocket motors (1940-1960), AIAA Paper 98-3978 (1998).

[19] P. W. M. Jacobs, H. M. Whitehead, Decomposition and combustion of ammonium perchlorate, Chemical Reviews, 69 (4) (1969) 551-590.

[20] K. Kishore, G. Prasad, A Review on decomposition/deflagration of oxidizer and binder in composite solid propellants, Defence Science Journal 29 (1979) 39-54.

[21] T. B. Brill, B. T. Budenz, Flash pyrolysis of ammonium perchlorate-hydroxyl terminated-polybutadiene mixtures including selected additives, Solid Propellant Chemistry, Combustion, and Motor Interior Ballistics (2000) 3-32.

[22] V. V. Boldyrev, Review – thermal decomposition of ammonium perchlorate, Thermochimica Acta 443 (2006) 1-36.

[23] S. M. Peiris, G. I. Pangilinan, T. P. Russell, Structural properties of ammonium perchlorate compressed to 5.6 GPa, J. Phys. Chem. 104 (47) (2000) 11188-11193.

[24] G. B. Manelis, V. A. Strunin, The mechanism of ammonium perchlorate burning, Combust. Flame 17 (1971) 69-77.

[25] S. Ramamurthy, P. G. Shrotri, Catalytic decomposition of ammonium perchlorate, J. Energetic Materials 14 (2) (1966) 97-126.

[26] G. B. Manelis, V. A. Strunin, Mechanism and elementary theory of burning of the composite solid propellants, Proc. Combust. Inst. 11 (1975) 97-104.

[27] C. U. Pittman, Location of action of burning-rate catalysts in composite propellant combustion, AIAA J. 7 (2) (1969) 328-344.

[28] H. Osada, N, Kakinouchi, Initiation of ignition of solid composite propellants, Kogyo Kayaku Kyokaishi 26 (1965) 200-211.

[29] J.D. Hightower, E. W. Price, Combustion of ammonium perchlorate, Proc. Combust. Inst. 9 (1963) 463-472.

[30] D. M. Watt., E. E. Petersen, Deflagration and deflagration limits of single crystals of ammonium perchlorate, AFOSR Scientific Report, AF-AFOSR (1968) 959-965.

[31] D. M. Watt, E. E. Petersen, The deflagration of single crystals of ammonium perchlorate, Combust. and Flame 14 (3) (1970) 297-302.

[32] E. E. Hackman, H. C. Beachell, Combustion characteristics of crystalline oxidizers, AIAA J. 6 (3) (1968).

[33] T. L. Boggs, K. J. Krauetle, Decomposition and deflagration of ammonium perchlorate, Naval Weapons Center, China Lake, CA, AD 842095 (1968).

[34] T. L. Boggs, Deflagration rate, surface structure, and subsurface profile of self-deflagrating single crystals of ammonium perchlorate, AIAA J. 8 (5) (1970) 867-873.

[35] T. L. Boggs, D. E. Zurn, D. W. Netzer, Ammonium perchlorate combustion: effects of sample preparation; ingredient type, and pressure, temperature and acceleration environments, Combust. and Flame 7 (1973) 177-183.

[36] T. L. Boggs, K. J. Kraeutle, D. E. Zurn, Decomposition, pyrolysis, and deflagration of pure and isomorphously doped ammonium perchlorate, AIAA J. 10 (1) (1972) 15-16.

[37] C. Price, T. Boggs, R. Derr, Modeling of solid monopropellant deflagration, AIAA 16th Aerospace Sciences Meeting, AIAA Paper 78-219 (1978).

[38] G. Lengelle, J. Duterque, J. F. Trubert, Physico-chemical mechanisms of solid propellant combustion, Solid Propellant Chemistry, Combustion, and Motor Interior Ballistics (2000) 287-334.

[39] M. L. Gross, M. W. Beckstead, Diffusion flame calculations for composite propellants using a vorticity-velocity formulation, J. Prop. Power 25 (1) (2009) 74-82.

[40] M. W. Beckstead, Overview of combustion mechanisms and flame structures for advanced solid propellants, Solid Propellant Chemistry, Combustion, and Motor Interior Ballistics (2000) 267-285.

[41] M. W. Beckstead, R. L. Derr, C. F. Price, A model of composite solid-propellant combustion based on multiple flames, AIAA J. 8 (12) (1970) 2200-2207.

[42] M. W. Beckstead, Recent progress in modeling solid propellant combustion, Combust. Explosion Shock Waves 42 (6) 2006 623-641.

[43] T. L. Jackson, Modeling of heterogeneous propellant combustion: a survey, AIAA J. 50 (5) (2012) 993-1006.

[44] R. R. Miller, Anomalous ballistic behavior of reduced smoke propellants with wide AP distributions, 15th JANNAF Combustion Meeting (2) 297 (1979) 265-269.

[45] R. R. Miller, Ballistic control of solid propellants, vol. 1 – experimental results and analysis, U.S. Air Force Rocket Propulsion Lab, TR-81-058 (1982).

[46] R. L. Foster, R. R. Miller, The influence of the fine AP/binder matrix on composite propellant ballistic properties, 17th JANNAF Combustion Meeting 3 (329) (1980) 91-104.

[47] R. L. Foster, J. A. Condon, R. J. Dale, Low exponent technology, U.S. Air Force Rocket Propulsion Lab., TR-82-060 (1982).

[48] M. K. King, Model for steady state combustion of unimodal composite solid propellants, AIAA Paper 78-216 (1978).

[49] C. W. Fong, R. F. Smith, The relationship between plateau burning behavior and ammonium perchlorate particle size in HTPB/AP composite propellants, Combust. Flame, 67 (3) (1987) 235-247.

[50] M. K. King, Experimental and theoretical study of the effects of pressure and crossflow velocity on composite propellant burning rate, Proc. Combust. Inst. 18 (1) (1981) 207-216.

[51] R. Bellec, J. Duterque, G. Lengelle, Modeling of aluminized solid propellants, ONERA, TR 37/7128 EN (1996).

[52] E. Rochford, *Temperature sensitivity measurements of solid rocket propellants*, M.S.E. Thesis, The University of Alabama, Huntsville, AL 1999.

[53] S. Hayakawa, M. Tanaka, C. Nakao, An effect of oxidizer particle size on combustion stability in composite propellants, 36th AIAA/ASME/SAE/ASEE Joint Propulsion Conference & Exhibit, AIAA Paper 2000-3700 (2000).

[54] R. Frederick, J. R. Osborn, Ballistic studies of wide distribution propellants, 36th AIAA/ASME/SAE/ASEE Joint Propulsion Conference & Exhibit, AIAA Paper 2000-3700 (2000).

[55] M. Kohga, Burning characteristics and thermochemical behavior of AP/HTPB composite propellant using coarse and fine AP particles, Prop. Explosives. Pyrotechnics 36 (1) (2011) 57-64.

[56] S. Isert, T. L. Connell, G. A. Risha, T. D. Hedman, R. P. Lucht, R. A. Yetter, S. F. Son, Near-surface flame structure and characterization of simplified ammonium perchlorate/hydroxyl-terminated polybutadiene compositions, Combust. Flame. 164 (2016) 201-211.

[57] S. Isert, T.D. Hedman, R. P. Lucht, S. F. Son, Oxidizer coarse-to-fine ratio effect on microscale flame structure in a bimodal composite propellant, Combust. Flame (163) (2016) 406-413.

[58] S. Isert, S. F. Son, The relationship between flame structure and burning rate for ammonium perchlorate composite propellants, Energetic Materials (2017).

[59] M. L. Gross, M. W. Beckstead, Diffusion flame calculations for composite propellants predicting particle-size effects, Combust. Flame 157 (2010) 864-873.

[60] M. L. Gross, M. W. Beckstead, Steady-state combustion mechanisms of ammonium perchlorate composite propellants, J. Prop. Power 27 (5) (2011) 1064-1078.

[61] E. W. Price, R. K. Sigman, Combustion of aluminized solid propellants, Solid Propellant Chemistry, Combustion, and Motor Interior Ballistics (2000) 663-687.

[62] Y. Chen, D. R. Guildenbecher, K. N. G. Hoffmeister, M. A. Cooper, H. L. Stauffacher, M. S. Oliver, E. B. Washburn, Study of aluminum particle combustion in solid propellant plumes using digital in-line holography and imaging pyrometry, Combust. Flame 182 (2017) 225-237.

[63] L. T. DeLuca, Burning of aluminized solid rocket propellants: from micrometric to nanometric fuel size, Theory and Practice of Energetic Materials 7 (2007) 277-289.

[64] M. W. Beckstead, A summary of aluminum combustion, RTO/VKI Special Course on Internal Aerodynamics in Solid Rocket Propulsion, RTO-EN-023-5 (2002) 1-46.

[65] R. A. Yetter, G. A. Risha, S. F. Son, Metal particle combustion and nanotechnology, Proc. Combust. Inst. 32 (2009) 1819-1838.

[66] Q. Yan, F. Zhao, K. K. Kuo, X. Zhang, S. Zeman, L. T. DeLuca, Catalytic effects of nano additives on decomposition and combustion of RDX-, HMX-, and AP-based energetic compositions, Prog. Energy Combust. Sci. 57 (2016) 75-136.

[67] A. Han, J. Liao, M. Ye, Y. li, X. Peng, Preparation of nano $MnFe_2O_3$ and its catalytic performance of thermal decomposition of ammonium perchlorate, Chin. J. Chem. Eng. 19 (6) (2011) 1047-51.

[68] K. Fujimura, A. Miyake, The effect of specific surface area of TiO_2 on the thermal decomposition of ammonium perchlorate, J. Therm. Anal. Calorim. 99 (1) (2010) 27-31.

[69] D. L. Reid, A. E. Russo, R. V. Carro, M. A. Stephens, A. R. LePage, T.C. Spalding, E. L. Petersen, S. Seal, Nanoscale additives tailor energetic materials, Nano Lett. 7 (7) (2007) 2167-61.

[70] M. Stephens, T. Sammet, R. Carro, A. LePage, D. Reid, S. Seal, E. L. Petersen, New additives for modifying the burn rate of composite solid propellants, AIAA Paper 2006-4948 (2006).

[71] D. L. Reid, R. Draper, D. Richardson, A. Demko, T. Allen, E. L. Petersen, S. Seal, In situ synthesis of polyurethane-TiO2 nanocomposite and performance in solid propellants, J. Mater. Chem. A. 2 (7) (2014) 2313-22.

[72] A. R. Demko, T. W. Allen, C. Dillier, T. Sammet, E. L. Petersen, D. L. Reid, S. Seal, Temperature sensitivity of composite propellants containing novel nano-additive catalysts, J. Propul. Power 34 (3) (2018) 795-807.

[73] O. R. Irwin, P. K. Salzman, W. H. Andersen, Mechanism of accelerated burning of ammonium perchlorate at high pressures, AIAA J. (1963) 1178-1180.

[74] C. K. Bastress, Modification of the burning rates of ammonium perchlorate solid propellants by particle size control, Ph. D. Dissertation, Aeronautical Engineering Dept., Princeton Univ. (1961).

[75] C. E. Hermance, A model of composite propellant combustion including surface heterogeneity and heat generation, AIAA J. 4 (1966) 1629-1637.

[76] C. E. Hermance, A detailed model of the combustion of composite solid propellants, Proc. 2nd ICRPG/AIAA Solid Propulsion Conference (1967).

[77] T. W. Allen, A. R. Demko, M. Johnson, T. Sammet, E. L. Petersen, D. L. Reid, R. Draper, S. Seal, Laboratory-scale burning of composite solid propellant for studying novel nanoparticle synthesis methods, 51st AIAA Aerospace Sciences Meeting, AIAA SciTech Forum, 2013.

[78] J. C. Thomas, A. R. Demko, T. E. Sammet, D. L. Reid, S. Seal, E. L. Petersen, Mechanical properties of composite AP/HTPB propellants containing novel titania nanoparticles, Propellants Explos. Pyrotech. 41 (2016) 822-834.

[79] A. R. Demko, C. Dillier, T. Sammet, E. L. Petersen, D. L. Reid, S. Seal, Ignition delay times of composite solid propellants using novel nano-additive catalysts, J. Propul. Power 34 (5) (2018) 1285-1296.

[80] M. Stephens, T. Sammet, R. Carro, A. Lepage, E. L. Petersen, Comparison of hand and mechanically mixed AP/HTPB solid composite propellants, 43rd AIAA/ASME/SAE/ASEE Joint Propulsion Conference & Exhibit, 2007.

[81] R. V. Carro, High pressure testing of composite solid rocket propellant mixtures: burner facility characterization, MS Thesis, Mechanical Engineering Dept., Univ. of Central Florida (2007).

[82] K. Kreitz, Catalytic nanoparticle additives in the combustion of AP/HTPB composite solid propellant, MS Thesis, Mechanical Engineering Dept., Texas A&M Univ. (2010).

[83] C. A M. Dillier, A. R. Demko, J. M. Stahl, T. Sammet, E. L. Petersen, Temperature sensitivity of AP/HTPB-based rocket propellants using a new high-pressure strand burner, 55th AIAA Aerospace Sciences Meeting, AIAA SciTech Forum, 2017.

[84] J. C. Thomas, G. R. Morrow, C. A. M. Dillier, E. L. Petersen, Comprehensive study of AP particle size and loading effects on the burning rates of composite AP/HTPB propellants, AIAA Paper 2018-4874, 54th AIAA/ASME/SAE/ASEE Joint Propulsion Conference, 2018.

[85] M. L. Gross, T. D. Hedman, S. F. Son, T. L. Jackson, and M. W. Beckstead, Coupling micros and meso-scale models of AP/HTPB propellants, Combust. Flame 160 (5) (2013) 982-992.

[86] J. C. Thomas and E. L. Petersen, Updated three-flame modeling of composite AP/HTPB propellants, 27th ICDERS, 2019.

[87] G. Kosiba, Multidimensional modeling of composite solid propellant combustion, Ph. D. Dissertation, Mechanical Engineering Dept., Rensselaer Polytechnic Institute (2017).

[88] C. Frazier, Modeling solid propellant strand burner experiments with catalytic nanoparticle additives, Ph. D. Dissertation, Mechanical Engineering Dept., Texas A&M Univ. (2011).

[89] J. Kalman, T. Hedman, B. Varghese, and G. Dagliyan, Nano-computed tomographic measurements of partially decomposed ammonium perchlorate particles, Propellants Explos. Pyrotech. 42 (9) (2017) 1111-1116.

[90] M. W. Beckstead, A model for solid propellant combustion, Proc. Combust. Inst. 18 (1) (1981) 175-185.

APPENDIX A

CDF CURVES FOR AP PARTICLE SIZE DISTRIBUTIONS

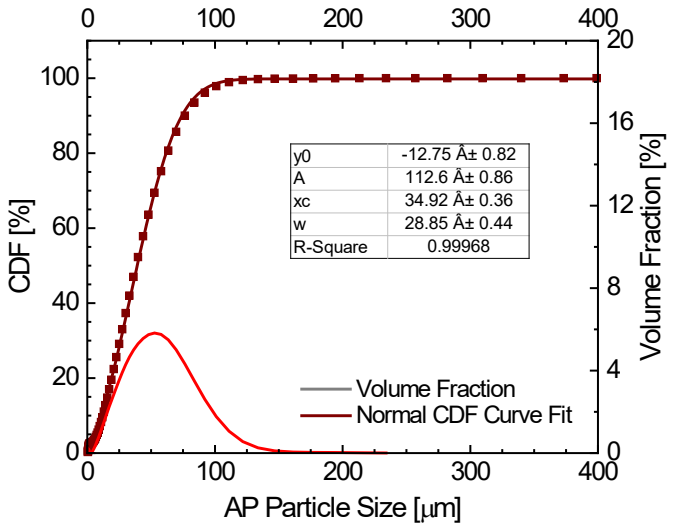

Figure A1. CDF curve for 46μm-AP particle size distribution.

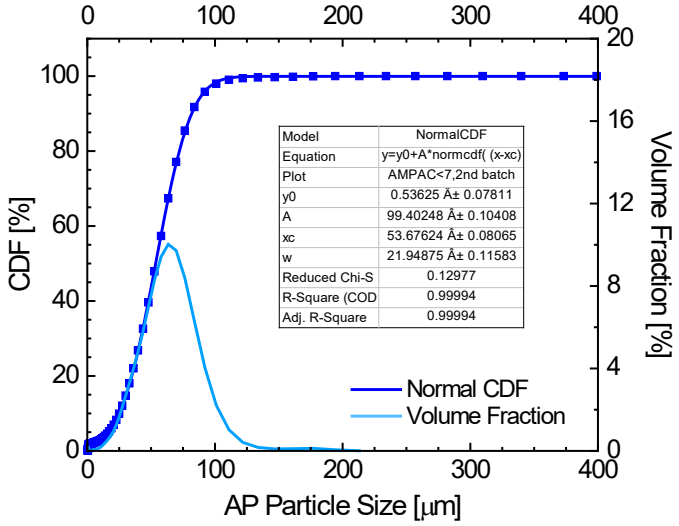

Figure A2. CDF curve for 59um-AP particle size distribution.

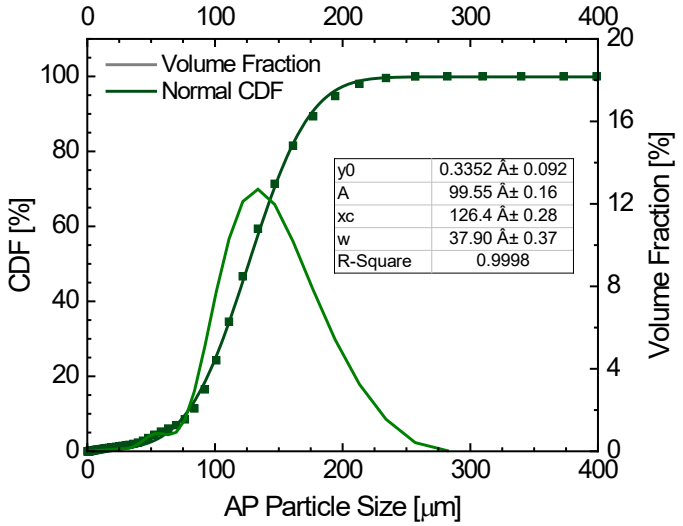

Figure A3. CDF curve for 138.9µm-AP particle size distribution.

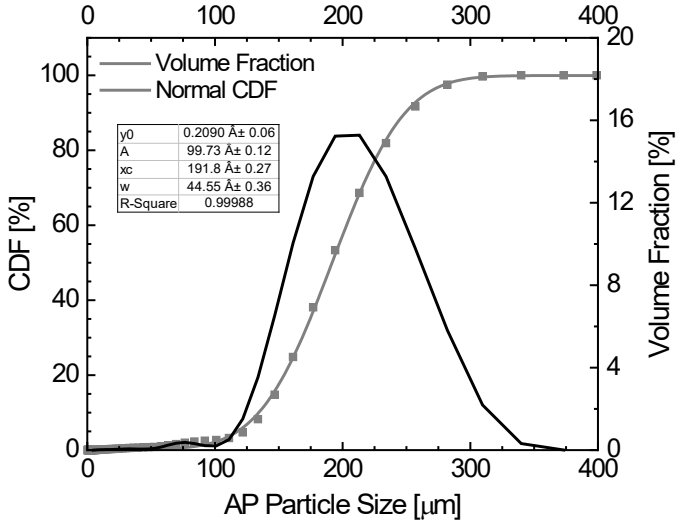

Figure A4. CDF curve for 210.3µm-AP size distribution.

APPENDIX B

SUPPLEMENTARY PLOTS

B.1 Irwin et al.'s Geometric Model

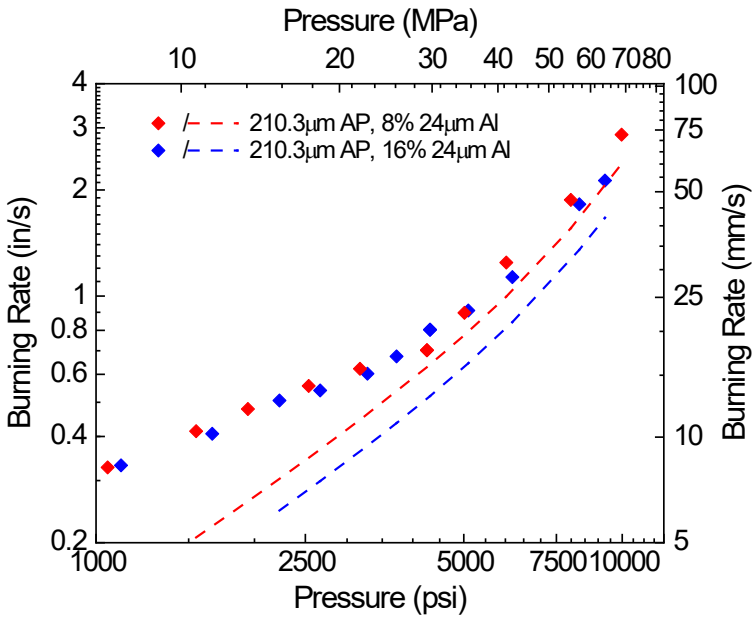

Figure B1. Comparison of Irwin's model burning rate predictions to experimental burning rates for aluminized formulations [6].

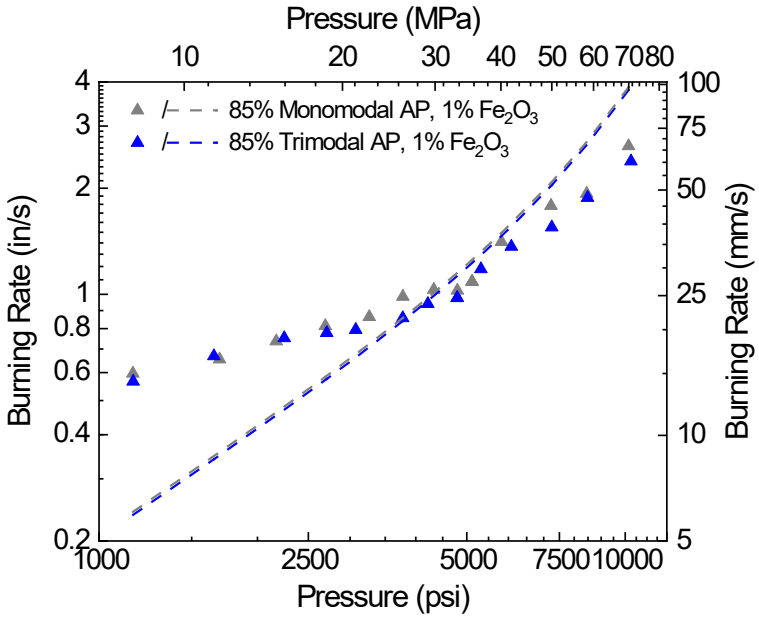

Figure B2. Comparison of Irwin's model burning rate predictions to experimental burning rates for formulations containing MACH I iron oxide and varying AP distributions [6].

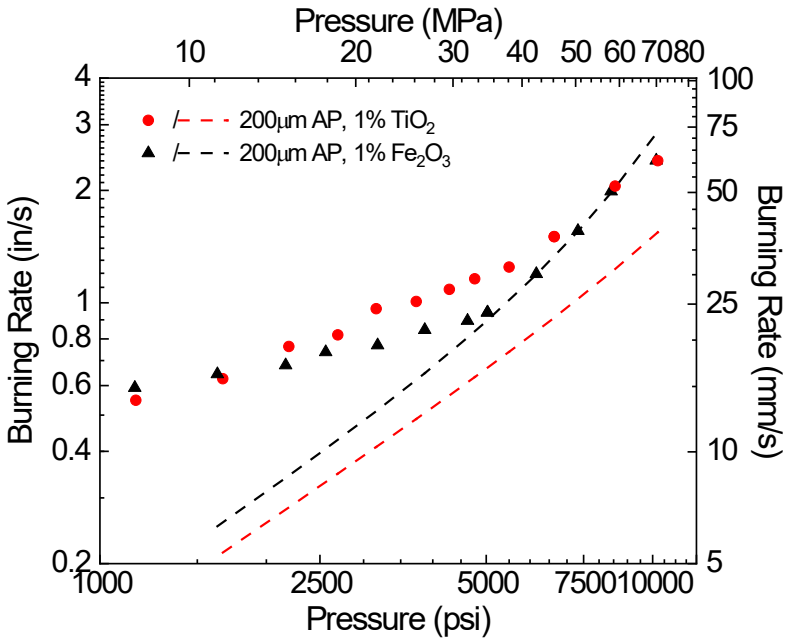

Figure B3. Comparison of Irwin's model burning rate predictions to experimental burning rates for formulations containing 200µm AP and MACH I additives [6].

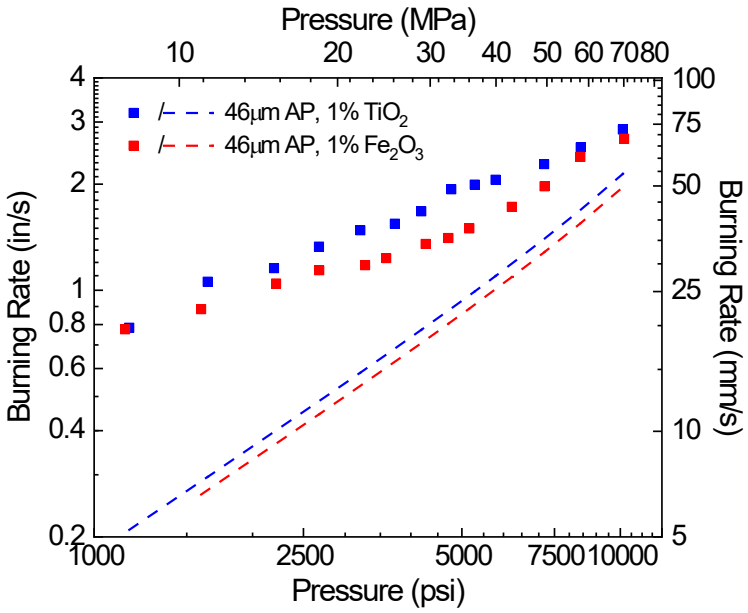

Figure B4. Comparison of Irwin's model burning rate predictions to experimental burning rates for formulations containing 46µm AP and MACH I additives [6]**.**

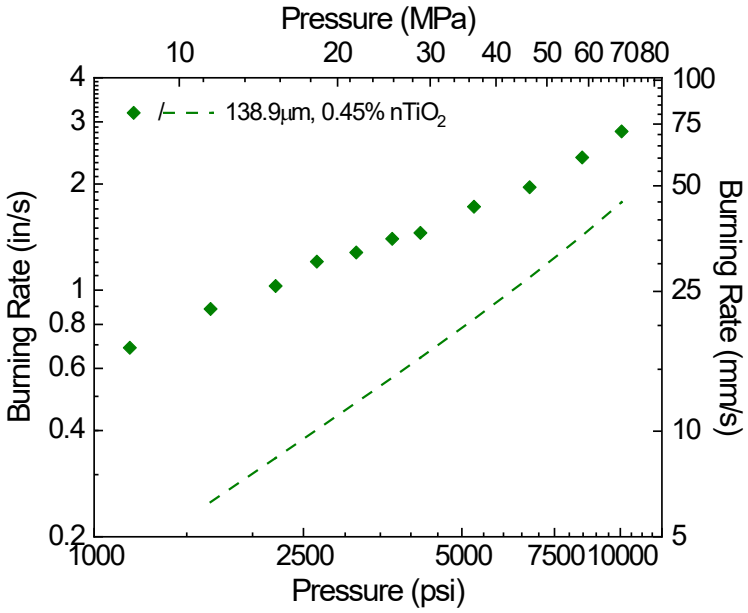

Figure B5. Comparison of Irwin et al.'s predicted burning rates and experimental results for the formulation containing 138.9µm AP and *insitu* titania [6].

B.2 Thomas et al. Ammonium Perchlorate Composite Propellant Model Details

Table B1. Complete list of input parameters for the Thomas et al. ammonium perchlorate composite propellant model [84].

	Parameter	Range	Value	Units	Reference
	Computational Input Parameters				
α_{ox}	Oxidizer Concentration	0.50 – 0.85	0.50 – 0.85	% x 10^3	-
D_{ox}	Oxidizer Particle Size	2 – 400	2 – 400	µm	-
T_0	Initial Temperature	-	298	K	-
P	Pressure	100 – 5000	100 - 5000	psia	-
	Oxidizer (AP) Ignition Parameters				
K	Oxidizer Ignition Delay Prefactor	-	4.321	s/cm^{n-1}	[90]
n	Oxidizer Ignition Delay Particle Diameter Exponent	-	1.7	-	[90]
	Oxidizer (AP) Parameters				
ρ_{ox}	Oxidizer Density	-	1950	kg/m^3	-
c_s	Specific Heat of Condensed Oxidizer	-	0.3903	cal/g-K	[88]
ΔH_s	Latent Heat of Condensed Oxidizer	-	138.5	cal/g	[87]
ΔH_{ev}	Latent Heat of Vaporization of Oxidizer at T_{ref}	-	526.5	cal/g	[87]
ΔH_g	Latent Heat of Oxidizer Decomposition Products	-	142.59	cal/g	[87]
A_s	Kinetics Prefactor of Oxidizer Surface Decomposition	-	2.5 x 10^7	g/cm^2-s	[87]
E_s	Activation Energy of Oxidizer Surface Decomposition	-	30	kcal/mol	[87]
A_{ox}	Kinetics Prefactor of Oxidizer Subsurface Reactions	1 x 10^7 – 1 x 10^9	1.56 x 10^8	g/cm^2-s	[1]
E_{ox}	Activation Energy of Oxidizer Subsurface Reactions	10 – 50	32	kcal/mol	[1]
A_{AP}	Kinetics Prefactor of Oxidizer Monopropellant Flame Reaction	1 x 10^3 – 1 x 10^5	5.45 x 10^4	g/cm^3-s-$atm^{\delta AP}$	[87-88]
E_{AP}	Activation Energy of Oxidizer Monopropellant Flame Reaction	10 – 50	30	kcal/mol	[1]
δ_{AP}	Reaction Order of AP Monopropellant Flame Reaction	1 – 2.5	2	-	[88]
T_{AP}	Oxidizer Monopropellant Flame Temperature	-	functional	K	[1]
c_g	Specific Heat of Oxidizer Combustion Product Gases	-	0.308	cal/g-K	[88]
λ_g	Thermal Conductivity of Oxidizer Combustion Product Gases	-	5.15 x 10^{-4}	cal/cm-s-K	[1]
	Fuel (HTPB) Parameters				
ρ_f	Fuel Density	-	920	kg/m^3	-
Q_f	Heat of Fuel Decomposition	-100 – 100	-66	cal/g	[87]
A_f	Kinetics Prefactor of Fuel Surface Decomposition	1 x 10^3 – 1 x 10^5	3 x 10^3	g/cm^2-s	[1]
E_f	Activation Energy of Fuel Surface Decomposition	5 – 30	15	kcal/mol	[1]
	Primary Flame Parameters				
A_{fh}	Average Flame Height Factor with Respect to Oxidizer	0 – 1	0.3	-	[1]
A_{PF}	Kinetics Prefactor of Primary Flame Reaction	1 x 10^3 – 1 x 10^5	2.41 x 10^3	g/cm^3-s-$atm^{\delta PF}$	[87]
E_{PF}	Activation Energy of Primary Flame Reaction	5 – 30	16.9	kcal/mol	[87]
T_{PF}	Primary Flame Temperature	-	1800	K	[87]
δ_{PF}	Reaction Order of Primary Flame Reaction	1 – 2.5	2	-	[1]

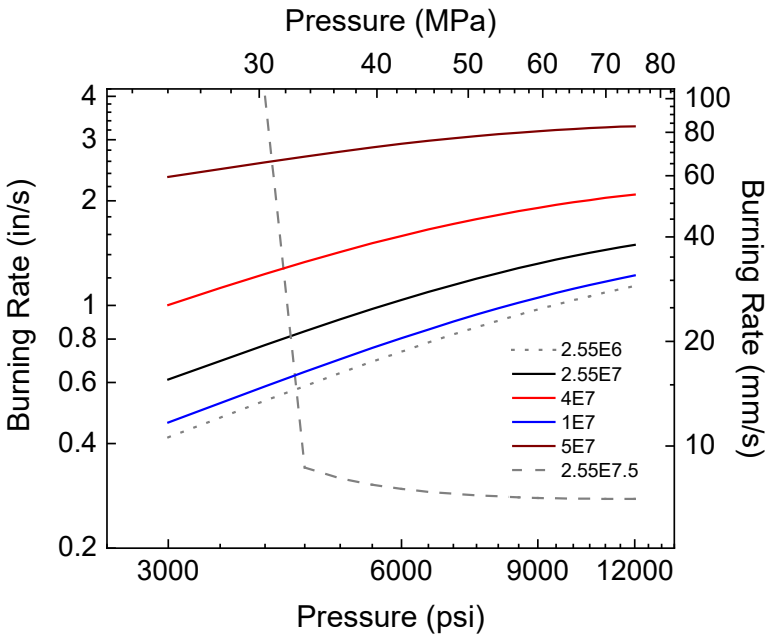

Figure B6. Effect of modifying the kinetics pre-factor of the oxidizer subsurface reactions, A_s, on the burning rate prediction of an 80% 210.3µm-AP propellant.

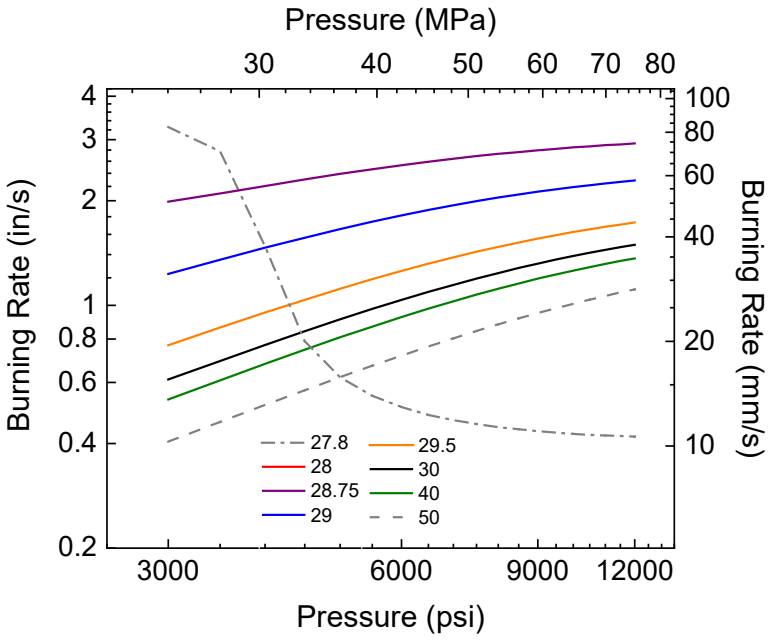

Figure B7. Effect of modifying the activation energy of the oxidizer subsurface reactions, E_s, on the burning rate prediction of an 80% 210.3µm-AP propellant.

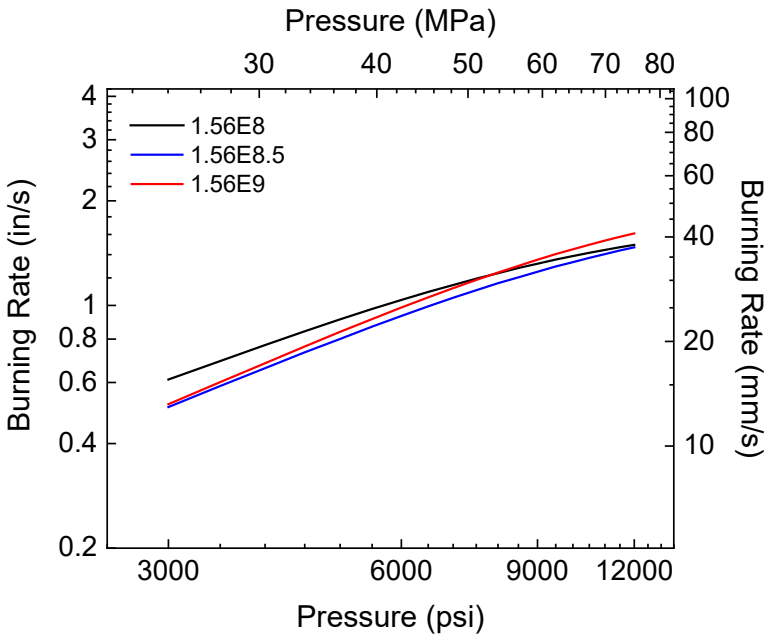

Figure B8. Effect of modifying the kinetics prefactor of the oxidizer surface decomposition, A_{ox}, on the burning rate prediction of an 80% 210.3µm-AP propellant.

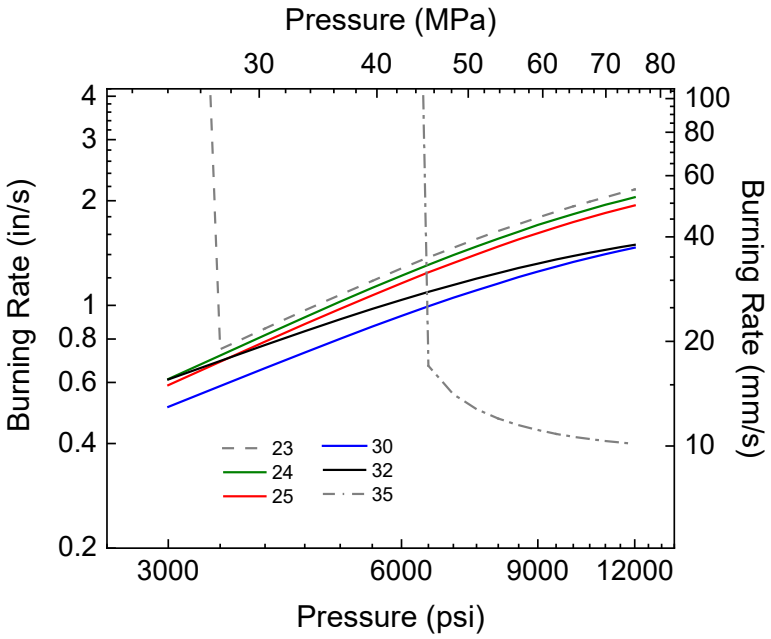

Figure B9. Effect of modifying the activation energy of the oxidizer surface decomposition, E_{ox}, on the burning rate prediction of an 80% 210.3µm-AP propellant.

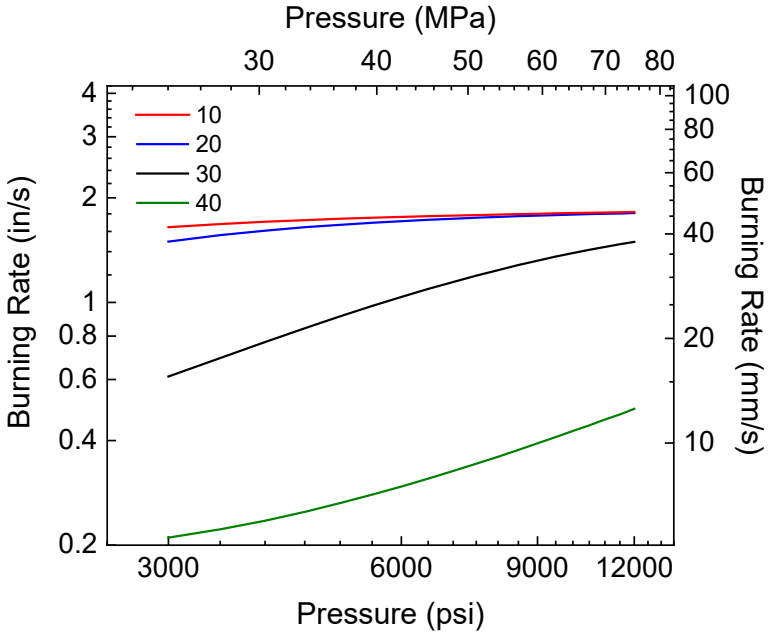

Figure B10. Effect of modifying the activation energy of the oxidizer monopropellant flame reaction, E_{AP}, on the burning rates of an 80% 210.3μm-AP propellant.

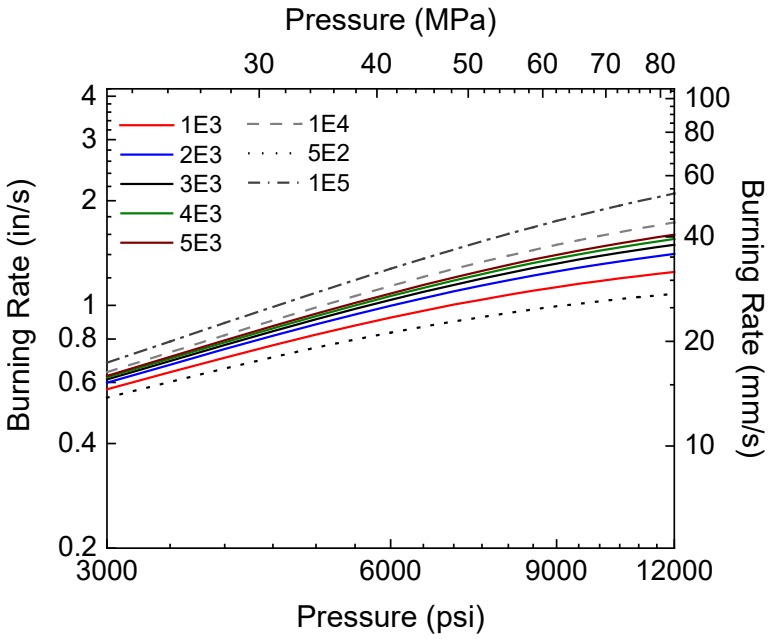

Figure B11. Effect of modifying the kinetics pre-factor of the fuel surface decomposition, A_f, on the burning rate predictions of an 80% 210.3μm-AP propellant.

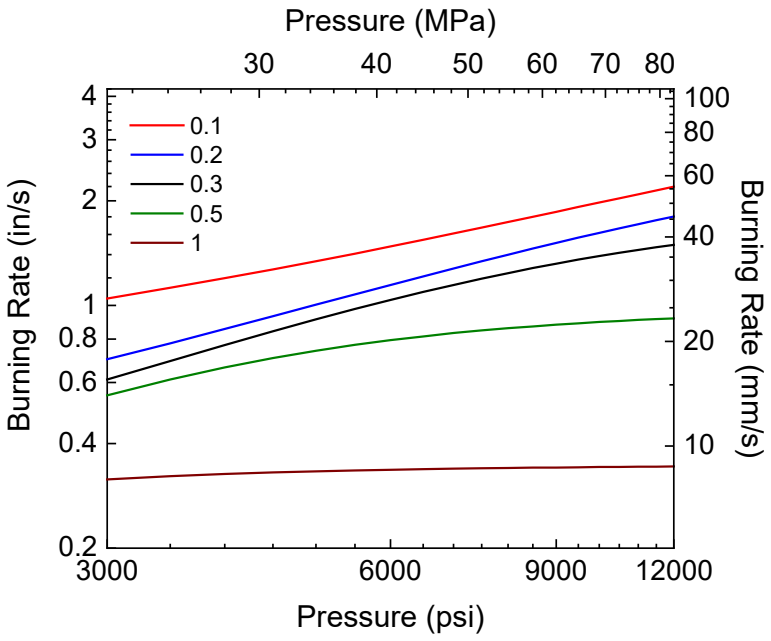

Figure B12. Effect of modifying the average diffusion flame height factor with respect to oxidizer, A_{fh}, on the burning rate prediction of an 80% 210.3µm-AP propellant.

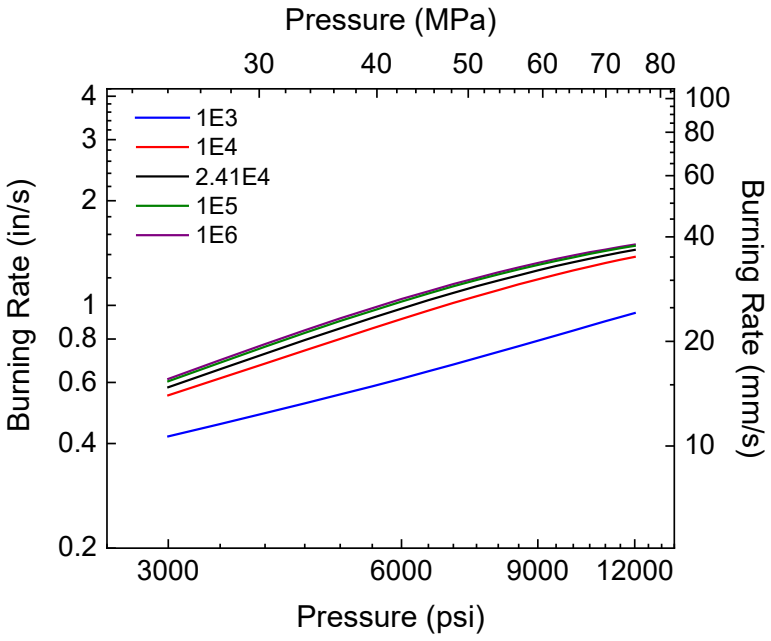

Figure B13. Effect of modifying the kinetics prefactor of the primary flame reaction, A_{PF}, on the burning rate predictions of an 80% 210.3µm-AP propellant.

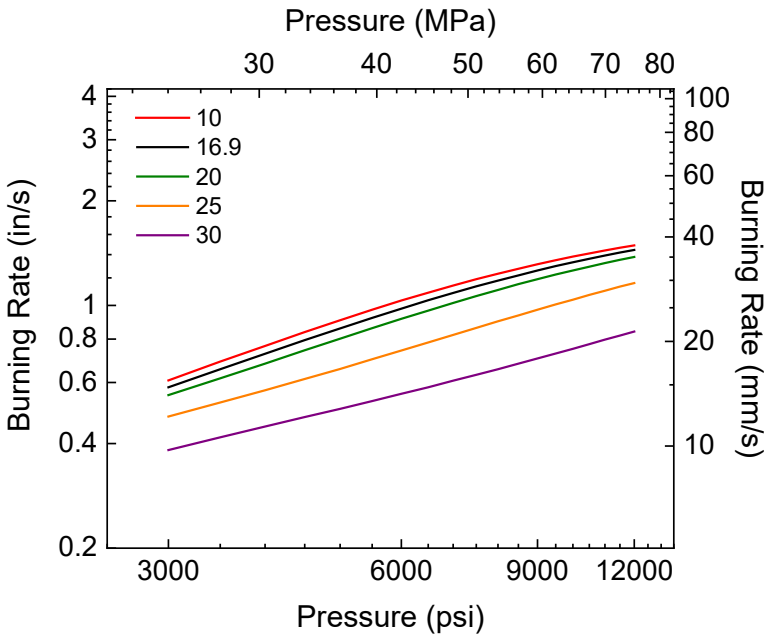

Figure B14. Effect of modifying the activation energy of the primary flame reaction, E_{PF}, on the burning rate prediction of an 80% 210.3μm-AP propellant.